CM Aprvd ISSUED 2009/09/18

911184
Revision 0

ENGINEERING SERVICES FOR THE NEXT GENERATION NUCLEAR PLANT (NGNP) WITH HYDROGEN PRODUCTION

Final Report – NGNP Core Performance Analysis, Phase 2

Prepared by General Atomics
For the Battelle Energy Alliance, LLC

Subcontract No. 00075309
Uniform Filing Code UFC:8201.3.1.2

GA Project 30302

GENERAL ATOMICS

Rolls-Royce

URS Washington Division

TOSHIBA Leading Innovation

OKBM

Korea Atomic Energy Research Institute

GENERAL ATOMICS

GA 1485 (REV. 08/06E)

ISSUE/RELEASE SUMMARY

☐ R & D ☐ DV&S ☒ DESIGN ☐ T&E ☐ NA	APPVL LEVEL	DISC	QA LEVEL	SYS	DOC. TYPE	PROJECT	DOCUMENT NO.	REV
	5	N	I	11	RGE	30302	911184	0

TITLE:

Final Report – NGNP Core Performance Analysis, Phase 2

CM APPROVAL/ DATE	REV	PREPARED BY	APPROVAL(S) ENGINEERING	QA	PROJECT	REVISION DESCRIPTION/ W.O. NO.
7 ISSUED SEP 1 8 2009		NGNP Project Staff	W. Scheffel for A. Shenoy	K. Partain K. Partain	J. Saurwein	Initial Issue A30302-0252

CONTINUE ON GA FORM 1485-1

NEXT INDENTURED DOCUMENT(S)

N/A

COMPUTER PROGRAM PIN(S)

N/A

LIST OF CONTRIBUTORS

Name	Organization
Alan Baxter	General Atomics
John Bolin	General Atomics
David Carosella	General Atomics
Jesse Crozier	General Atomics
Chris Ellis	General Atomics
Mike Fikani	General Atomics
David Hanson	General Atomics
Richard Luu	General Atomics
John Saurwein	General Atomics
Chuck Charman	C Squared, LLC

EXECUTIVE SUMMARY

GA was tasked by the Battelle Energy Alliance (BEA) to perform a core performance analysis (CPA) for a prismatic annular Modular Helium Reactor (MHR) core having the basic parameters given in Table E-1. The primary objective of the CPA was to determine if an acceptable core design can be achieved using a single-fuel-particle design or whether a binary-fuel-particle system (i.e., including a fissile particle and a fertile particle of different designs as described in Table E-1) is necessary. By definition, an acceptable core design is a design that provides for adequate fuel cycle length and efficient use of nuclear material, and that meets core design requirements with acceptable margin, including fuel performance and fission product release on a total core basis.

Per BEA's request, GA imposed two key constraints on the core physics design effort. One was to achieve an equilibrium fuel cycle length of 540 EFPD from cycle startup to shutdown, and the second was to limit compact packing fractions as shown in Table E-1. These compact packing fraction (PF) limits are based on the current nominal PF of about 35% for the compacting process developed by the NGNP/AGR Fuel Development and Qualification Program.

The overall conclusion of the CPA is that use of a single fuel particle having either a single U-235 enrichment or two U-235 enrichments appears feasible for a prismatic MHR operating with a reactor outlet helium temperature of 900°C. This conclusion is based on the success of the CPA effort in producing a single-fuel-particle/single-enrichment core design that meets the cycle length and PF requirements, is comparable to the best binary-fuel-particle core design achieved in the CPA with respect to predicted fuel performance and gaseous fission product release, and has predicted metallic fission product release that is only about a factor of two to three higher than for the best binary-fuel-particle core design. The CPA effort also produced two single-fuel-particle/two-enrichment core designs that have approximately the same predicted fuel performance and fission product release as the best binary-fuel-particle core design, but the maximum PF limit specified for the CPA was moderately exceeded in these designs. However, as discussed below, the fission product release for both the best single-fuel-particle and best binary-fuel-particle core designs achieved in the CPA did not meet the provisional MHR design limits for any of the fission products considered in the CPA. Consequently, further core design optimization would be required to achieve designs that are acceptable with respect to these requirements.

Table E-1. Key Parameters for NGNP Core Performance Analysis

Parameter	Value
Power level	600 MWt
Minimum fuel cycle length	540 EFPD
Core inlet helium temperature	540°C
Core mixed-mean outlet helium temperature	900°C
Core bypass flow fraction	0.15*
Fraction of power produced outside active core	0.05 (30 MWt)
Max. time-averaged fuel temperature	1250°C**
Fuel particle systems	(1) Binary-fuel-particle system: UCO fissile particle (350-μm kernel and ~19.7-wt% enrichment and a UCO (or UO_2) fertile particle (500-μm kernel and 0.72-wt% enrichment) (2) Single fissile fuel particle: UCO TRISO, ~14-wt% U-235 enrichment, 425-μm kernel
Fuel management	Two-batch re-load
Compact Packing Fraction	~30% for core average 35% maximum (goal) 35% - 40% for localized fuel zoning, if needed, not to exceed 5% of total core fuel compact volume

*The core bypass flow fraction in prior GA MHR designs has been 0.22. However, various reactor core design modifications that could reduce the core bypass flow fraction to about 0.10 were identified and evaluated in GA's NGNP pre-conceptual design studies report [PCDSR 2007]. Such core design modifications to reduce the core bypass flow are considered essential to help control maximum fuel temperatures in a reactor operating with a reactor outlet helium temperature of 900°C. For this CPA, a core bypass flow fraction of 0.15 was assumed as a compromise between the past value of 0.22 and the lowest reasonably-achievable value of 0.10.

**Historically, GA has used a maximum time-average fuel temperature of 1250°C as a guideline only (and not a hard limit) in assessing the suitability of a core physics design. This is because even if the maximum time-averaged fuel temperature of a small fraction of the fuel should exceed 1250°C, this does not necessarily mean that the design is unacceptable because the high temperatures may not lead to fuel failure and fission product release, which are the ultimate figures of merit for a core design.

Scope

The CPA included a core physics analysis; a fuel temperature, performance, and fission product release analysis; a core transient thermal-hydraulic analysis; and an accident analysis based on the results of the other analyses. The CPA was divided into two phases. The objectives of Phase 1 were to update and/or verify the computer codes to be used in the CPA, and to complete the first-cut of a binary-fuel-particle core physics design that would serve as the point of departure for the more detailed core analyses to be performed during Phase 2. The computer code sequence used in the CPA is shown in Figure E-1.

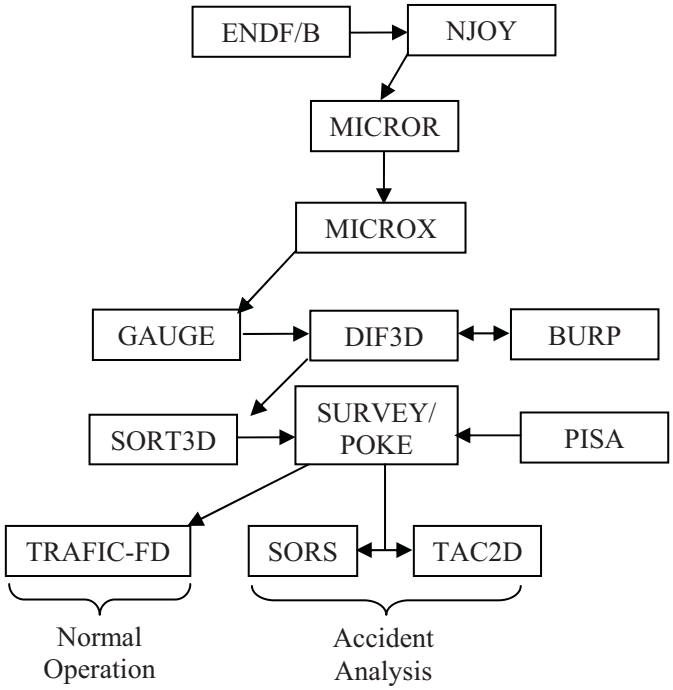

Figure E-1. Computer Code Flow Sequence for Core Performance Analysis

In Phase 1, the MICROX, GAUGE, BURP, DIF3D, SORT3D, TAC2D, TRAFIC-FD, SORS, and PISA codes were all ported from previous computing platforms to the new computing platform to be used in the CPA and were verified for running on the new platform. The SURVEY code, which is used to calculate fuel temperatures, fuel particle failure fractions, and fission gas release during normal reactor operation was updated and partially verified to ready it for use in Phase 2 to provide feedback to the physics design optimization effort. The SURVEY code results for the Phase 1 physics design indicated that while time-averaged fuel temperatures

were acceptable, there were fuel temperatures above 1600°C in a few locations in the core over some small time intervals. The results for Phase 1 were reported in Report 911160 [GA 2009a].

In the first part of Phase 2, verification of the SURVEY code was completed and the core physics design from Phase 1 was used as the starting point to develop an optimized binary-fuel-particle core design based on fuel temperature, fuel-performance, and fission-gas-release feedback from the SURVEY code. The TRAFIC-FD code was also used to calculate metallic fission product release. The work to develop an optimized core design for the binary-fuel-particle system was reported in the interim Phase 2 report [GA 2009b].

In subsequent work in Phase 2, the optimized binary-fuel-particle core design was used as the point of departure to develop a core design utilizing a single fissile fuel particle. The primary effort was to achieve an acceptable design for a single fuel particle with a single U-235 enrichment, but core design variations utilizing two identical fuel particles (i.e., a single-fuel-particle design) and two different U-235 enrichments were also evaluated. Work was also initiated to determine if the binary-fuel-particle and single-fuel-particle core designs could be further improved by using fuel shuffling (i.e., re-location of fuel elements within the core during refueling). Modifications were made to the SORT3D, SURVEY, and TRAFIC-FD codes to implement fuel shuffle capability, and one binary-fuel-particle, fuel-shuffle case, which did not provide any improvement relative to the non-shuffle cases, was performed, but the planned fuel shuffle work was not completed within the time constraints of the CPA. A depressurized conduction cooldown (DCC) event was also analyzed for the final binary-fuel-particle core design using the TAC2D and SORS codes, and the calculations indicated that the accident condition performance of the core design is acceptable with respect to temperature, fuel performance, and fission product release. The results for the single-fuel-particle core design work, the limited fuel-shuffle work, and the core accident conditions analysis are documented in this report.

Summary of Results

As discussed in [GA 2009b], design iterations were performed in the first part of Phase 2 to optimize the initial binary-fuel-particle core physics design developed in Phase 1. In all, 12 design iterations were performed. Design Case 7.9 is considered the best binary-fuel-particle core design achieved within the PF limits, cycle-length requirement, and time constraints of the CPA. Case 7.9 has a maximum PF of 38.5%, and 6.1% of the total core fuel compact volume is between 35% and 38.5%. This is within the maximum PF limit of 40%, but slightly exceeds the limit of 5% on the total core fuel compact volume having a PF greater than 35%. The minimum fuel cycle length goal of 540 EFPD (startup to shutdown) was achieved for all cycles except cycle 2, which ran for 530 EFPD.

The maximum predicted fuel temperature for Case 7.9 is 1488°C, and the maximum time-averaged fuel temperature is 1222°C, which is less than the 1250°C design guideline "limit". Fuel temperatures in the vicinity of 1488°C are clearly excessive and will cause SiC coating failure if they persist for a significant period of time. However, only a very-small volume of the fuel was predicted to experience such temperatures, and these temperatures did not persist for very-long periods of time. The predicted fuel performance and fission product release for Case 7.9 is summarized in Table E-2 below.

The focus of the single-fuel-particle core design work was to achieve an acceptable core design for a single fuel particle having a single U-235 enrichment. This work also involved a series of design iterations that primarily investigated fuel loading zoning and fixed burnable poison zoning to achieve a design that meets the PF and cycle length requirements, and which has predicted fuel performance and fission product release approximately equivalent to that for binary-fuel-particle core design Case 7.9. These iterations resulted in design Case 8.9.3, which is considered the best single-fuel-particle/single-enrichment core design achieved within the PF limits, cycle-length requirement, and time constraints of the CPA.

As indicated in Table E-1, the U-235 enrichment in the single-fuel-particle/single enrichment core design is supposed to be ~14%. This is consistent with the U-235 enrichment of the fuel particle that is currently being developed and qualified by the NGNP/AGR Fuel Program. However, it was determined during the binary-fuel-particle core design work that a U-235 enrichment of 14% is not compatible with the PF limits and the cycle-length goal imposed on the CPA. Consequently, a U-235 enrichment of 15.5% was selected for the fuel particles in the single-fuel-particle/single-enrichment design iterations based on the effective enrichment in the reloads in binary-fuel-particle core design Case 7.9.[1] Use of a single fuel particle having a U-235 enrichment would simply reduce the fuel cycle length from 540 EFPD to about 490 EFPD.

Case 8.9.3 has a maximum PF of 32.6% for the initial core and 38.3% for the reloads, with 5.9% of the fuel compact volume in the reloads having a PF greater than 35%. This is within the maximum PF limit of 40%, but slightly exceeds the limit of 5% on the total core fuel compact volume having a PF greater than 35%. The minimum fuel cycle length goal of 540 EFPD was achieved for all cycles except cycle 2 and cycle 3, which ran for 530 EFPD. The maximum predicted fuel temperature for Case 8.9.3 is 1534°C, and the maximum time-averaged fuel temperature is 1249°C, which is less than the 1250°C design guideline "limit".

[1] Subsequent to Case 8.9.3, Case 8.10 was performed to determine the cycle length that can be achieved within the PF constraints of the CPA using a single 14% enriched fissile particle. This analysis showed that a cycle length of 486 EFPD (equivalent to 90% availability over a 540 calendar day cycle) is achievable (with reactivity margin).

Although fuel temperatures are important with respect to fuel performance, limits on fuel temperatures are not sufficient figures-of-merit for a core design because of the influence of other parameters (e.g., burnup, fast fluence, time at temperature, etc.) on fuel performance. Rather, the ultimate figure-of-merit for assessing a core design from the standpoint of fuel performance is fission product release. Provisional fission product release limits and the attendant fuel failure limits for an NGNP prismatic reactor were first proposed in 2008 [Hanson 2008]. These limits were recently determined to be appropriate provisional limits for the prismatic reactor design considered in the CPA [Hanson 2009]. Table E-2 summarizes the provisional fuel failure and fission product release limits and compares the corresponding maximum predicted values for Cases 7.9 and 8.9.3 with these limits. The "Maximum Expected" criteria are the relevant figures-of-merit for the CPA because the core performance results are best-estimate predictions.

Table E-2. Comparison of Case 8.9.3 with Case 7.9 and the Provisional Fuel Performance and Fission Product Release Limits

Parameter	"Maximum Expected" Limit	"Design" Limit	Case 7.9	Case 8.9.3
Fuel failure during normal operation (exposed kernel fraction)	$\leq 5.0 \times 10^{-5}$	$\leq 2.0 \times 10^{-4}$	1.3×10^{-5} (fissile) 4.4×10^{-6} (fertile)	1.4×10^{-5}
In-service SiC failure	N/A	N/A	5.4×10^{-5}	1.0×10^{-4}
Kr-88 R/B	$\leq 8.3 \times 10^{-7}$	$\leq 3.3 \times 10^{-6}$	9.2×10^{-7}	1.1×10^{-6}
I-131 R/B	$\leq 2.0 \times 10^{-6}$	$\leq 8.0 \times 10^{-6}$	2.2×10^{-6}	2.5×10^{-6}
Cs-137 fractional release	$\leq 1.0 \times 10^{-5}$	$\leq 1.0 \times 10^{-4}$	4.2×10^{-5}	7.6×10^{-5}
Ag-110m fractional release	$\leq 5.0 \times 10^{-4}$	$\leq 5.0 \times 10^{-3}$	1.3×10^{-3}	5.7×10^{-3}

The total core exposed kernel fractions predicted for Case 7.9 and Case 8.9.3 are well below the in-service fuel failure limit of 5×10^{-5}. The contribution to the exposed kernel fraction from pressure vessel (PV) failure of standard fuel particles is negligible and the dominant sources of exposed kernels are PV failure of fuel particles with missing buffer layers, PV failure of fuel particles with defective or failed OPyC layers, and OPyC failure on fuel particles with defective or failed SiC layers.

The total core SiC failure fraction peaks at about 1.5 x 10^{-4} for Case 8.9.3, with as-manufactured SiC defects contributing about one-third of the total[2]. The predicted SiC failure is dominated by fission product (FP)/SiC reactions. The higher in-pile SiC failure in Case 8.9.3 relative to Case 7.9 is due to a higher volume fraction of the fuel operating at higher temperatures, primarily during the first two cycles. There is no limit per se on in-pile SiC failure, but SiC failure results in fission metal release, particularly of Cs isotopes, so SiC failure is practically limited by the allowed Cs-137 release fraction.

The results in Table E-2 show that neither the binary-fuel-particle core design nor the single-fuel-particle core design meet the "maximum expected" fission product release limits for any of the fission products considered in the CPA. The predicted maximum core-average R/B values for Case 8.9.3 are 1.1 x 10^{-6} for Kr-88 and 2.5 x 10^{-6} for I-131. These R/B values are slightly higher for Case 8.9.3 than for Case 7.9 because of the slightly higher exposed kernel fraction for Case 8.9.3.

The maximum Ag-110m cumulative release fraction for Case 8.9.3 is about an order of magnitude greater than the "maximum expected" limit of 5.0 x 10^{-4}, but only about three times greater than the maximum Ag-110m cumulative release fraction for Case 7.9. However, the maximum fuel temperatures and consequently the diffusive Ag-110m release for Case 8.9.3 decrease after cycle 2, and the Ag-110m cumulative release fraction drops to only about 1.5 x 10^{-3}, which is only about a factor of three greater than the "maximum expected" limit, by the end of cycle 5. The maximum predicted Cs-137 cumulative release fraction for Case 8.9.3 exceeds the "maximum expected" limit of 1 x 10^{-5} by a factor of about eight, but exceeds the maximum Cs-137 cumulative release fraction for Case 7.9 by only a factor of about two. The very-high localized fuel temperatures observed in both Case 7.9 and Case 8.9.3 are responsible for most of the predicted SiC failure (and therefore most of the Cs-137 release) and at least some of the Ag-110m release.

An alternative to using a single fuel particle with a single enrichment would be to use two UCO fuel particles that are identical except with respect to their U-235 enrichment. Because these two particles would be geometrically identical, they are considered to be a single fuel particle having two different enrichments. Two single-fuel-particle/two-enrichment cases were evaluated in the CPA.

In the first single-fuel-particle/two-enrichment case (Case 8.1), the fertile and fissile particles in Case 7.9 were redefined to have the same design (425-micron diameter UCO kernel and fissile-particle coating properties), but the U-235 enrichments were kept at 19.8% for the fissile particle

[2] The fraction of as-manufactured defective particles present in the core is conservatively assumed to be at the specification limit for each defect type specified in the Fuel Product Specification.

and 0.72 (natural uranium) for the fertile particle. Due to the high fertile-particle uranium loading in the initial core, retaining the same uranium loading with the smaller fertile particles (425 microns vs. 500 microns) had a significant impact on PF, increasing the maximum PF to 42.1% with a large fraction of the compacts (36%) above 35% PF. However, in the reloads, the PFs decreased relative to Case 7.9 because of the larger fissile particles (425-micron microns vs. 350 microns) and the reduced fertile particle uranium loading. The impact on PFs from using a single-fuel-particle design with a 350-micron kernel for both the fissile and fertile particles was also calculated and was found to be prohibitive. Specifically, the maximum PF in the initial core increased to 57% with 53% of the compacts having a PF greater than 35%. The maximum PF in the reload segments increased to 40% with 38% of the compacts having a PF greater than 35%.

The second single-fuel-particle/two-enrichment case (Case 8.5) used two identical fuel particles having two different U-235 enrichments in the initial core (cycle 1), but only one of these fuel particles was used in the reloads. The enrichment of the fuel particle used in the initial core and in the reloads was selected to be 15.5% such that the U-235 enrichment in the reloads is the same as the effective enrichment in Case 7.9. The enrichment of the second particle used in the initial core was selected to be 7.9% so that the effective enrichment of the initial core would be 10.9%, which is the same as the effective enrichment in the initial core in Case 7.9. The 7.9% enriched fuel particle was used only (and exclusively) in the first fuel load of Segment 1, which was removed after cycle 1. To limit the increase in PFs in the initial core (relative to Case 7.9) resulting from replacing the larger fertile particle and the more-highly-enriched fissile particle, the Segment 1 first-core uranium loading was reduced by 10% relative to Case 7.9. This resulted in a reduction of the initial core cycle length from 580 EFPD to 540 EFPD. The maximum PF in the initial core for this case is 40.6% with about 10% of the compacts having a PF greater than 35%. This does not meet the PF guidelines for the CPA, but it is a considerable improvement over Case 8.1. The PF guidelines are satisfied in the reloads, which have a maximum PF of 35% with only about 1% of the compacts having a PF greater than 35%.

The fuel performance in Case 8.5 was essentially unchanged relative to Case 8.1. The Ag-110m cumulative release fraction decreased by about a factor of two relative to Case 8.1, but there was also a modest increase in the Cs-137 cumulative release fraction. The predicted fuel failure and fission product release for both Cases 8.1 and 8.5 are approximately equivalent to the predicted fuel failure and fission product release for Case 7.9.

Conclusions

After an extensive code development and verification effort, and evaluation of a large number of physics design iterations utilizing both a binary-fuel-particle system and a single fuel particle,

GA was successful in producing binary-fuel-particle and single-fuel-particle core designs that: (1) meet the imposed cycle-length and PF requirements, the 1250°C design guideline for the time-averaged maximum fuel temperature, and the provisional “maximum expected” limit on in-service fuel failure; (2) have strong negative core temperature coefficients of reactivity; (3) have acceptable temperatures and fuel performance during a depressurized conduction cooldown event; and (4) have reasonable and similar axial and radial core power distributions and good uranium utilization. However, as discussed above, neither the best binary-fuel-particle core design nor the best single-fuel-particle core design achieved in the CPA meet the provisional fission product release limits for any of the fission products considered. Nevertheless, the results are encouraging for this initial core design effort given the relatively high fuel and graphite temperatures inherent in a prismatic MHR operating with an outlet helium temperature of 900°C and the potential that exists for further optimization of the core designs achieve in the CPA.

The results of the CPA work are considered to be supportive of an overall conclusion that use of a single fuel particle having either a single U-235 enrichment or two U-235 enrichments appears feasible for a prismatic MHR operating with a reactor outlet helium temperature of 900°C. This conclusion is based on the success of the CPA effort in producing a single-fuel-particle/single-enrichment core design (Case 8.9.3) that is comparable to the best binary-fuel-particle core design (Case 7.9) with respect to predicted fuel performance and gaseous fission product release, and that has predicted metallic fission product release that is only about a factor of two to three higher than for Case 7.9. The increased Ag-110m and Cs-137 release in Case 8.9.3 relative to Case 7.9 is primarily due to the higher fuel temperatures in the single-fuel-particle core design. This is as expected because a binary-fuel-particle system provides an inherent advantage relative to a single-fuel particle having a single U-235 enrichment because it allows U-235 enrichment zoning as well as uranium zoning and fixed burnable poison zoning. However, the differences in the results for the two designs are not particularly significant in view of the large uncertainties inherent in the calculation of fuel failure and fission product release.

The primary challenge associated with achieving a single-fuel-particle/single-enrichment core design that meets all requirements will be to reduce the metallic fission product release, which is greatest during the approach-to-equilibrium reactor operating cycles. Specifically, the maximum Ag-110 and Cs-137 cumulative release fractions for Case 8.9.3 are greater than the “maximum expected” limits by factors of 11 and 7, respectively. Design improvements that reduce the very-high localized temperatures observed not only in Case 8.9.3 but in all of the various design iterations, particularly during the approach-to-equilibrium cycles, will be necessary to reduce the Ag-110m and Cs-137 release fractions. The substantially lower metallic fission product release predicted for Case 8.9.3 Cycle 5, is noteworthy in that it suggests that the metallic fission product release fractions can be significantly reduced if a better physics design for the initial and

approach-to-equilibrium cycles can be developed.

The CPA effort also produced two single-fuel-particle/two-enrichment core designs (Cases 8.1 and 8.5) for which the predicted fuel performance and fission product release are approximately equivalent to the corresponding predictions for Case 7.9. Thus, the predicted Ag-110m and Cs-137 release fractions for these designs would have to be reduced by only about a factor of four to meet the provisional requirements. Use of a single-fuel-particle design with two U-235 enrichments is a potential fall back if an acceptable core design cannot ultimately be achieved with a single fuel particle and single U-235 enrichment. This is because a single-fuel-particle design with two U-235 enrichments should still require qualification of only one fuel particle because the irradiation and accident condition performance of the fuel particle having the higher U-235 enrichment should be bounding for the fuel particle having the lower U-235 enrichment. However, the maximum PF in both Case 8.1 and Case 8.5 moderately exceed the limit imposed on the CPA, so some relaxation of the PF constraints would be needed to accommodate these designs.

With respect to the PF limits imposed on the CPA, the PF constraints combined with the fuel cycle length goal of 540 EFPD (which requires relatively heavy fuel loadings) significantly limited the flexibility to use fuel zoning as a means of minimizing radial and axial power peaking in the core in either a binary-fuel-particle or single-fuel-particle core design. Consideration should be given to allowing PFs to increase up to about 45% given that the capability to make fuel compacts up to this PF without breaking fuel particles has already been demonstrated by the NGNP/AGR Fuel Program.

Although the physics design methodology changes investigated in Cases 7.9.1 and 7.9.4 to mitigate the localized fission rate spikes and resultant very-high, but short-term localized fuel temperatures caused by large incremental control rod movements did not have the anticipated effect, it is still clear from the SURVEY results that the very-high temperatures in the bottom of the core are the result of control rod withdrawal. Another potential means of reducing the impact of control rod withdrawal would be to modify the control rod operating scheme. There are 36 control rods located in the outer reflector elements, and the current approach used in the CPA is to operate these control rods in banks of three (one control rod per 120° sector of the core) and to completely withdraw each rod bank before initiating withdrawal of the next rod bank. A modified control rod operating scheme in which the control rods are withdrawn in banks of six rather than banks of three was evaluated in binary-fuel-particle core design Case 7.4, but this approach unexpectedly resulted in much-higher axial power factors and was not pursued further. Other control rod operating schemes could be investigated; for example, one in which all operating control rod groups are initially inserted about half-way into the core as opposed to having six of the twelve banks fully inserted and the other six withdrawn, as in the present

scheme. This would minimize control rod withdrawal for a required reactivity change and help to maintain an axial power shape tilted towards the top of the core.

In essentially all of the binary-fuel-particle and single-fuel-particle core design iterations, the highest calculated fuel temperatures are in the second and third cycles (i.e., the approach-to-equilibrium cycles). Based on these results, it is concluded that the design iterations performed in this study did not achieve sufficient optimization of the initial core and initial reload segments, and that further design iterations could result in significant improvement with respect to the high fuel temperatures observed in these cycles. However, given the extent to which the predicted Ag-110m and Cs-137 release fractions exceed the “maximum expected” limits in Cases 7.9 and 8.9,3, it is doubtful that these limits can be met by fuel and FBP zoning alone. Rather, it is likely that improvements to DIF3D (such as a control search capability) and/or relaxation of the constraints on PF and/or cycle length will be necessary to reduce the Ag-110m and Cs-137 release fractions to these levels. For example, allowing shorter cycle lengths during the approach-to-equilibrium might significantly improve fuel performance during cycles 2 and 3 without relaxing the constraint on PF.

Another potential means of improving the temperature, fuel failure, and fission product release results obtained for Cases 7.9 and 8.9.3 would be to modify the physics calculations to take advantage of the inverse relationship between reactivity and temperature. This option is available because all the physics calculations in the CPA were based on neutron cross sections generated for a single core-averaged temperature. This simplification minimized the complexity of the calculations to allow for reasonably-quick evaluation of many options, but it was also a conservatism that resulted in overestimation of peak power factors and temperatures to some degree. If temperature-dependent sets of cross sections were used throughout the core, the effect of the core negative temperature coefficient would be to reduce the neutron flux, and hence the power in the high temperature regions and to increase power in the low temperature regions. This would have the beneficial effect of lowering the highest fuel temperatures. It is possible to use multiple cross section sets in the DIF3D calculations, so the degree of conservatism associated with the use of a single cross section set could (and should) be evaluated. If the use of multiple cross sections sets is found to significantly reduce peak fuel temperatures, this methodology should be adopted for future core physics design work.

As indicated above, the relatively high fission product release fractions obtained for both the binary-fuel-particle and single-fuel-particle core designs in the CPA are at least partially due to the relatively high fuel and graphite temperatures that are inherent in a prismatic MHR operating with an outlet helium temperature of 900°C. It is expected that for a given reactor design, a reduction in the reactor outlet helium temperature would have a beneficial impact on fuel and graphite temperatures and therefore on fuel performance and fission product release.

Evaluation of the effect of reducing the reactor outlet helium temperature on fuel performance and fission product release was not within the scope of the CPA, but it was included in a companion task that was performed to develop fuel performance requirements and to ascertain the capability of various core designs to meet the requirements [Hanson 2009]. In the companion study, SURVEY and TRAFIC-FD calculations were performed for Case 7.9 from the CPA with a reactor outlet helium temperature of 750°C and a core inlet helium temperature of 390°C (thereby maintaining the same core temperature rise as for Case 7.9 in the CPA). The results for Case 7.9 with the different reactor outlet helium temperatures are compared in Table E-3 and confirm the expected benefit from reducing the reactor outlet helium temperature.

Table E-3. Case 7.9 Results for Different Reactor Outlet Helium Temperatures

Parameter	"Maximum Expected" Limit	Case 7.9 (900°C)	Case 7.9 (750°C)
Fuel failure during normal operation (exposed fissile kernel fraction)	$\leq 5.0 \times 10^{-5}$	1.3×10^{-5}	1.0×10^{-5}
In-service SiC failure	N/A	5.4×10^{-5}	1.4×10^{-6}
Kr-88 R/B	$\leq 8.3 \times 10^{-7}$	9.2×10^{-7}	5.3×10^{-7}
I-131 R/B	$\leq 2.0 \times 10^{-6}$	2.2×10^{-6}	1.6×10^{-6}
Cs-137 fractional release	$\leq 1.0 \times 10^{-5}$	4.2×10^{-5}	5.1×10^{-6}
Ag-110m fractional release	$\leq 5.0 \times 10^{-4}$	1.3×10^{-3}	4.4×10^{-5}

TABLE OF CONTENTS

LIST OF FIGURES

LIST OF TABLES

ACRONYMS AND ABBREVIATIONS

APF	Axial Power Factor
BEA	Battelle Energy Alliance (operators of the INL)
BOEC	Beginning of Equilibrium Cycle
BOIC	Beginning if Initial Cycle
CPA	Core Performance Analysis
DCC	Depressurized Conduction Cooldown
DOE	Department of Energy
EFPD	Effective Full Power Days
EOC	End of Cycle
EOEC	End of Equilibrium Cycle
FBP	Fixed Burnable Poison
FDDM	Fuel Design Data Manual
FIFA	Fissions per Initial Fissile Atom
FIMA	Fissions per Initial Metal Atom
GA	General Atomics
GDDM	Graphite Design Data Manual
GT-MHR	Gas Turbine-MHR
HTGR	High Temperature Gas-Cooled Reactor
INL	Idaho National Laboratory
LEU	Low-enriched Uranium
MHR	Modular Helium Reactor
MOEC	Middle of Equilibrium Cycle
NGNP	Next Generation Nuclear Plant
NRC	Nuclear Regulatory Commission
NU	Natural Uranium
NUCO	Natural UCO (Uranium Oxycarbide)
OPyC	Outer Pyrocarbon Coating Layer
PF	Packing Fraction
R/B	Fission Gas Release Rate/Fission Gas Birth Rate
RPF	Radial Power Factor
RSS	Reserve Shutdown System
SiC	Silicon Carbide
TRISO	TRI-material, ISOtropic (fuel particle coating system)

1 INTRODUCTION

GA was tasked by the Battelle Energy Alliance (BEA) to perform a core performance analysis (CPA) for a prismatic annular Modular Helium Reactor (MHR) core having the basic parameters given in Table 1-1. The primary objective of the CPA was to determine if an acceptable core design can be achieved using a single-fuel-particle design or whether a binary-fuel-particle system (i.e., including a fissile particle and a fertile particle of different designs as described in Table 1-1) is necessary.[3] By definition, an acceptable core design is a design that provides for adequate fuel cycle length and efficient use of nuclear material, and that meets core design requirements with acceptable margin, including fuel performance and fission product release on a total core basis.

Per BEA's request, GA imposed two key constraints on the core physics design effort. One was to achieve an equilibrium fuel cycle length of 540 EFPD from cycle startup to shutdown, and the second was to limit compact packing fractions as shown in Table 1-1. These compact packing fraction (PF) limits are based on the current nominal PF of about 35% for the compacting process developed by the NGNP/AGR Fuel Development and Qualification Program.

The CPA included a core physics analysis; a fuel temperature, performance, and fission product release analysis; a core transient thermal-hydraulic analysis; and an accident analysis based on the results of the other analyses. The CPA was divided into two phases. The objectives of Phase 1 were to update and verify the computer codes to be used in the CPA, and to complete the first-cut of a binary-fuel-particle core physics design that would serve as the point of departure for the more detailed core analyses to be performed during Phase 2. The computer code sequence being used in the CPA is shown in Figure 1-1.

In Phase 1, the MICROX, GAUGE, BURP, DIF3D, SORT3D, TAC2D, TRAFIC-FD, SORS, and PISA codes were all ported from previous computing platforms to the new computing platform to be used in the CPA and were verified for running on the new platform. The SURVEY code, which is used to calculate fuel temperatures, fuel particle failure fractions, and fission gas release during normal reactor operation was updated and partially verified to ready it for use in Phase 2 to provide feedback to the physics design optimization effort. The SURVEY code results for the Phase 1 physics design indicated that while time-averaged fuel temperatures were acceptable, there were fuel temperatures above 1600°C in a few locations in the core over some small time intervals. The results for Phase 1 were reported in Report 911160 [GA 2009a].

[3] GA has used both a fissile fuel particle and a fertile fuel particle in past GA core designs. GA has found that use of both fissile and fertile particles maximizes the ability to zone the core to minimize local power peaking and to maximize fuel cycle length. The traditional GA fissile and fertile particle designs were specified such that the particles would have different sizes to facilitate separation of the particles during reprocessing to recover the fissile material bred in the fertile particles.

Table 1-1. Key Parameters for NGNP Core Performance Analysis

Parameter	Value
Power level	600 MWt
Fuel cycle length	540 EFPD
Core inlet helium temperature	540°C
Core mixed-mean outlet helium temperature	900°C
Core bypass flow fraction	0.15*
Fraction of power produced outside active core	0.05 (30 MWt)
Max. time-averaged fuel temperature	1250°C**
Fuel particle systems	(1) Binary-fuel-particle system: UCO fissile particle (350-μm kernel and 19.9-wt% enrichment and a UCO (or UO2) fertile particle (500-μm kernel and 0.72-wt% enrichment) (2) Single fissile fuel particle: UCO TRISO, ~14-wt% U-235 enrichment, 425-μm kernel
Fuel management	Two-batch re-load
Compact PF***	~30% for core average 35% maximum (goal) 35% - 40% for localized fuel zoning, if needed, not to exceed 5% of total core fuel compact volume

*The core bypass flow fraction in prior GA MHR designs has been 0.22. However, various reactor core design modifications that could reduce the core bypass flow fraction to about 0.10 were identified and evaluated in GA's NGNP pre-conceptual design studies report [PCDSR 2007]. Such core design modifications to reduce the core bypass flow are considered essential to help control maximum fuel temperatures in a reactor operating with a reactor outlet helium temperature of 900°C. For this CPA, a core bypass flow fraction of 0.15 was assumed as a compromise between the previous value of 0.22 and the lowest reasonably achievable value of 0.10.

**Historically, GA has used a maximum time-average fuel temperature of 1250°C as a guideline only in assessing the suitability of a core physics design. This is because even if the maximum time-averaged fuel temperature of a small fraction of the fuel should exceed 1250°C, this does not necessarily mean that the design is unacceptable because the high temperatures may not lead to fuel failure and fission product release, which are the ultimate figures of merit for a core design. Thus, the a maximum time-averaged fuel temperature of 1250°C should be used only as a guideline in core design, not as a hard limit.

***These compact PFs are guidelines based on the current nominal PF of about 35% for the compacting process developed by the NGNP/AGR Fuel Development and Qualification Program. However, compacting studies performed at ORNL show that compact PFs well over 40% can be achieved with the current compacting process without damaging fuel particles. Because lower compacting forces are required for higher-packing-fraction compacts, there is a corresponding reduction in matrix density, but recent work at ORNL shows that a relatively high matrix density (i.e., >1.5 g/cc) can still be obtained for compacts with PFs as high as around 41%. There is a tradeoff between PF and matrix density with all MHR compact fabrication processes, and high-packing-fraction compacts (≥ 40%) having acceptable fuel quality can be fabricated at the expense of some reduction in matrix density. A modest reduction in matrix density has only modest implications for a prismatic MHR and can be fairly easily dealt with in the core design; whereas, limitations on compact PFs can have a serious impact on the economics of the reactor. Thus, the target PF constraints selected for the CPA should not necessarily be considered as hard limits for NGNP core design.

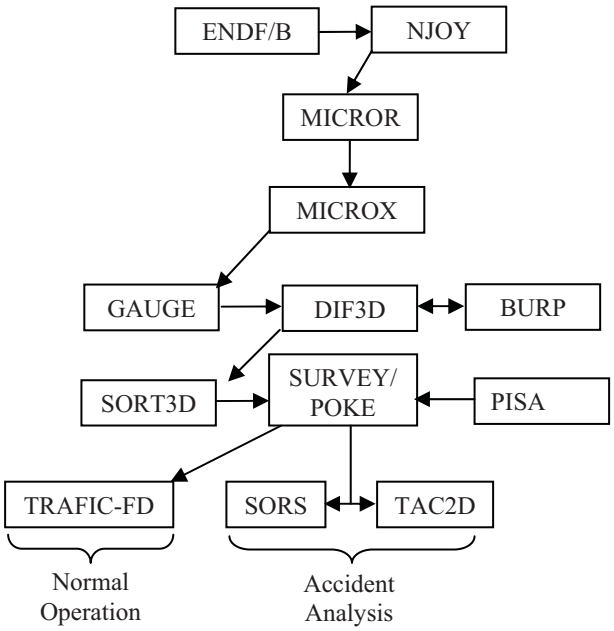

Figure 1-1. Computer Flow Sequence for Core Performance Analysis

In the first part of Phase 2, verification of the SURVEY code was completed and the core physics design from Phase 1 was used as the starting point to develop an optimized binary-fuel-particle core design based on fuel temperature, fuel-performance, and fission-gas-release feedback from the SURVEY code. The TRAFIC-FD code was also used to calculate metallic fission product release. The work to develop an optimized core design for the binary-fuel-particle system was reported in the interim Phase 2 report [GA 2009b] and is summarized in Section 3 of this report.

In subsequent work in Phase 2, the optimized binary-fuel-particle core design was used as the point of departure to develop a core design utilizing a single fissile fuel particle. The primary effort was to achieve an acceptable design for a single fuel particle with a single U-235 enrichment, but core design variations utilizing two identical fuel particles (i.e., a single-fuel-particle design) and two different U-235 enrichments were also evaluated. Work was also initiated to determine if the binary-fuel-particle and single-fuel-particle core designs could be further improved by using fuel shuffling (i.e., re-location of fuel elements within the core during refueling). A core accident analysis was performed for the optimized binary-fuel-particle core

design developed in the first part of Phase 2 [GA 2009b][4].

The results for the single-fuel-particle core design work, the fuel-shuffle work, and the core accident conditions analysis are documented in this report. Section 2 discusses the methods used in the CPA, Section 3 summarizes the work reported in [GA 2009b] to develop an optimized binary-fuel-particle core design, Section 4 describes the work to develop single-fuel-particle/single-enrichment and single-fuel-particle/2-enrichment core designs, Section 5 describes the fuel shuffle evaluation, and Section 6 describes the accident analysis. Section 7 provides the overall conclusions with respect to the feasibility of using a single fuel particle to achieve an acceptable core design for a prismatic MHR operating with a reactor outlet helium temperature of 900°C based on the work performed during Phase 2 of the CPA.

[4] The core accident analysis was performed on the final binary-fuel-particle core design, as planned, rather than a single-fuel-particle core design because of schedule constraints. The accident conditions for the single-fuel-particle should be similar to those for the binary-fuel-particle core because the power distributions are similar.

2 NGNP CORE ANALYSIS METHODS

Sections 2.1 and 2.2 present an overview of the core design and core physics methods. This information was previously presented in [GA 2009a] and [GA 2009b], but is repeated herein for completeness. Section 2.3 presents an overview of the fuel performance/fission product release methods.

2.1 Core Design Description

2.1.1 Core Configuration

The NGNP preconceptual design of the core consists of an array of hexagonal fuel elements in a cylindrical arrangement surrounded by a single ring of identically sized solid graphite replaceable reflector elements, followed by a region of permanent reflector elements all located within a reactor pressure vessel. The permanent reflector elements contain a 10 cm (3.94 in.) thick borated region at the outer boundary, adjacent to the core barrel. The borated region contains B_4C particles of the same design as in the FBP (see lower half of Table 2-8.), but dispersed throughout the entire borated region with a volume fraction of 61%.

The core is designed to provide 600 MWt at a power density of 6.57 MW/m^3. A core elevation view is shown in Figure 2-1 and a plan view is shown in Figure 2-2. The active core consists of hexagonal graphite fuel elements containing blind holes for fuel compacts and full length channels for helium coolant flow. The fuel elements are stacked to form columns (10 fuel elements per column) that rest on support structures as shown in Figure 2-1. The active core columns form a three row annulus with columns of hexagonal graphite reflector elements in the inner and outer regions (see Figure 2-2). Twelve core columns and 36 outer reflector columns contain channels for control rods. Eighteen columns in the core also contain channels for reserve shutdown material.

The annular core configuration was selected, along with the power density of 6.57 MW/m^3, to achieve maximum power rating and still permit passive core heat removal while maintaining the fuel temperature at ~ 1600°C (2912°F) during a conduction cooldown event. The active core effective outer diameter of 4.8 m (190.2 in.) is sized to maintain a minimum reflector thickness of 1 m (39.4 in.) within the 7.2 m (284.5 in.) inner diameter reactor vessel. These dimensions allow for a lateral restraint structure between the reflector and vessel. The height of the core with ten elements in each column is 7.9 m (312 in.), which allows a maximum power rating and axial power stability over the cycle.

The core reactivity is controlled by a combination of fixed burnable poison (FBP), movable poison, and a negative temperature coefficient. The fixed poison is in the form of lumped burnable poison compacts; the movable poison is in the form of metal clad control rods. Should

the control rods become inoperable, a backup reserve shutdown control (RSC) is provided in the form of boronated pellets that may be released into channels in the active core.

The control rods are fabricated from natural boron in annular graphite compacts with metal cladding for structural support. The control rods are located in row one of the core, and in the inner ring of the outer reflector (Figure 2-2). These control rods enter the core and outer reflector through the top reactor vessel penetrations in which the control rod drives are housed. The 36 control rods located in the outer reflector are the operating control rods, and are used for control during power operation, and for reactor trip. These operating rods can maintain the required 1% $\Delta\rho$ shutdown margin indefinitely under hot conditions, or for at least one day under cold conditions. Locating the operating rods in the outer reflector prevents damage during depressurized or pressurized passive heat removal. The twelve control rods in the core are the startup control rods, which are withdrawn before the reactor reaches criticality. With the startup and operating rods inserted, a 1% $\Delta\rho$ shutdown margin can be indefinitely maintained under cold conditions.

The RSC consists of boronated graphite pellets, housed in hoppers above the core. When the RSC is actuated, these pellets drop into channels in 18 columns of the active core. The RSC is used to institute reactor shutdown if the control rods become inoperable, or if necessary, to provide additional negative reactivity beyond that available in the inserted control rods.

The basic core nuclear design parameters are summarized in Table 2-1.

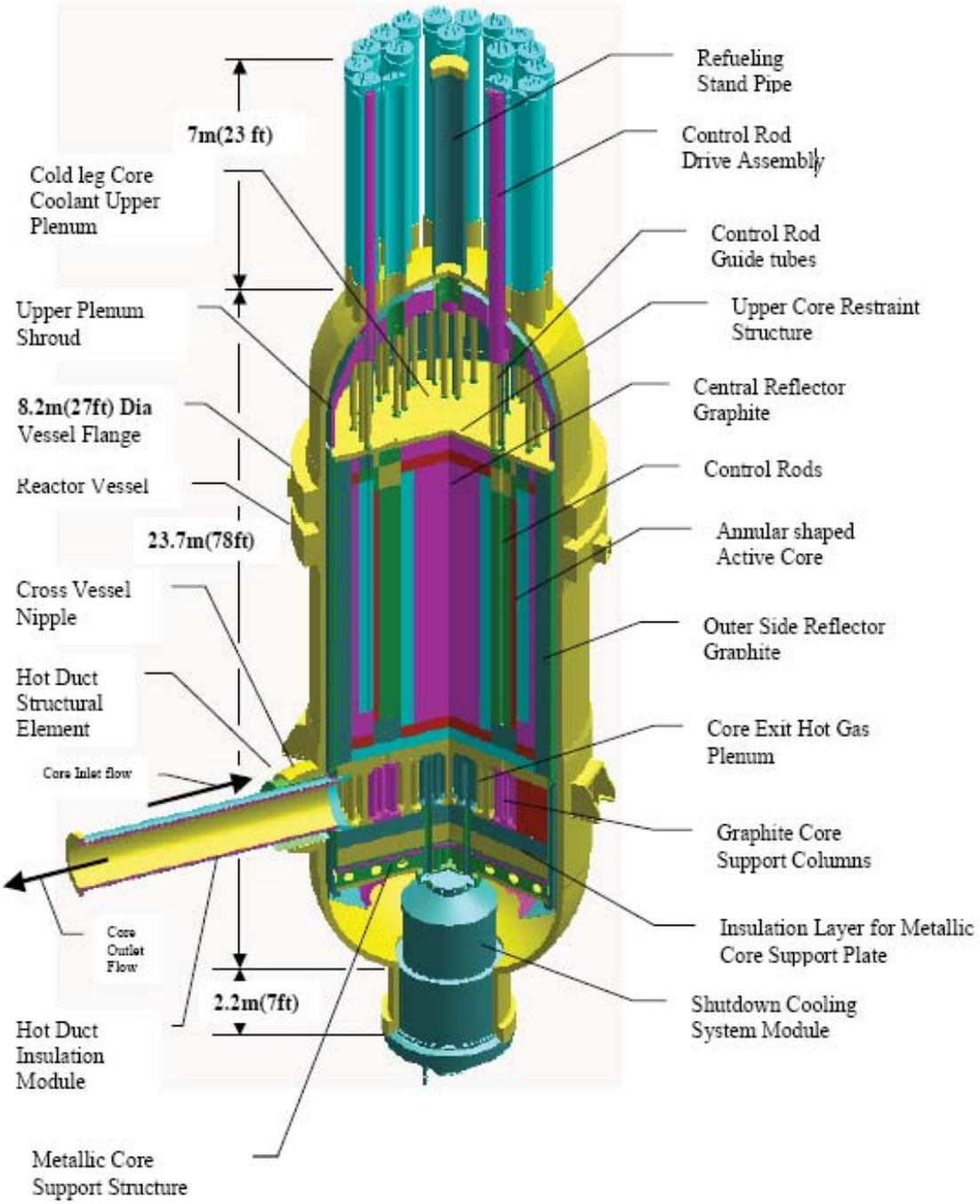

Figure 2-1. Reactor System

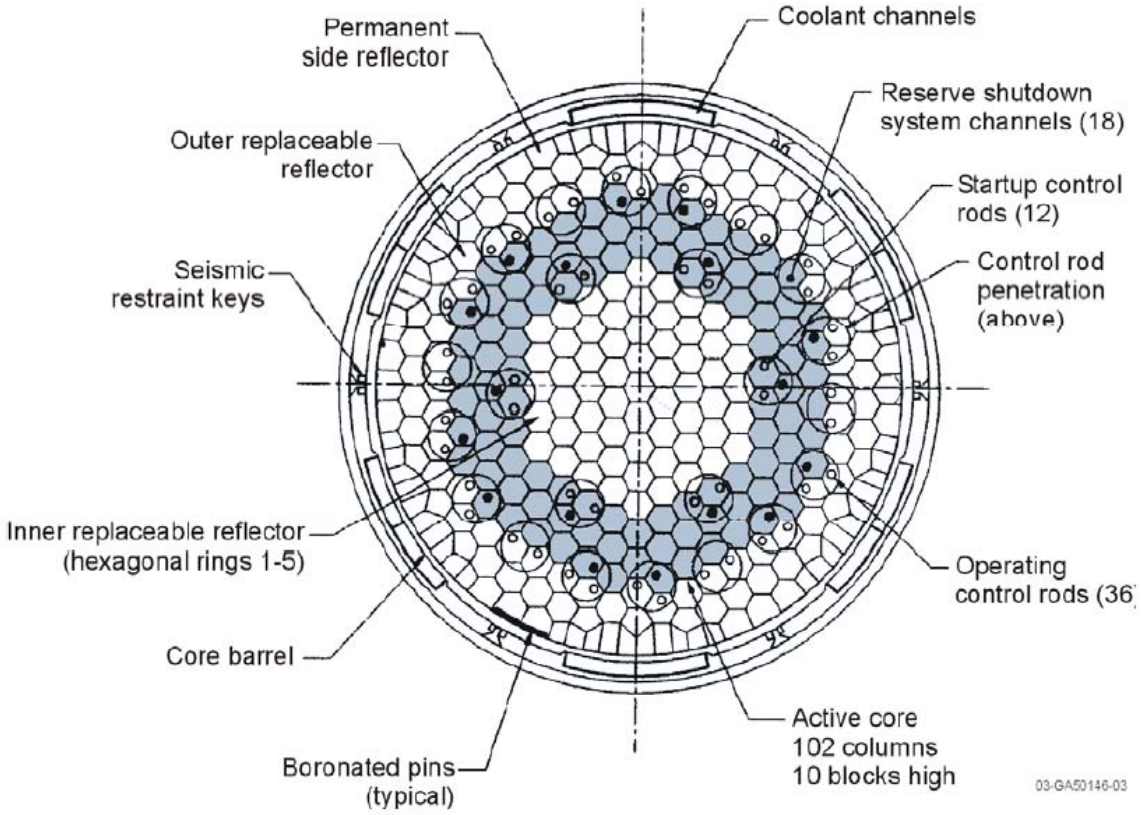

Figure 2-2. Core Cross Section at Vessel Midplane

Table 2-1. Core Design Parameters

Core power (MW(t))	600
Number of fuel columns	102
Thermal power density (MW/m^3)	6.57
Effective inner diameter of active core (m)	2.96
Effective outer diameter of active core (m)	4.83
Active core height (m)	7.93
Number of fuel elements (10 per column)	
Standard	720
Control	120
Reserve shutdown	180
Number of control rods	
In-core	12
Outer reflector	36
Number of RSC channels in the core	18
Fissile material in kernel (19.7974% enriched U)	$UC_{0.5}O_{1.5}$
Fertile material in kernel (natural U)	$UC_{0.5}O_{1.5}$
Refueling interval (months)	18
Number of columns per refueling segment	51
Time to refuel (days)	10
Availability factor (%)	98.6
Equilibrium cycle length (effective full-power days)	540
Core fuel loading (kg)	
Initial core, LEU	3457.83
NU	3006.82
Reloads, LEU	2132.75
NU	628.02
Weight of reload segment in core (kg)	
Carbon	76,771
Oxygen	278.9
Silicon	1215.7

2.1.2 Fuel Cycle Description

The fuel cycle uses two reload segments, so that 51 of the 102 columns core (half of the core) are replaced each reload. The control rod pattern (12 control rods in the core and 36 control rods in the outer reflector) allows refueling by 1/6 core sectors. The refueling operation is performed one sector at a time. Each refueling sector thus contains 17 core columns, with 10 fuel elements per column. In refueling each of the six refueling core sectors, the sector elements are removed one layer at a time until all of the core elements in the sector have been removed. Fresh reload elements and one-cycle-old elements are then reloaded into the sector. Thus, all 1020 core elements are removed from the reactor each reload, and the 510 two-cycle-old elements are reinserted with 510 fresh reload elements.

2.1.3 Fuel Element Design

There are three types of elements that contain fuel: standard elements, reserve shutdown elements that contain a channel for reserve shutdown control, and control elements that contain a control rod channel. Each standard element contains 3,126 fuel compacts, and each control element and RSC element contains 2,766 fuel compacts. Each compact contains fissile and fertile particles. Each particle contains a kernel of $UC_{0.5}O_{1.5}$ and coatings of carbon and silicon. The fissile kernels use 19.7974 weight % enriched uranium, while natural uranium is used in the fertile kernels.

The principal structural material of the fuel elements used in this analysis is nuclear grade PCEA AG (or equivalent) graphite (1.85 Mg/m^3) in the form of a right hexagonal prism 793 mm (31.2 in.) high and 360 mm (14.2 in.) across the flats. Fuel and coolant holes run parallel through the length of the prism in a regular triangular pattern of two fuel holes per coolant hole. The standard fuel element, shown in Figure 2-3, contains an essentially continuous pattern of fuel. Exceptions are the central handling hole, which is surrounded by smaller coolant holes, and six corner holes available for fixed burnable poison (FBP) compacts. The reserve shutdown and control fuel elements differ from the standard fuel elements in that they contain 95.3 mm (3.75 in.) and 101.6 mm (4.0 in.) diameter channels, respectively (see Figure 2-4). Those channels replace 24 fuel and 11 coolant holes. The pitch of the coolant and fuel-hole array is 18.8 mm (0.74 in.). The minimum web thickness between a 15.9 mm (0.63 in.) coolant hole and a 12.7 mm (0.5 in.) fuel hole is 4.5 mm (0. 18 in.). Both of these types of fuel elements have the exact same geometry as the corresponding fuel elements in the Fort St. Vrain high-temperature gas-cooled reactor.

A 35.0 mm (1.38 in.) diameter handling hole, located at the center of the element and extending down about one-third of the height, is used to lift the element during loading or unloading from the core. The hole has a ledge where the grapple of the fuel handling machine engages. The

25.4 mm (1.0 in.) diameter tooling hole at the bottom of the element is created during manufacturing of the element. The edge bevels prevent breakage of the graphite during loading or unloading of the elements. Each dowel extends above the top surface of the element. Each element also has dowel holes on the bottom surface to provide alignment for refueling and coolant channels, and transfer of seismic loads from fuel elements. Thus, when one element is placed on top of another element in the core, the dowels screwed into the bottom element fit into the dowel holes on the bottom surface of the element above it. This assures that proper vertical alignment is maintained in a column of elements.

The design of the fuel elements is summarized in Table 2-2. This data was used to calculate the volume of the components in the standard, control, and RSC elements, and the volumes, and volume fractions for the entire core. Table 2-3 gives the volumes of the solid components, volumes of the open voids where coolant can directly flow, and volumes for the closed voids that are internal to the element.

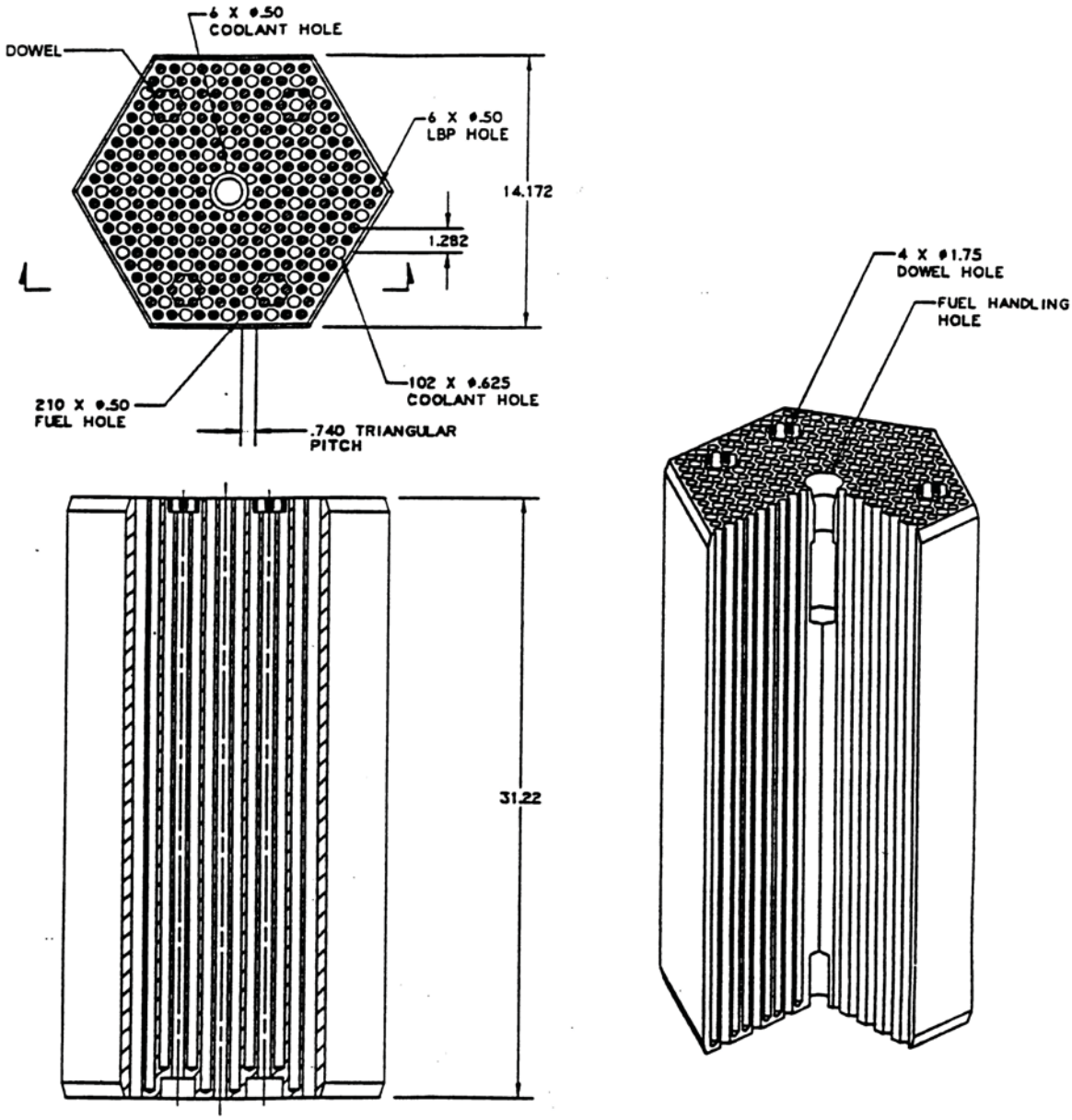

Figure 2-3. Standard Fuel Element Design (dimensions in inches)

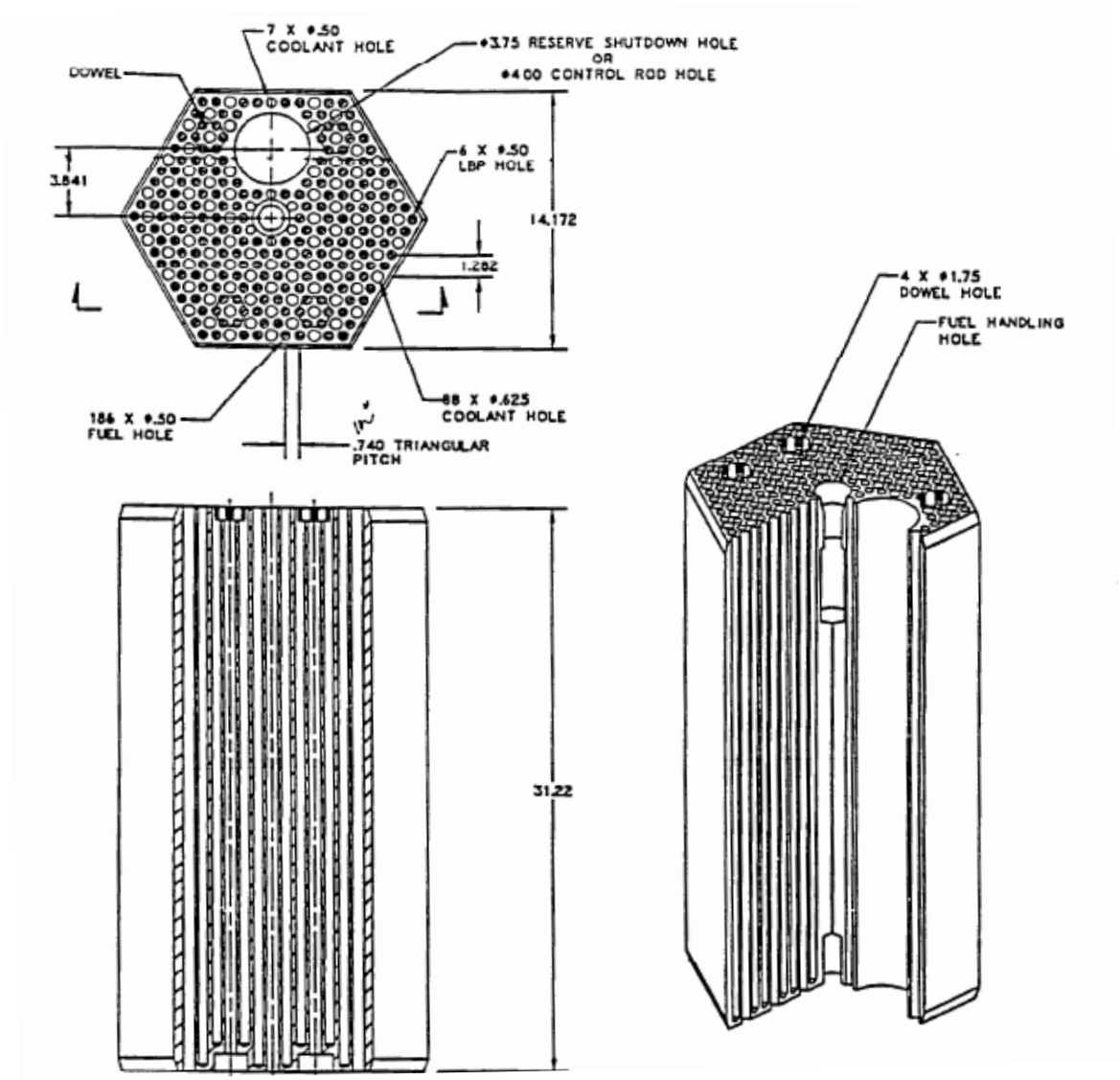

Figure 2-4. Control or Reserve Shutdown Fuel Element (dimensions in inches)

Table 2-2. Fuel Element Design Data

Shape	Hexagonal Prism
Type of graphite	Nuclear Grade PCEA AG or Equivalent
Block graphite density (g/cm^3)	1.85
Dimensions (mm, (in.))	793, (31.22) in length
	360, (14.172) across flats of hexagon – not including gaps
	361, (14.212) across flats of hexagon – including gaps
Control rod hole diameter (mm, (in.))	101.6, (4.0)
RSC hole diameter (mm, (in.))	95.25, (3.75)
Coolant holes per element, small/large	
Standard element	6 / 102
Control and RSC element	7 / 88
Coolant hole diameter (mm, (in.))	15.88, (0.625) for larger holes
	12.7, (0.5) for the 6 smaller holes near the center of the block
Pitch of coolant/fuel-hole array (mm, (in.))	18.8, (0.74)
FBP holes per element	6
FBP hole diameter (mm, (in.))	12.7, (0.5)
FBP hole length (mm, (in.))	781.5, (30.77)
FBP compact diameter (mm, (in.))	11.43, (0.45)
FBP compact length (mm, (in.))	51.56, (2.03)
FBP compacts per hole	14
Fuel holes under dowels / not under dowels	
Standard element	24 / 186
Control and RSC element	24 / 162
Fuel hole diameter (mm, (in.))	12.7, (0.5)
Fuel hole length (mm, (in.))	752.6, (29.63) under dowels
	781.5, (30.77) not under dowels
Fuel compacts per fuel hole	14 for holes under dowels
	15 for holes not under dowels
Fuel compacts per element	
Standard element	3,126*
Control and RSC element	2,766*
Fuel compact diameter (mm, (in.))	12.45, (0.49)
Fuel compact length (mm, (in.))	49.28, (1.94)*
Fuel compacts in core	3,080,520*
Fissile particles in compact, reload average	6,663*
Fertile particles in compact, reload average	673*

*These values are based on the MHTGR and GT-MHR nominal compact length of 1.94 in. The nominal length of the fuel compact being developed in the NGNP/AGR Fuel Program is currently 0.97 in. (i.e. half length)

Table 2-3. Element and Core Volumes

	Standard Element (m^3)	Control/RSC Element (m^3)	Entire Core (m^3)	Volume Fraction (%)
Solid Volumes				
Graphite block & dowels	5.040E-2	4.845E-2/4.923E-2	50.965	55.834
Fuel compacts	1.874E-2	1.658E-2	18.468	20.232
FBP rods	4.444E-4	4.444E-4	0.453	0.497
Fuel & FBP hole plugs	1.738E-4	1.544E-4	0.171	0.188
Total			70.057	76.750
Open Void Volumes				
Control holes	0	6.429E-3/5.651E-3	1.789	1.959
Coolant holes	1.661E-2	1.452E-2	16.316	17.874
Gaps between blocks	5.03E-4	5.03E-4	0.513	0.562
Handling hole	4.588E-4	4.588E-4	0.468	0.513
Tooling hole	2.574E-5	2.574E-5	0.026	0.029
Edge bevels	1.134E-4	1.134E-4	0.116	0.127
Dowel holes	5.361E-5	5.361E-5	0.055	0.060
Total			19.283	21.124
Closed Void Volumes				
Fuel holes	1.817E-3	1.616E-3	1.793	1.964
FBP holes	1.448E-4	1.448E-4	0.148	0.162
Total			1.941	2.126
Total Volume			91.281	100.000

2.1.4 Fuel Compact Design

The TRISO particles are bonded into fuel compacts to prevent mechanical interaction between the fuel particles and moderator graphite by maintaining the fuel as a free standing non-structural component of the fuel element, to maximize the thermal conductivity in the fuel, and to provide a secondary barrier to metallic fission product release through absorption mechanisms. The fuel compacts, which are contained within the fuel holes in the fuel elements, have a 12.45 mm (0.49 in.) diameter with a length of 49.3 mm (1.94 in.).[5]

[5] The nominal length of the fuel compact being developed in the NGNP/AGR Fuel Program is currently 0.97 in. (i.e. half length). Whether the compact length is 1.94 in. or 0.97 in. (in which case twice as many compacts will be needed) has no impact on the core performance analysis.

Each fuel compact is a mixture of fissile and fertile fuel particles bonded by a carbonaceous matrix.[6] These compacts are stacked in the fuel holes. The six stacks under each of the four dowels contain 14 fuel compacts; all other stacks contain 15 fuel compacts. A nominal radial gap of 0.127 mm (0.005 in.) between the fuel compact and the fuel hole allows for fuel element loading and precludes interference between the fuel compact and the graphite block during operation. Graphite plugs cemented into the tops of the fuel holes enclose the fuel compact stacks. A gap between the top of the fuel compact stack and the graphite plug also precludes interference during operation.

2.1.5 Fuel Particle Design

The reference fuel cycle employs low-enriched uranium and natural uranium. The fissile fuel is 19.7974% enriched uranium having an oxygen-to-uranium ratio of 1.5 in fresh fuel, and a carbon-to-uranium ratio of 0.5. The fertile fuel is the same composition as the fissile fuel, except that natural uranium is used rather than enriched uranium. Natural uranium, rather than depleted uranium, was selected for the fertile material because of the presence of more U-235 in natural uranium.

The core has a double-heterogeneous fuel configuration. The first level of heterogeneity consists of the TRISO coated particle design. As depicted in Figure 2-5, the fuel kernel is surrounded by a buffer (porous) layer of graphite and two high-density pyrocarbon layers with a silicon carbide layer in between. The buffer layer allows for limited kernel migration and provides some retention of gas particles. The silicon carbide layer ensures the structural integrity of the particle under constant pressure and also helps retain metallic fission products. These TRISO particles are dispersed in a graphite compact matrix to form fuel compacts, which are inserted into vertical fuel channels arranged in the fuel element, and produce the second level of heterogeneity. Details of the TRISO particle designs are given in Table 2-4. The reasons for the specified properties of each TRISO particle component are given in Table 2-5. The fuel quality and performance limits are given in Table 2-10 in Section 2.3.3

[6] The compact fabrication process currently being developed by the NGNP/AGR Fuel Program does not include use of graphite shim particles, which were used in GA's compacting process. However, it may be necessary to use shim particles in NGNP/AGR fuel compacts to occupy compact volume in compacts having relatively low fuel particle PFs (in the event that such compacts are required by the core design).

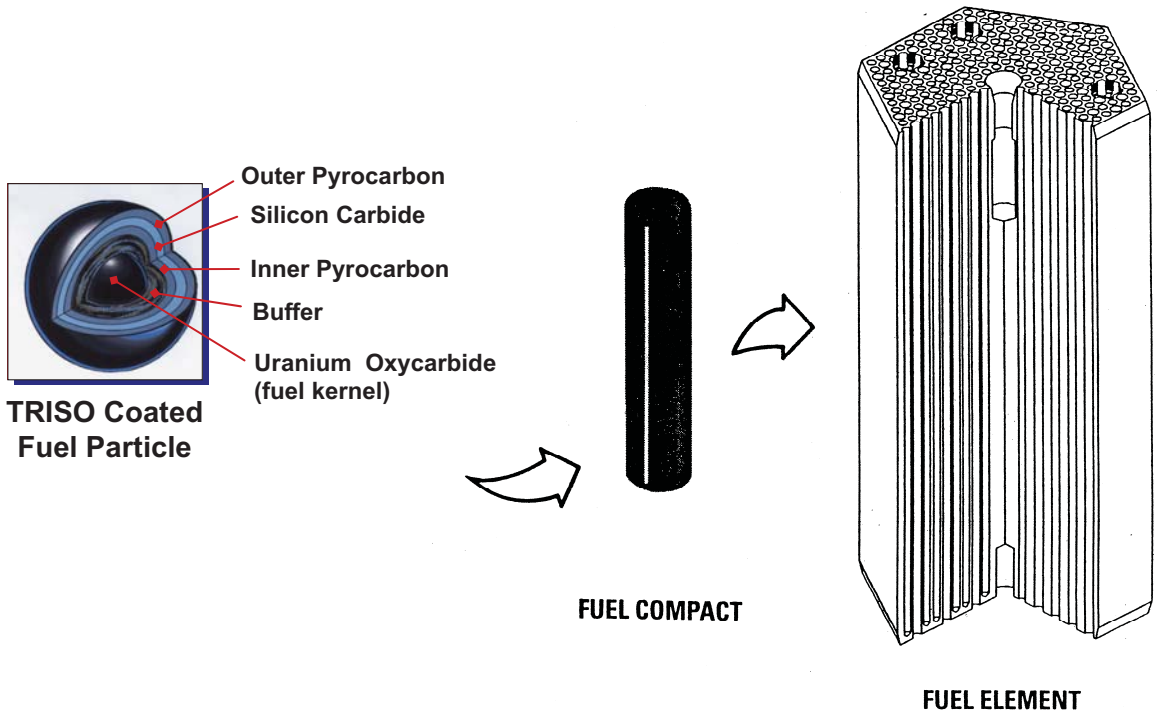

Figure 2-5. Standard Fuel Element and its Components

Table 2-4. Coated Particle Design

	Fissile Particle (LEU)	Fertile Particle (NU)
Composition	$UC_{0.5}O_{1.5}$	$UC_{0.5}O_{1.5}$
Uranium enrichment (weight %)	19.7974	0.711
Kernel diameter (μm)	350	500
Coating thickness (μm)		
Buffer	100	65
Inner pyrolytic	35*	35
Silicon carbide	35	35
Outer pyrolytic	40	40
Particle diameter (μm)	770	850
Coating thickness/Kernel diameter	0.6	0.35
Densities (g/cm^3)		
Kernel	10.5	10.5
Buffer	1.0	1.0
Inner pyrolytic	1.9	1.9
Silicon carbide	3.2	3.2
Outer pyrolytic	1.9	1.9
Elemental content per particle (μg)		
Carbon	314.2	387.1
Oxygen	21.2	61.5
Silicon	105.8	133.2
Uranium	209.3	610.3
Total	650.4	1192.2
Design burnup % FIMA MWd/MT	 26 260,000	 7 70,000
*The nominal mean value for the fissile particle currently being developed by the NGNP/AGR Fuel Development and Qualification Program is 40 μm. The impact of using 35 μm rather than 40 μm for the mean IPyC thickness in the CPA is very small		

Table 2-5. Basis for TRISO-Coated Fuel Properties

Particle Component	Specified Property	Purpose
Kernel	Diameter	Assure adequate heavy metal
		Control power production per particle
		Control pressure vessel failure
	Density	Assure adequate heavy metal
		Minimize fission gas release
Buffer	Thickness and Density	Control gas pressure
IPyC	Thickness and Density	Assure impermeability to chlorine during SiC deposition
		Provide structural support to SiC layer throughout irradiation
		Assure maximum irradiation stability with minimum permeability
SiC	Thickness and Density	Control pressure vessel failure
		Contain metallic and gaseous fission products
OPyC	Thickness	Provide structural support to SiC layer throughout irradiation
		Provide backup to SiC for gaseous fission product containment
	Density	Assure maximum irradiation stability with minimum permeability

2.1.6 Fixed Burnable Poison Design

The FBP consists of boron carbide (B_4C) granules dispersed in graphite compacts. The B_4C granules are pyrocarbon (PyC) coated to limit oxidation and loss from the system. The amount of burnable poison is determined by reactivity control requirements, which may vary with each reload cycle. The diameters of the FBP rods are specified according to requirements for self-shielding of the absorber material to control its burnout rate relative to the fissile fuel burnout rate. The goals are to achieve near complete burnout of the material when the element is replaced, and to minimize the hot excess reactivity swing over the cycle. The current design uses six FBP rods per element in all core layers, while axial zoning is performed through having relatively less FBP mass in the top and bottom layers compared to the middle layers of the core. Axial FBP zoning will be used to maintain the axial power shape during burnup and to prevent xenon induced axial power oscillations. The current design also uses a constant FBP compact diameter of 11.43 mm (0.45 in.) for all cycles. Details of the FBP design are given in Table 2-6, assuming that each FBP rod contains 14 compacts.

Table 2-6. Characteristics of Fixed Burnable Poison

FBP holes per element	6			
FBP compacts per FBP rod	14			
Compact diameter (mm, (in.)	11.43 (0.45)			
Compact length (mm, (in.))	51.56 (2.03)			
Rod length (mm, (in.))	721.87 (28.42)			
Volume fraction of B_4C particles plus shim particles	0.61			
FBP Component	Composition	Diameter (μm)	Thickness (μm)	Density (g/cm^3)
B_4C particle				
Kernel	B_4C	200	-	2.47
Buffer coating	C	-	18	1.0
Pyrolytic coating	C	-	23	1.87
Shim particle	C	-	-	1.65
Matrix	C	-	-	0.94

2.1.7 Hexagonal Reflector Elements

The hexagonal reflector elements are nuclear grade PCEA AG (or equivalent) graphite. Their size, shape, and handling hole are similar to the fuel elements, except that some of the reflector elements are half-height or three-quarter height. The volumes of the reflector components are given in Table 2-7.

Table 2-7. Reflector Element Volumes

Reflector Element Type:	Radial Standard	Radial Control	Axial Standard	Axial Control	Axial RSC
Solid Volumes (m^3)					
Graphite block & dowels	8.849E-2	8.204E-2	7.187E-2	6.753E-2	6.83E-2
Open Void Volumes (m^3)					
Control holes	0	6.429E-3	0	6.429E-3	5.651E-3
Coolant holes	0	0	1.661E-2	1.452E-2	1.452E-2
Gaps between blocks	5.03E-4	5.03E-4	5.03E-4	5.03E-4	5.03E-4
Handling hole	4.588E-4	4.588E-4	4.588E-4	4.588E-4	4.588E-4
Tooling hole	2.574E-5	2.574E-5	2.574E-5	2.574E-5	2.574E-5
Edge bevels	1.134E-4	1.134E-4	1.134E-4	1.134E-4	1.134E-4
Dowel holes	5.361E-5	5.361E-5	5.361E-5	5.361E-5	5.361E-5
Total	1.155E-3	7.584E-3	1.777E-2	2.201E-2	2.132E-2
Total Volume (m^3)	8.964E-2	8.962E-2	8.964E-2	8.962E-2	8.962E-2
Carbon volume fraction (%)	98.712	91.538	80.18	75.342	76.211
Void volume fraction (%)	1.288	8.462	19.82	24.658	23.789

The reflector above the active core is composed of two layers: one layer of full-height elements above a layer of half-height elements, for total reflector height of 1.2 m (46.8 in.). The top reflector elements channel coolant flow to the active core and provide for the insertion of reserve shutdown material into the active core. They have the same array of coolant holes as the fuel element and the same holes for the insertion of reactivity control devices.

The reflector below the active core has a total height of 1.6 m (62.4 in.). It consists of two layers: one layer of two half-height reflector elements above a layer of two half-height flow distribution and support elements. The bottom two elements provide for the passage of coolant from the active core into the core support area. This is accomplished by directing the coolant channel flow to the outside of the core support pedestal. The channels for the control rods and reserve shutdown material (RSS) stop at the top of the lower reflector so that neither the rods nor the RSS material can exit the core at the bottom. However, small holes are drilled through the reflector below the control rod channels so that adequate cooling is provided for the rods when they are inserted in the core or side reflectors without excessive coolant flow through these channels when the rods are withdrawn from the core.

The outer side reflector includes one full row and a partial second row of hexagonal reflector columns as shown in Figure 2-2. The outer row of hexagonal elements is solid, with the exception of the handling holes. Thirty-six of the elements in the inner row of the outer side reflector also have a control rod channel as shown in Figure 2-6. The control rod channel has a diameter of 102 mm (4 in.) and stops at an elevation just below the active core. Crushable graphite matrix at the lower end of each control rod channel will limit the load between the control rod assembly and reflector element in the event that the neutron control assembly support fails. The control rod channel is centered on the flat nearest the active core 102 mm (4.028 in.) from the center of the reflector element. The distance from the flat of the reflector block to the edge of the control rod channel is 27 mm (1.06 in.).

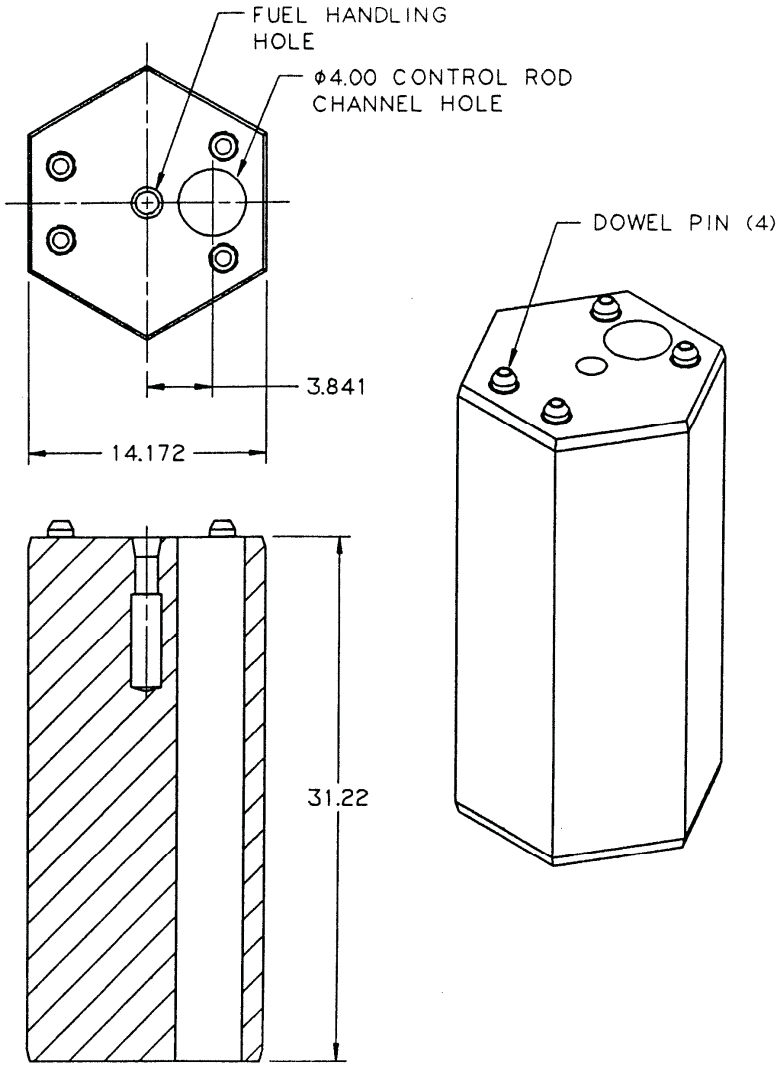

Figure 2-6. Reflector Control Element

The inner (central) reflector includes 61 columns of hexagonal elements. The central and side reflector columns consist of, from top down, one three-quarter height element, eleven full-height elements, one three-quarter height element, and two half-height elements, above the core support pedestal. The total reflector height for the equivalent 13.5 elements above the top of the core support pedestal is 10.7 m (421.5 in.). The dowel/socket connection at each axial element-to-element interface provides alignment for refueling and control rod channels, and transfers seismic loads from reflector elements.

2.1.8 Control Rods and Reserve Shutdown Control

Figure 2-7 shows the control rod design. The neutron absorber material consists of B_4C granules uniformly dispersed in a graphite matrix and formed into annular compacts. The boron is enriched to 90 weight percent B-10 and the compacts contain 40 weight percent B_4C. The compacts have an inner diameter of 52.8 mm, an outer diameter of 82.6 mm, and are enclosed in Incoloy 800H canisters for structural support. Alternatively, carbon-fiber reinforced carbon (C-C) composite canisters, or SiC, may be used for structural support. The control rod consists of a string of 18 canisters with sufficient mechanical flexibility to accommodate any postulated offset between elements, even during a seismic event.

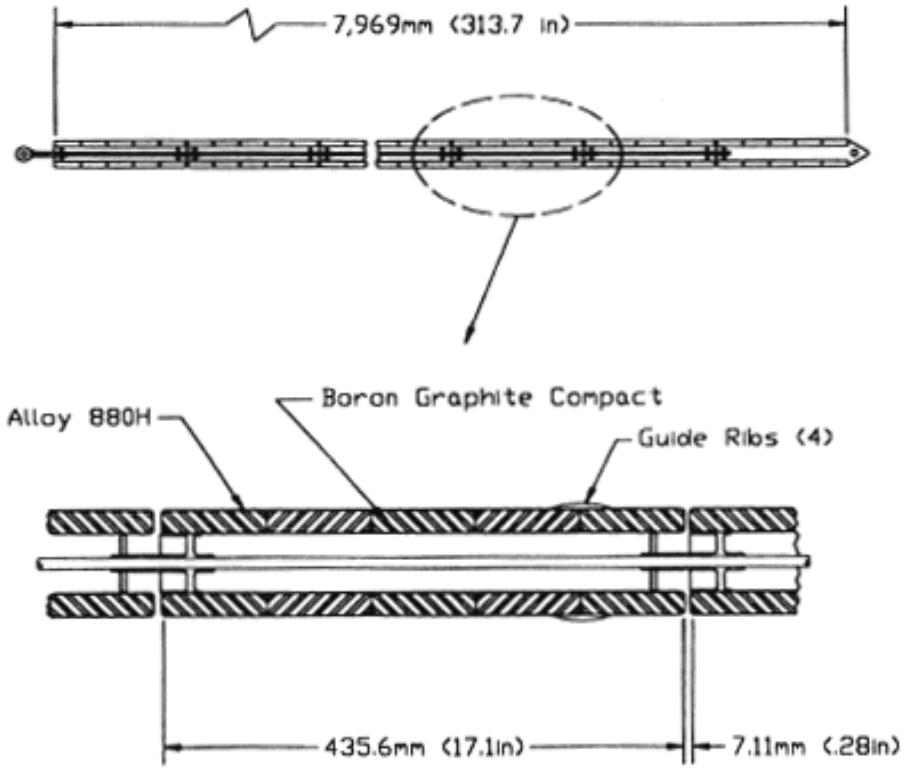

Figure 2-7. Control Rod Design

The reserve shutdown control material consists of 40 weight percent natural boron in B_4C granules dispersed in a graphite matrix and formed into pellets. The B_4C granules are coated with PyC to limit oxidation and loss from the system during high temperature, high moisture events. When released into the reserve shutdown channel in the fuel element, the pellets have a PF of ≥ 0.55.

The control rods are withdrawn in groups with three control rods in each group. The three control rods in each group are symmetrically located around the core, so that one rod is located in each 120° sector of the core. Figure 2-8 shows the locations of the control rod groups in a 1/3 section of the 102-column 600 MWt core. Control rod groups 1 through 12 in the outer reflector are the operating control rods, and groups 13 through 16 are the startup control rods. For startup from a cold condition, the control rod withdrawal sequence begins with the withdrawal of group 16 and progresses through groups 15, 14, 13, 12, 11, etc.

During normal power operation, control is accomplished with only the operating control rods (the startup control rods are in the fully withdrawn position.) These rods are operated automatically on the demand signal from the Plant Control Data Instrumentation System (PCDIS) in symmetric groups, with three control rods per group. The neutron flux level is continuously monitored by the ex-vessel detectors that supply signals to the PCDIS, the Investment Protection System (IPS) and the Reactor Protection System (RPS).

For a planned shutdown, the operating control rods are sequentially inserted, in the order indicated in Figure 2-8, to obtain a subcritical reactor. The I-135, Xe-135 and other radioactive nuclides will then decay, and the temperature of the core and reflectors will decrease, depending on the time dependence of the coolant flow and inlet temperature. When it is necessary to maintain a cold shutdown, the startup control rods will be inserted after a predetermined delay time. The delay time is long enough to ensure the rods would not be damaged in the event of a subsequent loss of forced core cooling.

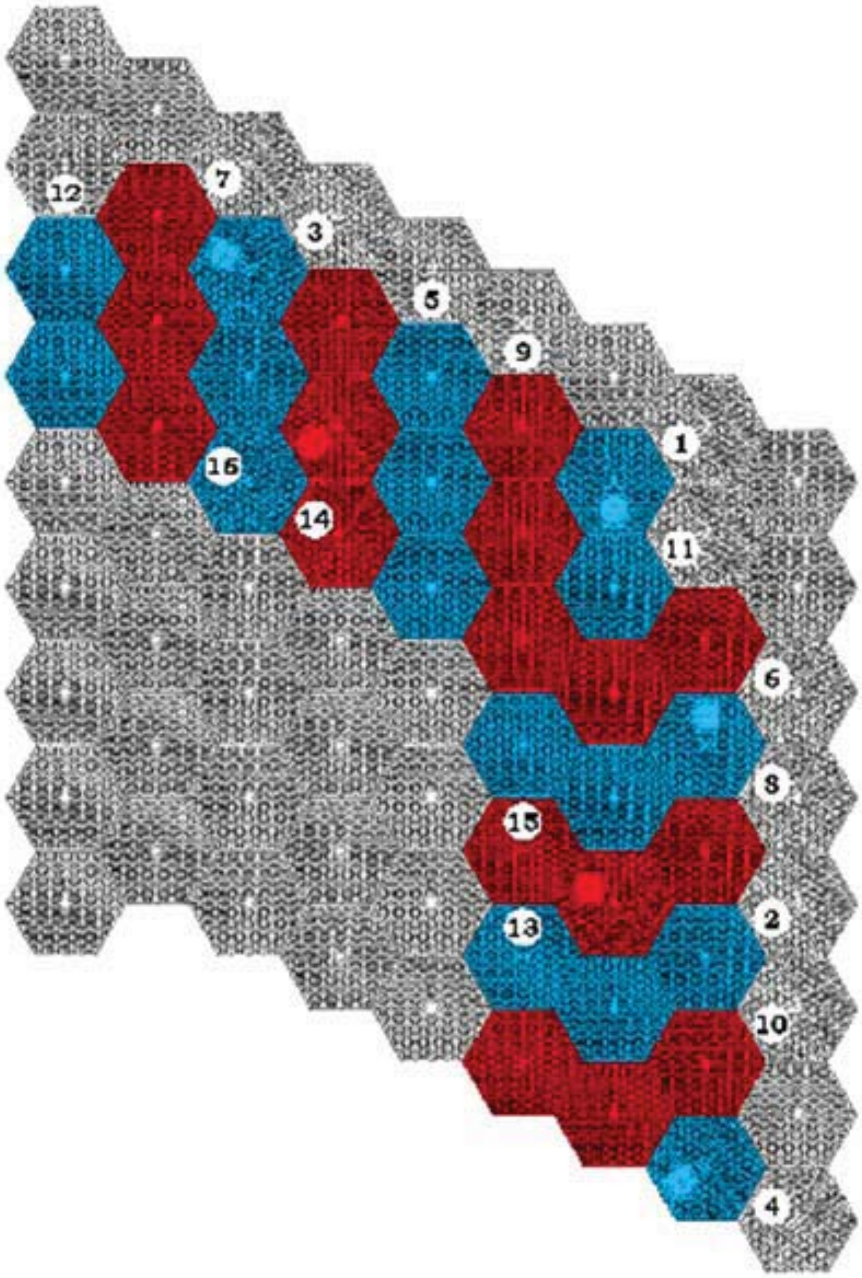

Key:
Blue columns = reload segment A
Red columns = reload segment B
Grey columns = reflector
Circle w/ number = control rod bank number
Circle w/o number = RSC location

Figure 2-8. One-third symmetrical reactor geometry model (excluding ring 9 and beyond)

2.1.9 Permanent Reflector Design

To allow for a 900°C helium outlet temperature, it was determined that direct vessel cooling is necessary and that the permanent reflector should be redesigned to have holes for helium core inlet flow [PCDSR 2007]. The current design uses 54 coolant holes equally spaced around the reactor, each 20.32 cm (8 in.) in diameter. The volume fraction occupied by these holes (in the non-borated region of the permanent reflector) is 0.29.

Neutron shielding of the reactor structural equipment consists of graphite permanent reflector elements containing a 10 cm (3.94 in.) thick borated region at the outer boundary, adjacent to the core barrel. The borated region contains B_4C particles of the same design as the FBP (see lower half of Table 2-6.) As opposed to containing the particles in compacts, the current design assumes B_4C particles are dispersed throughout the entire borated region, and the volume fraction the particles occupy within the borated region is 0.61. Figure 2-9 [Richards 2008a] shows a 1/12th core sector illustration of the permanent side reflector.

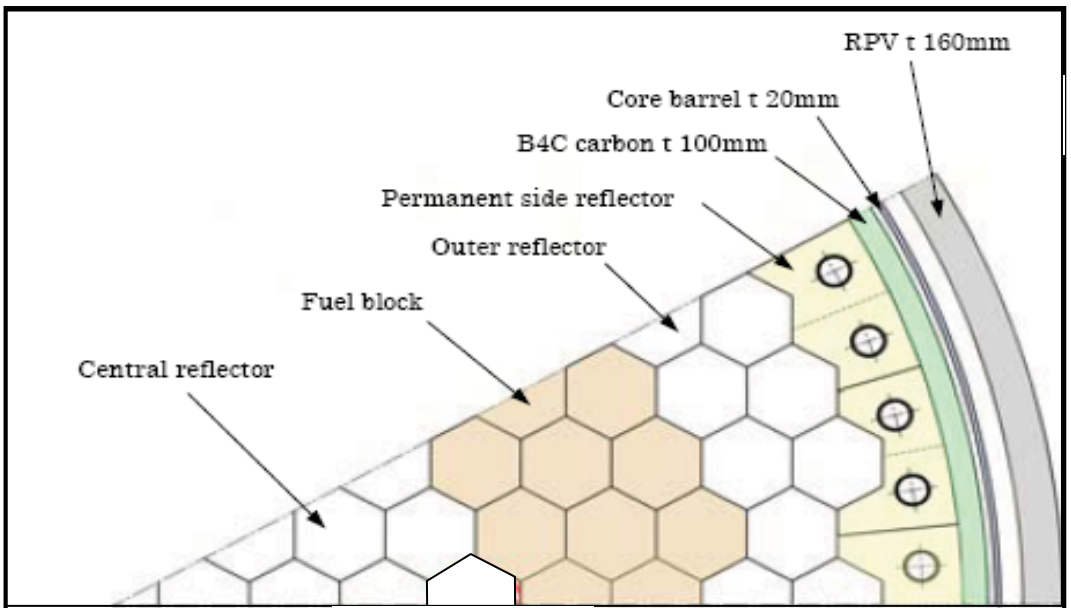

Figure 2-9. Permanent Reflector Design

2.2 Core Physics Methods

For multi-group cross-sections, fuel particle and fuel compact heterogeneities must be accounted for in the calculation of the microscopic cross-sections to account for shielding of resonances in the fuel kernel and in the fuel compact for cold and hot conditions. GA accounts for these heterogeneities using the MICROX code. MICROX is an integral transport theory flux spectrum code, which solves the thermalization and neutron slowing-down equations on a detailed energy grid for a two-region lattice cell [Walti 1972]. Fluxes in these two regions are coupled by collision probabilities based upon a flat flux approximation. GA uses the MICROX code to account for the rod and particle self-shielding in the calculation of multi-group and transport cross-sections. MICROX uses a model with two cylindrical regions. Region 1, which is the inner cylinder, is used to model a cylindrical fuel compact containing up to two types of particles. The cylindrical region 2, which surrounds region 1, is used to homogenize everything else in the fuel elements. Fuel particles cannot be modeled in region 2. MICROX calculates a fine group spectrum, with 92 fast groups from 15 MeV down to 2.3824 eV, plus 101 thermal points from 2.38 eV down to 0.001 eV. This 193 fine group spectrum has been used to collapse the cross-section data down to 9 groups (5 fast + 4 thermal) as shown in Table 2-8.

Table 2-8. Broad Group Energy Structure

Group #	Type	Lower Energy (eV)
1	Fast	1.8316×10^5
2		961
3		17.61
4		3.9279
5		2.38
6	Thermal	1.275
7		0.825
8		0.13
9		0.001

Microscopic core cross-sections for a total of 54 different nuclides are calculated with MICROX for use in all diffusion analysis. Since there are two particle types (fissile and fertile,) two separate sets comprising of sixteen heavy metal nuclide cross-sections were developed which gives the ability to independently track the depletion of each particle type during a core burnup. A complete list of these nuclides is given in Table 2-9 where:

- NSAG35 and NSAG49 represent non-saturating aggregates from U-235 and Pu-239, respectively (these aggregates help estimate a lumped reactivity worth of the remaining fission products);
- B-10 represents the boron within the FBP;
- B-Nat is natural boron;
- BIMP is burnable impurities within graphite in terms of boron worth;
- NBIMP is non-burnable impurities within graphite in terms of boron worth;
- C-Fuel represents graphite within fuel compacts;
- C-Mod represents graphite within FBP and the graphite blocks.

Note that in Table 2-9, separate carbon atom densities are given due to carbon in the fuel compacts and carbon in the graphite block to allow flexibility in modeling carbon at different temperatures.

Table 2-9. Nuclide Listing for Diffusion Calculations

Nuclide	Nuclide-Type	Nuclide	Nuclide-Type	Nuclide	Nuclide-Type
U-235	Heavy Metal	Tc-99	Fission Product	Sm-151	Fission Product
U-236	Heavy Metal	Rh-103	Fission Product	Sm-152	Fission Product
U-238	Heavy Metal	Rh-105	Fission Product	Eu-151	Fission Product
Np-237	Heavy Metal	Ag-109	Fission Product	Eu-152	Fission Product
Np-239	Heavy Metal	Ag-110m	Fission Product	Eu-153	Fission Product
Pu-238	Heavy Metal	I-135	Fission Product	Eu-154	Fission Product
Pu-239	Heavy Metal	Xe-131	Fission Product	Eu-155	Fission Product
Pu-240	Heavy Metal	Xe-135	Fission Product	NSAG35	Fission Product
Pu-241	Heavy Metal	Cs-133	Fission Product	NSAG49	Fission Product
Pu-242	Heavy Metal	Cs-134	Fission Product	B-10	Structural
Am-241	Heavy Metal	Cs-136	Fission Product	B-Nat	Structural
Am-242m	Heavy Metal	Nd-143	Fission Product	BIMP	Structural
Am-243	Heavy Metal	Nd-145	Fission Product	NBIMP	Structural
Cm-242	Heavy Metal	Pm-147	Fission Product	Silicon	Structural
Cm-243	Heavy Metal	Pm-148m	Fission Product	Oxygen	Structural
Cm-244	Heavy Metal	Pm-148g	Fission Product	C-Fuel	Structural
Kr-83	Fission Product	Sm-149	Fission Product	C-Mod	Structural
Mo-95	Fission Product	Sm-150	Fission Product	Hydrogen	Structural

For hot conditions, core cross-sections for the nuclides associated with the fuel rods were performed at 1130K, while the graphite blocks were performed at 1080K. The methods applied in generating core cross-sections do not take into account any direct temperature feedback. Instead, only one set of core cross-sections at a specified temperature is used for hot conditions for diffusion burnup calculations for all time points from beginning of initial cycle (BOIC) to end of equilibrium cycle (EOEC.) The set applied was derived from a BOIC core spectrum. As explained in [Ellis 2009a], this is a reasonable assumption and is also conservative from the standpoint of fuel cycle length.

Additional information on the single core unit cell model includes LEU and NU volume fractions of kernels within a compact of 0.0201 and 0.0175, respectively. The volume fraction of fuel compacts in the model is 0.202.

A detailed discussion how these nuclides were processed for the 2D and 3D models, how impurities within the graphite were modeled and how self-shielding factors were applied, are given in [Ellis 2009a].

Two-dimensional diffusion burnup calculations were performed with the GA code GAUGE based upon a triangular spatial mesh [Archibald 1983]. In GAUGE, a single fuel column (called a “patch”) is divided into seven homogenous burnup regions, as shown in Figure 2-10. These burnup regions are called “subcolumns”. Weighting factors already exist in the physics input database to account for the difference between the subcolumn boundaries and the actual fuel element boundary. GAUGE uses a one-third symmetrical reactor geometry model for the physics calculations as shown previously in Figure 2-8. Figure 2-10 shows this symmetrical layout and gives the column and subcolumn numbering scheme. The core is divided into two fuel segments, or batches denoted ‘A’ and ‘B’, indicating that half the core is removed during reloads. Note that segment ‘A’ is the first to be reloaded. When modeling the entire reactor on a subcolumn level, it is crucial to draw a detailed map for the code-user to follow and is shown in Figure 2-11. Note that this model is utilized in both two-dimensional and three-dimensional nuclear calculation methods, so Figure 2-11 contains critical information needed for all physics codes involved. Figure 2-11 represents the physics model only, which is a homogenized version of the actual physical core. For example, the yellow circles in the figure refer to the subcolumn regions which contain homogenized boron that mocks-up the borated region used in the permanent side reflector to shield the vessel. The location of these borated regions is illustrated in Figures 2-2 and 2-9. It should also be noted that the physics model shown in Figure 2-11 has hexagonal regions outside of the edge of the core barrel border, shown by the dashed circular line on the figure. These regions contain low density graphite to represent a void and are used in the DIF3D model to ensure that the calculations converge correctly to a solution. The ‘ring number’ and ‘hex number’ in Figure 2-11 are required by DIF3D in defining

region locations for hexagonal models (see 'hexes within same ring' to better understand.) Burnup time-step design consisted of an initial 0 Effective Full Power Days (EFPD), followed by 3 EFPD for xenon equilibrium, and a time step at every additional 10 cumulative EFPD from time 0.

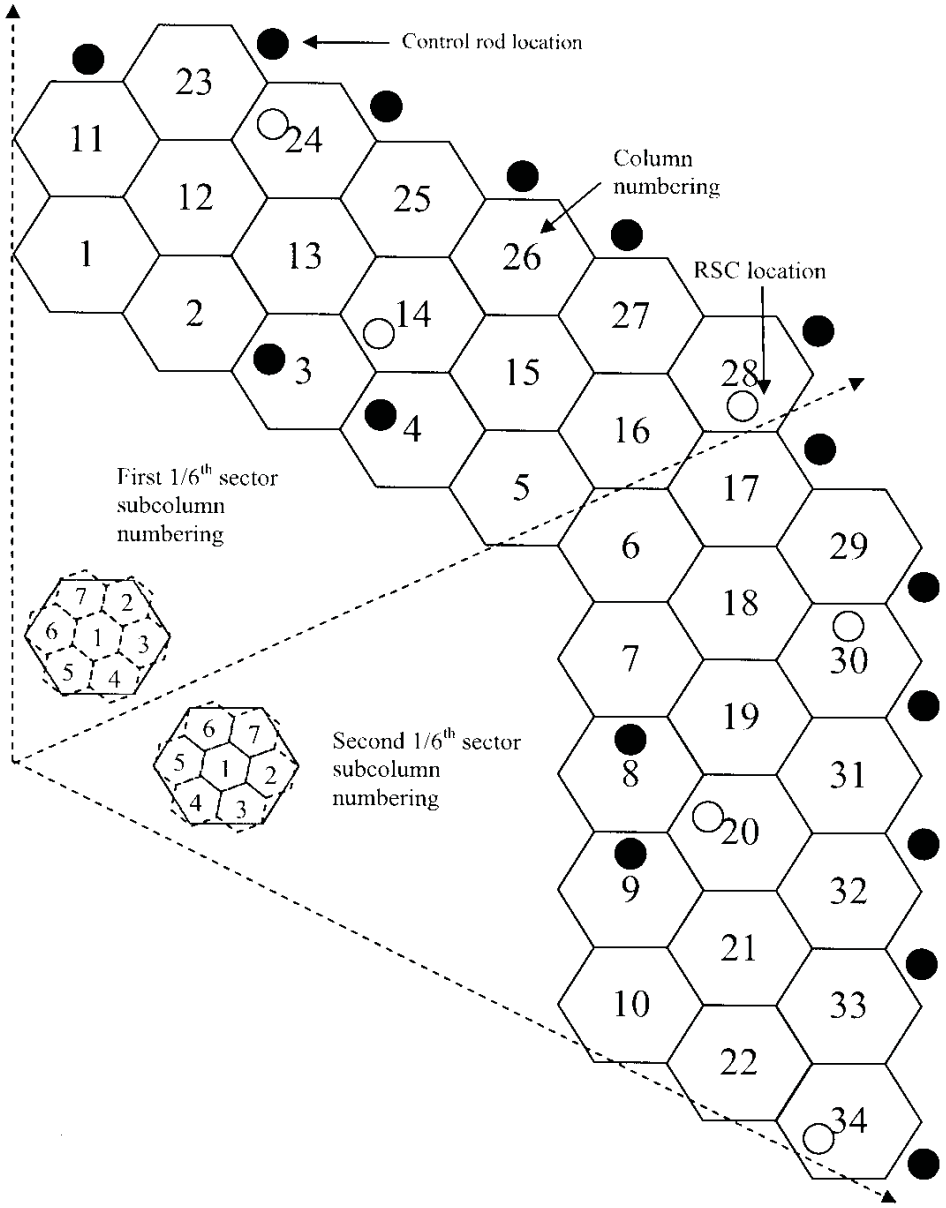

Figure 2-10. Diffusion Model Used for Subcolumn Depletion Calculations

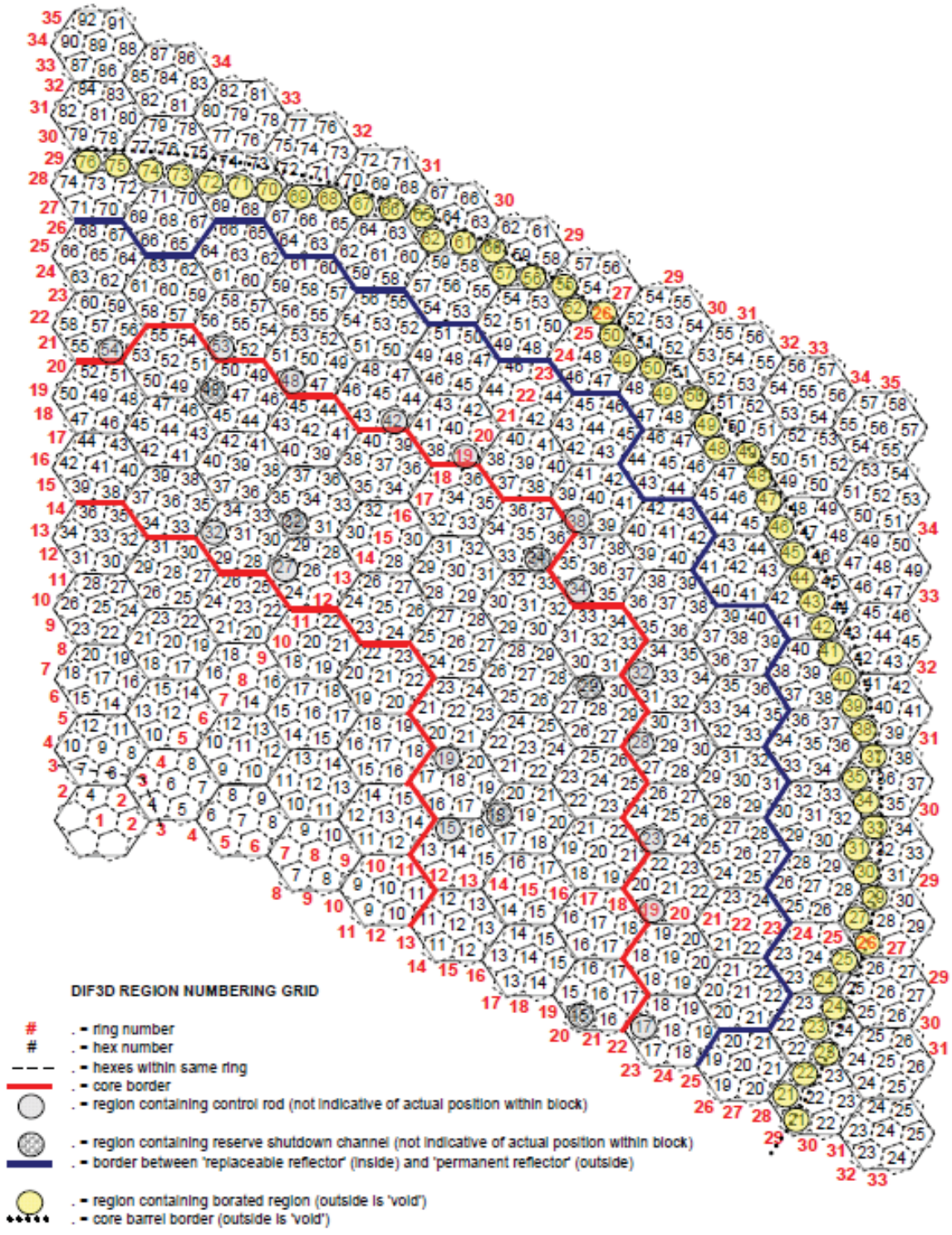

Figure 2-11. Radial subcolumn map design for entire one-third symmetrical reactor model

A critical feature GAUGE has is its ability to determine the operating control rod sequence during normal operation. Based on the user providing a desired K_{eff} range and the control rod bank sequence pattern, GAUGE will calculate which control rod banks are fully inserted, fully withdrawn, and which bank (if needed) is partially inserted. GAUGE calculates these positions at every burnup time-step.

Three-dimensional diffusion burnup calculations were performed with a combination of two codes: the commercial (Argonne National Laboratory) code DIF3D, Version 6.0 [Derstine 1984] and the GA code BURP [Sherman 1993]. DIF3D solves the multigroup diffusion theory eigenvalue, adjoint, fixed source and criticality problems in 1, 2, and 3 space dimensions for orthogonal (rectangular or cylindrical), triangular, and hexagonal geometries. The solution flux file from DIF3D is then used by BURP to perform nuclide depletion calculations. This cycle of calculations is then repeated at many time-steps to simulate reactor operation.

Similar to GAUGE, DIF3D uses the same depletion model and one-third symmetrical reactor geometry model previously shown in Figures 2-8, 2-10 and 2-11. The main difference is that the axial design of the reactor is also taken into account within DIF3D, and includes the top and bottom reflectors. In Phase 1, the axial extent of a DIF3D core region was over the length of a single fuel element. For Phase 2, the model was modified to include five axial nodes per fuel element for a finer axial resolution. The control rod bank insertion/withdrawal pattern determined by GAUGE as a function of burnup time-step is read into a curve-fit of the three-dimensional s-curve and used to build control rod position files for the BURP model. The control rod group withdrawal pattern is described in Section 2.1.7, and the control rod banks involved are identified in Figure 2-8.

The core physics methods used in the CPA have been described in detail in this section. Of necessity they involve some approximations in modeling the behavior of the core. Generally speaking, the approximations, which include the choice of the broad group cross section number and energy boundaries, the modeling of the TRISO fuel particles, and the simplified modeling of fission products, have been carefully developed for application to graphite-moderated, helium-cooled, reactor cores, and have been checked against critical experiments and operating reactor data to validate their accuracy and applicability.

A couple of additional approximations were used in the CPA. These included the use of a single set of broad group cross sections derived from a BOIC spectrum, the use of cross sections derived at a single core temperature, and the method for calculating control rod bank motion to maintain core criticality with burnup. These approximations were used in the CPA so that multiple design variations could be evaluated in a reasonable time, and because their use should give conservative results in terms of a slight underestimation of fuel cycle length, and

higher-than-actual power peaking results.

The effect of the use of a single broad group cross section set was evaluated during Phase 1 of the CPA by comparing the reactivity change with burnup over the initial core cycle using this set with the results of a calculation in which the cross sections were re-averaged at each time point. The reactivity behavior from the two calculations was almost identical, with the values based on the multiple cross section case being slightly higher throughout the cycle. In addition, an end-of-cycle k_{eff} of 1.02 was assumed in all 2D calculations and an EOC k_{eff} of 1.005 was assumed in all 3D calculations to conservatively account for this and other modeling approximations. The use of a single, core average, fuel temperature for generating cross sections will tend to overestimate power peaking compared to a more detailed model. This is because in a more detailed model where cross sections are generated at local temperatures the negative temperature coefficient (see Section 4.1.4) would reduce local fission density and hence local power peaking.

2.3 Fuel Performance/Fission Product Release Calculation Methods

This section provides an overview of the design methods used to predict fuel performance and fission product release from a prismatic core during normal operation. It also includes the proposed NGNP fuel performance requirements by which the adequacy of the various core designs can be judged.

2.3.1 Thermal Analysis Methods

The design methods for predicting the core temperature distributions during normal plant operation are presented in detail in [Shenoy 1974]. This methodology is utilized in both the POKE code [Kapernick 1993] and in SURVEY/THERM [Pfremmer 2002]. The requisite material property data are obtained from various GA design manuals, including the Fuel Design Data Manual [FDDM/F 1987] and the Graphite Design Data Manual [GDDM/A 1984] and standard engineering handbooks (e.g., for helium thermal properties, etc.).

The calculation of fuel temperatures from the core power distribution and coolant flow distribution is of fundamental importance to predicting fuel performance and fission product release. The dominant variables in determining the fuel temperatures were illustrated in a recent parametric study performed by GA and KAERI for the NGNP Project [Richards 2008b]. Figure 2-12 shows a typical radial temperature distribution in a fuel element from the fuel compact to the coolant and Figure 2-13 shows a typical axial temperature distribution. As illustrated in Figures 2-12 and 2-13 [Richards 2008b], the fuel temperatures at a given location in the core result from the addition of a number of temperature rises: (1) the temperature rise in the coolant from the sensible heat added as the coolant flow transverses the core; (2) the film

temperature rise from the flowing helium coolant to the surface of the coolant channels in the graphite fuel blocks (forced convection); (3) the temperature rise across the graphite web separating the coolant holes from the adjacent fuel holes (conduction); (4) the temperature rise across the small gap between the fuel hole and fuel compacts (conduction and radiation), and (5) the temperature rise from the fuel compact surface to the compact centerline. Both POKE and SURVEY/THERM perform a one-dimensional thermal analysis in the radial plane which is judged to be adequate for fuel performance and fission product release analyses.

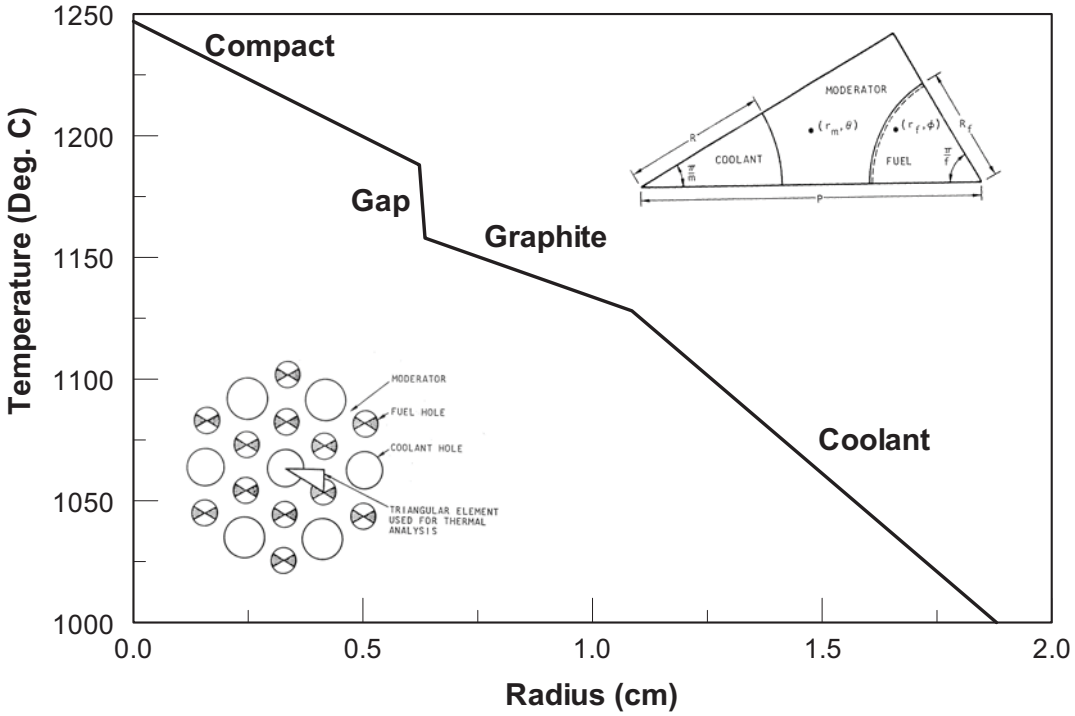

Figure 2-12. Typical Radial Temperature Distribution in Fuel Element

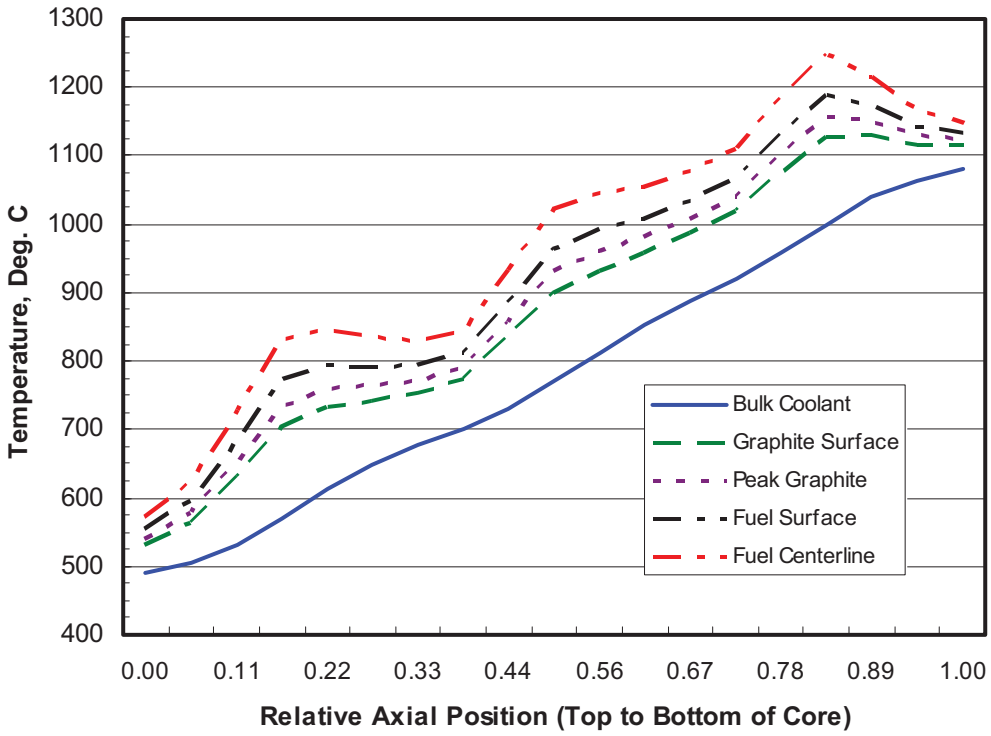

Figure 2-13. Typical Axial Temperature Distribution in Prismatic Core

The core design utilized in the GA/KAERI parametric study incorporated a fuel shuffling scheme that effectively reduced the radial peaking factors [Richard 2008a]. Consequently, peak fuel temperatures of 1250°C were predicted even with a reactor outlet helium temperature of 950°C. Presumably, the fuel shuffling schemes to be investigated during the remainder of this Phase 2 study will yield a similar benefit of reduced RPFs and the attendant lower peak fuel temperatures.

The axial temperature distributions in Figure 2-13 demonstrate why it is highly desirable for the power distribution to be skewed to the top of the core. At the bottom of block #2 ("Relative Axial Position" = 0.2), the coolant temperature is ~600°C, and the temperature rise from the coolant to the fuel compact centerline is ~250°C, resulting in a peak fuel temperature at that elevation of 850°C. However, in block #8 where the coolant temperature is 1000°C, this same 250°C temperature rise results in a peak fuel temperature of 1250°C. With the axial power distribution used to generate Figures 2-12 and 2-13, the largest contribution to peak fuel temperatures in blocks #4 through #10 is the temperature rise in the coolant channel to a given axial position.

2.3.1.1 Fuel Performance Analysis Methods

During the past four decades, a number of mechanisms have been identified - and quantified - which can compromise the capability of the coated fuel particles to retain radionuclides (i.e., functional failure of the coated particle). A considerable number of documents have been prepared on the topic of coated particle failure mechanisms. [TECDOC-978 1997] provides a good summary along with an extensive bibliography.

The reference GA component models and material property correlations are contained in the Fuel Design Data Manual [FDDM/F 1987]. FDDM/F has several notable limitations; in particular, it presents models and correlations along with extensive references, but it does not include the experimental data from which they were derived. In recognition of the above limitations, Martin of ORNL prepared a compilation in 1993 which collected the GA models and the supporting data base under a single cover [Martin 1993]. The component models in FDDM/F for predicting fuel failure and fission gas release are incorporated into the PERFOR module of the SURVEY code.

The following failure mechanisms have been identified as capable of causing partial or total failure of the TRISO coating system under irradiation and/or during postulated accidents; these mechanisms are shown schematically in Figure 2-14. Phenomenological performance models, typically inspired by first principles and correlated with experimental data, have been developed to model each of these mechanisms.

1. Coating damage during fuel manufacture, resulting in heavy metal contamination on coating surfaces and in the fuel compact matrix.
2. Pressure vessel failure of standard (“intact”) particles (i.e., particles without manufacturing defects).
3. Pressure vessel failure of particles with defective or missing coatings.
4. Irradiation induced failure of the OPyC coating;
5. Irradiation induced failure of the IPyC coating and potential SiC cracking;
6. Failure of the SiC coating due to kernel migration in the presence of a temperature gradient.
7. Failure of the SiC coating caused by fission product/SiC interactions.
8. Failure of the SiC coating by thermal decomposition.
9. Failure of the SiC coating due to heavy-metal dispersion in the IPyC coating.

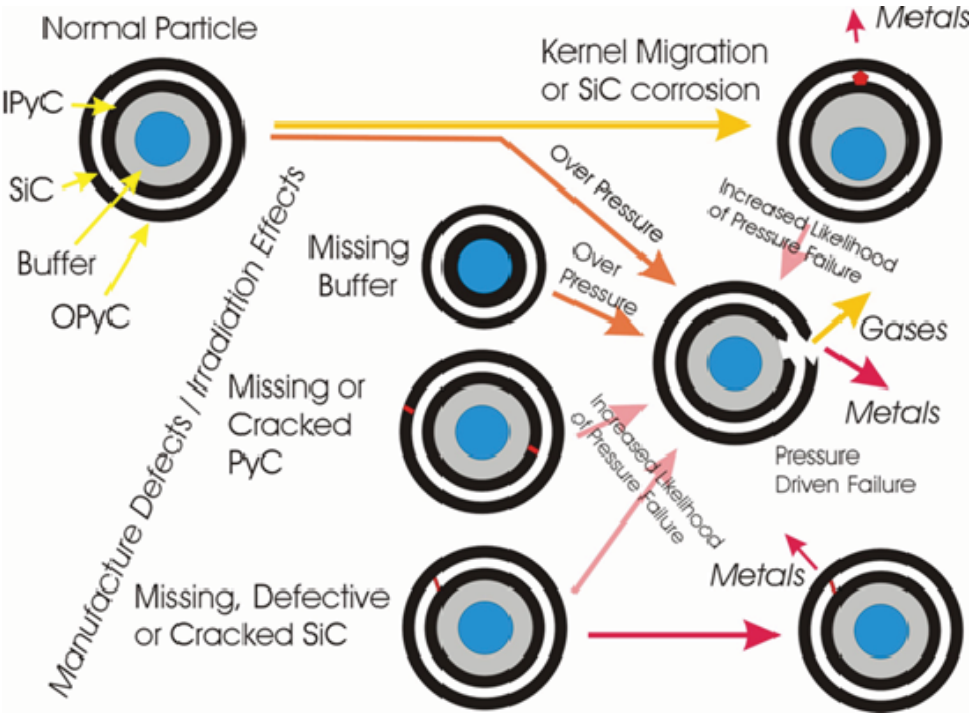

Figure 2-14. TRISO Particle Failure Mechanisms

The first mechanism listed above – as-manufactured heavy-metal contamination - is not an in service failure mechanism *per se* but rather an extreme case of as-manufactured coating defects whereby trace amounts of heavy metal (HM) are not encapsulated by a single intact coating layer (analogous to “tramp uranium” in LWR fuel). Modern fuel product specifications only allow small fractions of HM contamination (~10^{-5} is typical); nevertheless, it is an important source of fission product release.

2.3.2 Fission Product Release Analysis Methods

The two dominant sources of fission product release from the core are as-manufactured, heavy-metal contamination and failed particles. In addition, the volatile metals (e.g., Cs, Ag, Sr) can, at sufficiently high temperatures for sufficiently long times, diffuse through the SiC coating and be released from intact TRISO particles; however, diffusive release from intact particles during normal operation is only significant compared to other sources for silver (and tritium) release. Fission products resulting from fissions in HM contamination outside of the particles are obviously not attenuated by the kernels or coatings, nor are the fission products produced in the kernels of failed particles appreciably attenuated by the failed coatings. In these cases, the fission products must be controlled by limiting the respective sources and by the fuel-element graphite in the case of the fission metals and actinides.

Expressed in the simplest terms, the fractional release of a radionuclide from the core is given by the following relationship:

$$(f.r.)_{core} = \frac{C(f.r.)_c + F(f.r.)_F + [1-C-F](f.r.)_D}{AF_{graphite}} \quad (2\text{-}1)$$

where:

$(f.r.)_{core}$ = fractional release from core

C = heavy-metal contamination fraction

$(f.r.)_C$ = fractional release from contamination

F = failure fraction

$(f.r.)_F$ = fractional release from failed particles

$(f.r.)_D$ = fractional diffusive release from intact particles

$AF_{graphite}$ = graphite attenuation factor[7]

In reality, the problem of calculating the full-core fractional release is much more complicated than implied by Eqn. (2-1). For example, the fissile and fertile particle failure fractions are generally different and vary in space and time, the fractional releases from contamination and failed particles and graphite attenuation factors vary in space and time, and "partially" failed particles (i.e., particles with a failed SiC coating but with intact IPyC and/or OPyC coatings) must also be considered. Full-core computer codes are needed to keep track of all these effects; nevertheless, the results given by Eqn. (2-1) are quite intuitive. Fission gas release, which is expressed as a release rate-to-birth rate ratio (R/B), is calculated in SURVEY/PERFOR, and fission metal release is calculated with TRAFIC-FD.

The transport of radionuclides from the location of their birth through the various material regions of the core to their release into the helium coolant is a relatively complicated process. The principal steps and pathways are shown schematically in Figure 2-15. Also for certain classes of radionuclides, some steps are eliminated (e.g., noble gases are not diffusively released from intact TRISO particles, but noble gases are not significantly retarded by the compact matrix or fuel-element graphite).

[7] Graphite attenuation factor = fission product release from fuel compact/release into coolant.

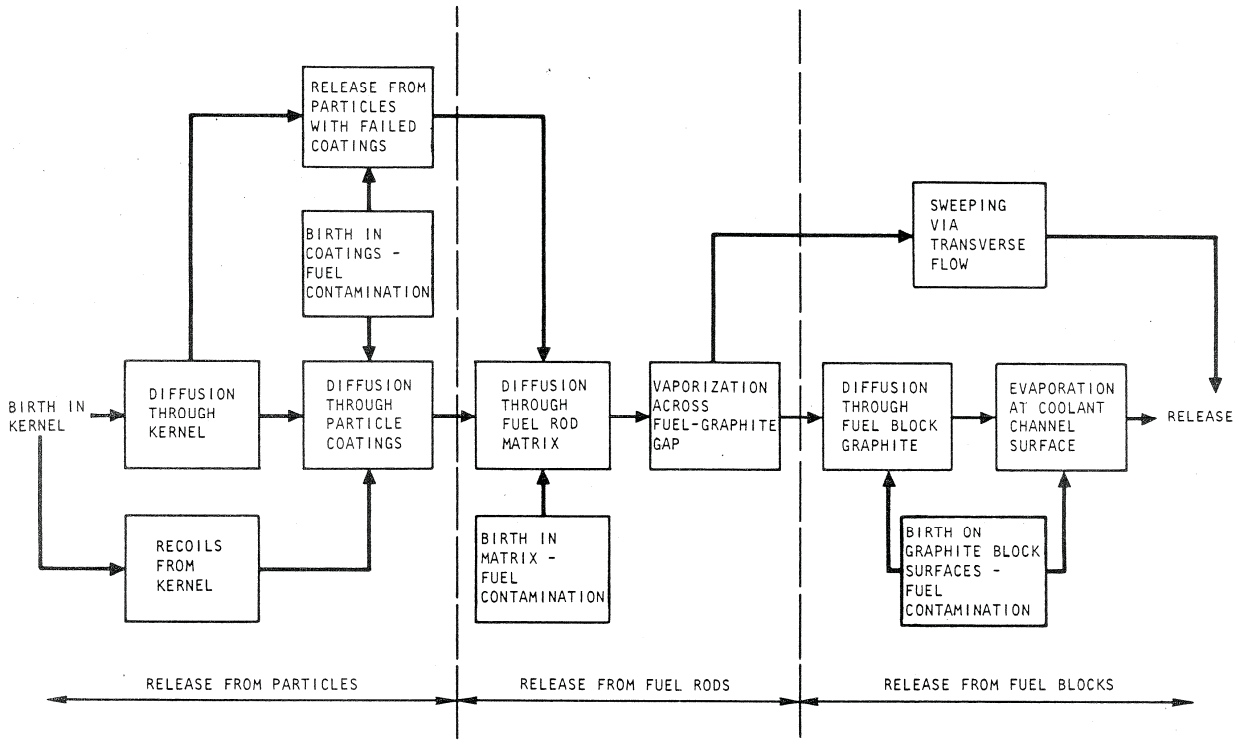

Figure 2-15. Principal Steps in Radionuclide Release from a Prismatic Core

As implied by Eqn. (2-1), radionuclide transport must be modeled in the fuel kernel, in the particle coatings, in fuel-compact matrix, and in the fuel-element graphite. While the actual radionuclide transport phenomena in an HTGR core are complex and remain incompletely characterized after four decades of modeling efforts, the basic approach remains unchanged; radionuclide transport is essentially treated as a transient solid-state diffusion problem with various modifications and/or additions to account for the effects of irradiation and heterogeneities in the core materials.

2.3.3 Provisional NGNP Fuel Requirements

Quantitative figures-of-merit are needed to judge the adequacy of the various core designs evaluated under the current Phase 2 workscope. GA has long cautioned that the often cited "limits" on maximum fuel temperature during normal operation and core heatup accidents are simply rules-of-thumb that are insufficient by themselves. The ultimate figure-of-merit for assessing fuel performance is fission product release. Provisional fission product release limits and the attendant fuel failure and as-manufactured fuel quality for the NGNP were first proposed in 2008 [Hanson 2008]. The as-manufactured fuel quality limits proposed therein were consistent with those adopted earlier for the 600-MWt commercial GT-MHR [Munoz 1994].

These limits were recently determined to be appropriate provisional limits for the prismatic reactor design evaluated in the CPA [Hanson 2009]. The various limits are listed in Table 2-10.

Table 2-10. Provisional NGNP Fuel Requirements

Parameter	NGNP – 900°C Core Outlet Temperature	
	"Maximum Expected"	"Design"
As-Manufactured Fuel Quality		
HM contamination	$\leq 1.0 \times 10^{-5}$	$\leq 2.0 \times 10^{-5}$
Missing or defective buffer	$\leq 1.0 \times 10^{-5}$	$\leq 2.0 \times 10^{-5}$
Defective SiC	$\leq 5.0 \times 10^{-5}$	$\leq 1.0 \times 10^{-4}$
Missing or defective IPyC	$\leq 4.0 \times 10^{-5}$	$\leq 1.0 \times 10^{-4}$
In-Service Fuel Failure (FGAS)		
Normal operation	$\leq 5.0 \times 10^{-5}$	$\leq 2.0 \times 10^{-4}$
Core heatup accidents	$[\leq 1.5 \times 10^{-4}]$	$[\leq 6.0 \times 10^{-4}]$
Core Release Limits for Gases		
Kr-88 R/B	$\leq 8.3 \times 10^{-7}$	$\leq 3.3 \times 10^{-6}$
I-131 R/B	$\leq 2.0 \times 10^{-6}$	$\leq 8.0 \times 10^{-6}$
Core Release Limits for Metals		
Cs-137 fractional release	$\leq 1.0 \times 10^{-5}$	$\leq 1.0 \times 10^{-4}$
Ag-110m fractional release	$\leq 5.0 \times 10^{-4}$	$\leq 5.0 \times 10^{-3}$

For previous gas-cooled reactor designs, the requirements for as-manufactured quality and in-service performance of coated-particle fuel have been based on a two-tier set of radionuclide design criteria (allowable core release rates), referred to as the "Design" and "Maximum Expected" criteria. The "Design" criteria represent upper limits for all normal operating conditions and any off-normal events that are expected to occur during operation of the plant. These criteria are used when assessing the impact of plant operation on public safety, to size helium purification and radwaste systems, and to design plant hardware and shielding. The "Design" criteria account for uncertainties in the design methods and supporting data, and represent a design margin over the "Maximum Expected" criteria, which are used for applications where "best-estimate" results are appropriate, including developing component removal and maintenance procedures. The fuel and reactor core are to be designed such that there is at least a 50% probability that the radionuclide releases will be less than the "Maximum

Expected" criteria, and at least a 95% probability that the releases will be less than the "Design" criteria. The "Maximum Expected" criteria are the relevant figures-of-merit for the CPA because the core performance results are best-estimate predictions.

2.4 Computer Code Verification

The GA physics codes used for core design have been formally verified, but have been run previously on a DecAlpha UNIX platform, which is no longer available. Consequently, it was necessary to port the codes from the DecAlpha UNIX platform to the SGI ALTIX supercomputer platform and to re-verify the codes for running on the new platform. During Phase 1, the following physics codes were verified for running on the SGI ALTIX supercomputer:

- MICROX
- GAUGE
- BURP
- DIF3D
- SORT3D

The GA codes used for the fuel performance and fission product release and transport analysis were also ported to the SGI ALTIX supercomputer and verified for running on that computing platform. These codes include:

- SURVEY
- TRAFIC-FD
- POKE
- PISA
- SORS
- TAC2D[8]

With the exception of SURVEY and POKE, the codes in the above lists were verified for running on the SGI ALTIX by comparing the results obtained on the SGI ALTIX with results obtained from a verified version of the code that was run previously on the GA DecAlpha computer. A report was prepared to document the verification of each of the codes verified in this manner. A summary of the Phase 1 code verification task is provided in [GA 2009a] and references to the code verification reports are provided therein.

The SURVEY code was also verified, but this required a substantially greater effort and a

[8] TAC2D was previously ported to the SGI ALTIX and verified for running on that platform [DelBene 2000]; consequently, platform verification of TAC2D was not necessary as part of the CPA

different approach than used for the other codes because the following major modifications to the code were necessary to make it useable for the CPA.

- The code was converted to Fortran 90, and a generalized dimensioning protocol was introduced
- The POKE code, which calculates the coolant flow distribution in the core, was incorporated into SURVEY
- Fuel performance models were developed and incorporated for the natural-enriched UCO TRISO fertile particle
- The number of coolant and fuel holes for each subcolumn (seven subcolumns per fuel element) was supplied to SURVEY/THERM from SORT3D in order to refine the calculated coolant flow rates and fuel temperatures
- SURVEY was re-dimensioned and re-compiled to accommodate a finer axial mesh (five axial points per fuel block rather than one point per fuel block)

These modifications are summarized below and are discussed in more detail in Section 4.2.2 of [GA 2009b].

Because there is no previously verified two-particle test case available for running with the new modified version of SURVEY, SURVEY was verified by comparison with analogous calculations using other computer codes. The SURVEY/THERM module, which calculates coolant flow rates and fuel temperatures, was verified by comparison with the POKE code. The SURVEY/PERFOR module, which calculates fuel particle performance and fission gas release, was verified by comparison with the CAPPER code, a local-point code that was developed to analyze fuel irradiation capsules. Both SURVEY/PERFOR and CAPPER contain the same fuel performance and fission gas release component models from the GA Fuel Design Data Manual, Issue F (FDDM/F).

The methodology used to verify the modified SURVEY code is summarized in [GA 2009b] and is fully documented in the SURVEY code verification report [Crozier 2009]. The agreement between the SURVEY results and the results obtained with POKE and CAPPER was judged to be sufficiently good to warrant a conclusion that the current modified version of SURVEY has been verified and is suitable for use in the CPA.

3 BINARY-FUEL-PARTICLE CORE DESIGN

A series of core design iterations were performed in the first part of Phase 2 to optimize the initial binary-fuel-particle core physics design developed in Phase 1. In all, 12 design iterations were performed. The details of this work are described in [GA 2009b] and [Ellis 2009b] so only a brief summary is provided herein.

3.1 Core Physics Analysis

Design Case 7.9 is considered the best binary-fuel-particle core design that was achieved within the PF limits, cycle-length requirements, and time constraints of the CPA. Case 7.9 has a maximum PF of 38.5% and 6.1% of the total core fuel compact volume is between 35% and 38.5%. This is within the maximum PF limit of 40%, but slightly exceeds the limit of 5% on the total core fuel compact volume having a PF greater than 35%. The minimum fuel cycle length goal of 540 EFPD (startup to shutdown) was achieved for all cycles except cycle 2, which ran for 530 EFPD.

The fuel cycle for the binary-fuel-particle core design is summarized in Table 3-1. The optimization strategy used for the fuel cycle keeps the fissile and fertile loadings constant for every reload, but allows the cycle time to vary to obtain the required K_{eff} at the end of each cycle. The effective core enrichments for the initial core and reload cycles are 10.9% and 15.5%, respectively. For the initial cycle, Segments A and B contain 0.303 kg and 1.691 kg of FBP, respectively.

Table 3-1. Fuel Cycle Design

	Cycle Time		Fuel Loading (kg)		FBP Loading (kg)	EOC GAUGE K_{eff}
Reload	EFPD	Months	LEU	NU		
0	580	19.3	3457.83	3006.821	1.994	1.021
1	530	17.7	2132.754	628.017	1.5	1.02
2	540	18	2132.754	628.017	1.5	1.022
3	540	18	2132.754	628.017	1.5	1.02
Equilibrium	540	18	2132.754	628.017	1.5	1.021

The fuel burnup in each cycle is given in Table 3-2 in megawatt-days per initial metric ton (MWd/MT) of fissile plus fertile uranium in each reload segment. The denominator term in the calculation of the fissions per initial metal atom (FIMA) includes all heavy metal atoms in the reload segment, and was taken from SURVEY output. The denominator term in the calculation

of the fissions per initial fissile atom (FIFA) includes all U-235 atoms in the reload segment.

Table 3-2. Discharge Fuel Burnup for Each Cycle

Reload	EFPD	Burnup (MWd/MT)	Average				Peak	
			LEU		NU		LEU	NU
			FIMA	FIFA	FIMA	FIFA	FIMA	FIMA
0	580	53,831	0.095	0.474	0.019	2.702	0.148	0.028
1	530	115,185	0.158	0.789	0.046	6.393	0.202	0.063
2	540	117,359	0.153	0.764	0.044	6.045	0.196	0.058
3	540	117,359	0.154	0.771	0.044	6.176	0.197	0.058
Equilibrium	540	117,359	0.152	0.762	0.044	6.057	0.197	0.059

Table 3-2 shows that the average FIMA in the fissile particles in the equilibrium cycle is 15.2% and the peak FIMA in the fissile particles in the equilibrium cycle is 19.7%. The peak burnup is about 20.2% for the fissile particle and 6.3% for the fertile particle in Cycle 1, which are less than the design burnup limits of 26% and 7%, respectively. The peak fast fluence for design Case 7.9 is about 4.2×10^{25} n/m^2 (E >0.18 Mev), which is less than the design limit of $\leq 5 \times 10^{25}$ n/m^2.

One additional case (Case 7.10) was run specifically to investigate the potential to improve the thermal and fuel performance characteristics of the design by loosening the PF constraints. In this case, the axial power distribution was more strongly tilted toward the top of the core by moving fuel from the bottom two layers of blocks to the top two layers of blocks. The fuel redistribution resulted in a 45.5% PF in the top two layers. This case was run with the coarse-axial-mesh model because of the much-shorter computing time for this model relative to the fine-axial-mesh model. The fuel zoning change resulted in a modest reduction in power peaking at the location of the maximum fuel temperature, reductions in the maximum fuel temperature and maximum time-average fuel temperature, and reduced SiC failure and exposed kernel fractions relative to the other cases run with the course axial mesh. Based on the results for Cases 7.7 and 7.9, which were run using the fine-axial-mesh model, it is anticipated that the Case 7.10 results would be significantly improved if this case were run with the fine-axial-mesh model. The results for Case 7.10 suggest that the thermal and fuel performance of the design can likely be somewhat improved relative to Case 7.9 by pushing more power to the top of the core and allowing the maximum PF to increase up to at least 45%.

3.2 Performance Assessment of Phase 2 Binary-Fuel-Particle Core Design (Case 7.9)

The modified SURVEY code (version SURVEY_August_2009) was run for design Case 7.9 using the binary input data file generated by SORT3D from DIF3D output. All of the spatial and temporal data generated by DIF3D was processed by SORT3D and utilized by SURVEY. Using the SURVEY output results as input, TRAFIC-FD was used to calculate Cs-137 and Ag-110m release.

Core-volume-temperature-distribution plots for Case 7.9 are presented in [GA 2009b] and are therefore not presented herein. However, given that fuel failure and fission gas release are strongly dependent on temperature and that limiting fuel temperatures is therefore a key to achieving an acceptable core design, the fuel temperatures for the hottest 5% of the core are of particular interest. Table 3-3 summarizes this information for design Case 7.9.

Table 3-3. Maximum Fuel Temperatures in Hottest 5% Core Volume for Case 7.9

Segment & Fuel Load	Maximum Temperature (°C)	Temperature Range for Hottest 5% of Core (°C)
Segment 1		
Fuel Load 1	1254	~1160 – 1254
Fuel Load 2	1488	~1350 – 1488
Fuel Load 3	1456	~1330 – 1456
Segment 2		
Fuel Load 1	1341	~1200 – 1341
Fuel Load 2	1456	~1290 – 1456
Fuel Load 3	1419	~1280 – 1419

As shown in Table 3-3, the maximum calculated fuel temperature is 1488°C, and about 5% of the fuel volume is operating at temperatures in excess of about 1300°C in fuel loads 2 and 3 of both Segments 1 and 2. The time-averaged maximum fuel temperature for Case 7.9 is 1222°C in segment 1, fuel load 2.[9] This is well below the design guideline of 1250°C that GA has used for previous MHR core designs.

The highest fuel temperatures tend to occur in subcolumns in the bottom fuel elements of columns that are adjacent to the outer reflector and also adjacent to a control rod. These subcolumns are called buffered subcolumns. The high temperatures in these subcolumns

[9] The time-averaged maximum fuel temperature for segment 2, fuel load 3 is reported as 1249°C in report 911176, but this time-averaged maximum fuel temperature is for only one cycle rather than 2 (because the DIF3D depletion analysis was terminated after 5 cycles.

suggest that it would be desirable to further reduce the radial power peaking in these areas. Reducing the heavy-metal loadings in the four fuel rows adjacent to fuel element-reflector interface in these buffered subcolumns, especially in the bottom axial fuel zone, should also have a beneficial effect in reducing maximum fuel temperatures. However, either of these changes would likely result in some increase in the maximum PFs. Also, as discussed in Section 3.1, the results for Case 7.10 suggest that the thermal and fuel performance of the physics design can likely be somewhat improved relative to Case 7.9 by pushing more power to the top of the core and allowing the maximum PF to increase up to at least 45%.

Although fuel temperatures are important with respect to fuel performance, limits on time-average fuel temperature and/or maximum fuel temperature are not sufficient figures-of-merit for a core design because of the influence of other parameters (e.g., burnup, fast fluence, time at temperature, etc.) on fuel performance. Rather, the ultimate figure-of-merit for assessing fuel performance is fission product release. Table 3-4 compares the results for Case 7.9 with the provisional fuel failure limits and fission product release limits given in Table 2-10. The "Maximum Expected" criteria are the relevant figures-of-merit because the core performance results are best-estimate predictions.

Table 3-4. Comparison of Case 7.9 Results with Provisional Requirements

Parameter	"Maximum Expected" Limit	"Design" Limit	Case 7.9
Fuel failure during normal operation (exposed kernel fraction)	$\leq 5.0 \times 10^{-5}$	$\leq 2.0 \times 10^{-4}$	1.3×10^{-5} (fissile) 4.4×10^{-6} (fertile)
Kr-88 R/B	$\leq 8.3 \times 10^{-7}$	$\leq 3.3 \times 10^{-6}$	9.2×10^{-7}
I-131 R/B	$\leq 2.0 \times 10^{-6}$	$\leq 8.0 \times 10^{-6}$	2.2×10^{-6}
Cs-137 fractional release	$\leq 1.0 \times 10^{-5}$	$\leq 1.0 \times 10^{-4}$	4.2×10^{-5}
Ag-110m fractional release	$\leq 5.0 \times 10^{-4}$	$\leq 5.0 \times 10^{-3}$	1.3×10^{-3}

The predicted fuel performance for case 7.9 is quite good considering the rather high fuel temperatures that are inherent in a reactor operating with a nominal reactor outlet helium temperature of 900°C. The total core exposed kernel fraction is 1.3×10^{-5} for fissile fuel particles and 4.4×10^{-6} for fertile particles, both of which are well below the in-service fuel failure limit of 5×10^{-5}. The dominant sources of exposed kernels are: (1) pressure vessel (PV) failure of fuel particles with missing buffer layers, (2) PV failure of fuel particles with defective or failed OPyC layers, and (3) OPyC failure on fuel particles with defective or failed SiC layers. The

contribution from PV failure of standard fuel particles is negligible. Exposed kernels result in release of both fission gases and fission metals.

The maximum SiC defect fractions are 1.0 x 10^{-4} and 6.4 x 10^{-5} for the fissile and fertile particles, respectively, with as-manufactured SiC defects contributing about 50% of the fissile particle total[10] The predicted in-service SiC failure fraction for the fissile particles is about two-times higher than for the fertile particles because the FP/SiC corrosion model has weak burnup dependence. The amount of in-service SiC failure peaks at the end of cycle 3 and is less than the as-manufactured SiC defect fraction in cycles 4 and 5. The predicted SiC failure is dominated by fission product (FP)/SiC reactions. SiC failure due to kernel migration and SiC thermal decomposition are negligible. This FP/SiC corrosion failure, which is strongly temperature dependent, is a consequence of the excessively-high fuel temperatures that occur in a small volume of the core. This SiC failure primarily results in fission metal release, especially the release of Cs isotopes. To a lesser degree, SiC failure also contributes to the exposed kernel fraction to the extent that OPyC layers are initially defective and/or fail in service.

The release-rate to-birth-rate (R/B) ratios (equivalent to the fractional release at steady-state) for 2.8-hr Kr-88 and 8-day I-131 were also calculated by SURVEY/PERFOR using the FDDM/F fission gas release models. These two radionuclides were chosen because they are dominant contributors to off-site accident doses. The R/B ratios were conservatively calculated using the models for hydrolyzed UCO fuel because the GA and AREVA preferred candidate prismatic NGNP configurations currently include a stream generator in the primary circuit. The predicted maximum core-average R/B values are 9.2 x 10^{-7} for Kr-88 and 2.2 x 10^{-6} for I-131. Because the predicted exposed kernel fraction is very low, the predicted fission gas release is completely dominated by the contribution from heavy-metal contamination in the as-manufactured fuel, which is assumed to be present at the specification limit of 1 x 10^{-5}. Nevertheless, the peak predicted R/Bs are at the provisional limits because of the high average fuel temperatures that are practically unavoidable with a 900°C reactor outlet helium temperature. The most effective way of reducing these R/Bs would be to tighten the specification on heavy-metal contamination.

The SURVEY results for Case 7.9 were supplied as input to the TRAFIC-FD code, which was used to calculate releases of 250-day Ag-110m and 30.1-year Cs-137. The material property data (e.g., FP diffusivities in SiC coatings) required as input to TRAFIC-FD was taken from FDDM/F with two important exceptions. First, the KFA correlation for Ag diffusion in SiC coatings [Moormann 1987], [TECDOC 1997] was used instead of the FDDM/F correlation as recommended by a critical review of the Ag transport data [Acharya 1994]. Use of the FDDM/F

[10] The fraction of as-manufactured defective particles present in the core is conservatively assumed to be at the specification limit for each defect type specified in the Fuel Product Specification.

correlation would likely increase the calculated Ag-110m fractional release by a factor of five or more relative to the values reported herein based upon previous core analysis [PC-MHR 1994]. Secondly, no credit was taken for Cs retention in exposed kernels. The FDDM/F correlation for Cs diffusion in UCO kernels has an extremely large burnup dependence (i.e., FIMA to the fourth power]. This large burnup dependence for UCO kernels was inferred from the observed burnup dependence for Cs diffusion in ThO_2 kernels in the 1 - 6% FIMA range [Martin 1993]. This FDDM/F correlation was shown to grossly underpredict Cs release from UCO kernels at low burnups (2.5% FIMA) in the COMEDIE BD-1 test [Medwid 1993]; consequently, its use is not considered justified. An alternative would have been to use the German correlation for Cs diffusivity in LEU UO_2 which has no burnup dependence; however, this correlation would not necessarily be conservative for burnups greater than about 10% FIMA.

The predicted cumulative fractional release[11] of Ag-110m into the coolant is shown in Figure 3-1. Very little Ag-110m is released from the fuel particles during the first cycle because the SiC failure fraction and exposed kernel fraction are low, and the Ag-110m diffusing through the SiC layers of intact TRISO particles has not yet broken through. However, diffusive release of Ag-110m from intact TRISO particles becomes dominant in cycle 2 and remains dominant in subsequent cycles. The cumulative fractional release of Ag-110m peaks at ~1.3×10^{-3} at the end of cycle 2, and then decreases, but remains above ~5×10^{-4} throughout the subsequent cycles. Nearly all of the Ag-110m that escapes from the fuel particles is released into the coolant because there is minimal hold up of Ag-110m by the fuel compact matrix and the fuel element graphite. The predicted maximum cumulative fractional release of Ag-110m exceeds the limit of 5×10^{-4} by about a factor of three at the end of cycle 2, but is close to this limit in subsequent cycles.

The predicted cumulative fractional release of Cs-137 is shown in Figure 3-2. The predicted behavior of Cs-137 is similar to, but somewhat different than that of Ag-110m because its half life is much longer (30.1 years vs. 0.68 year for Ag-110m) and the Cs-137 release model in

[11] The cumulative fractional release of Ag-110m at a given time point is defined as the cumulative release into the helium coolant from time zero up to that time point divided by the cumulative birth of Ag-110m in the core from time zero up to that time point, with both the releases and bred inventories corrected for decay.

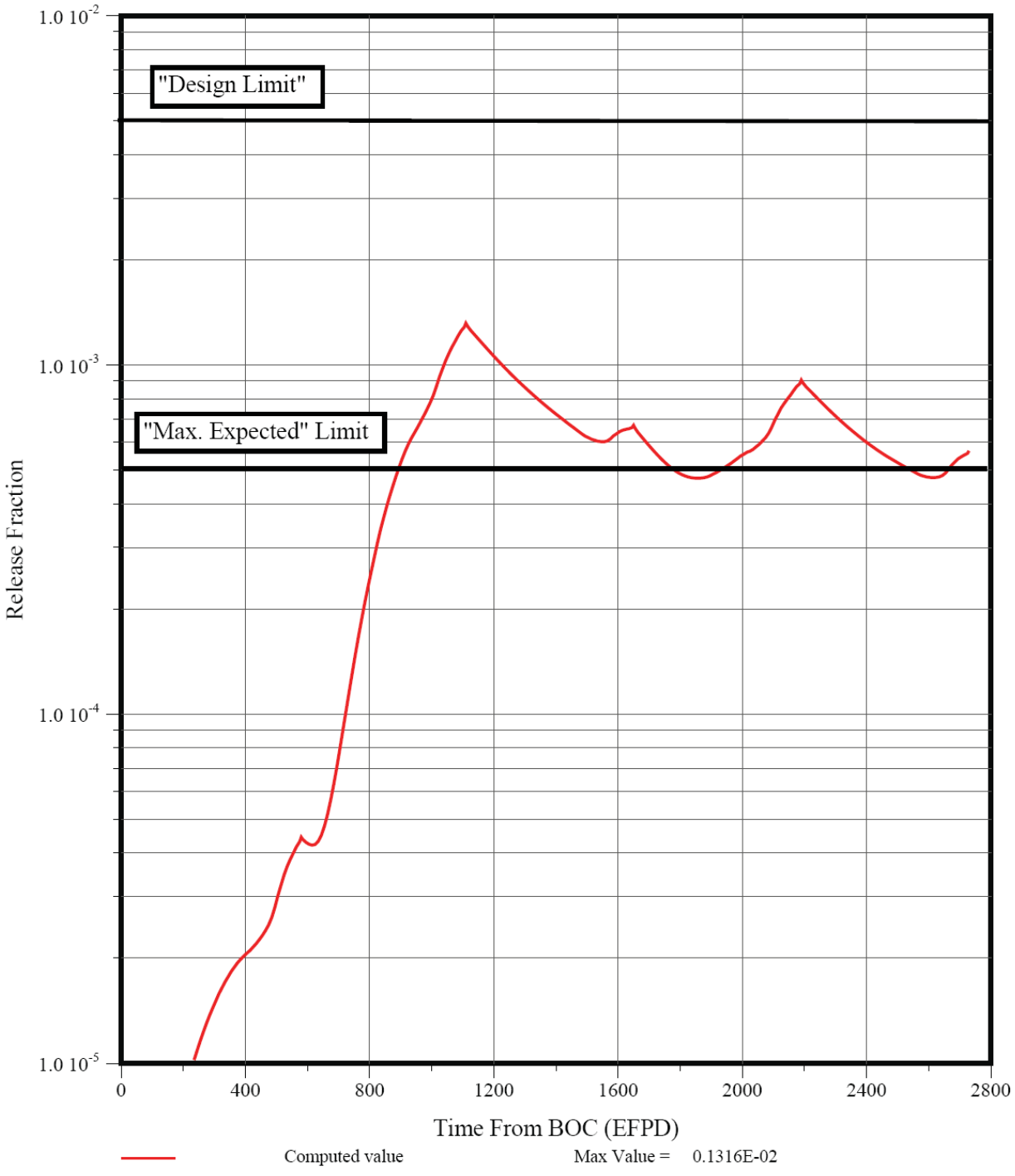

Figure 3-1. Cumulative Fractional Release of Ag-110m (Case 7.9)

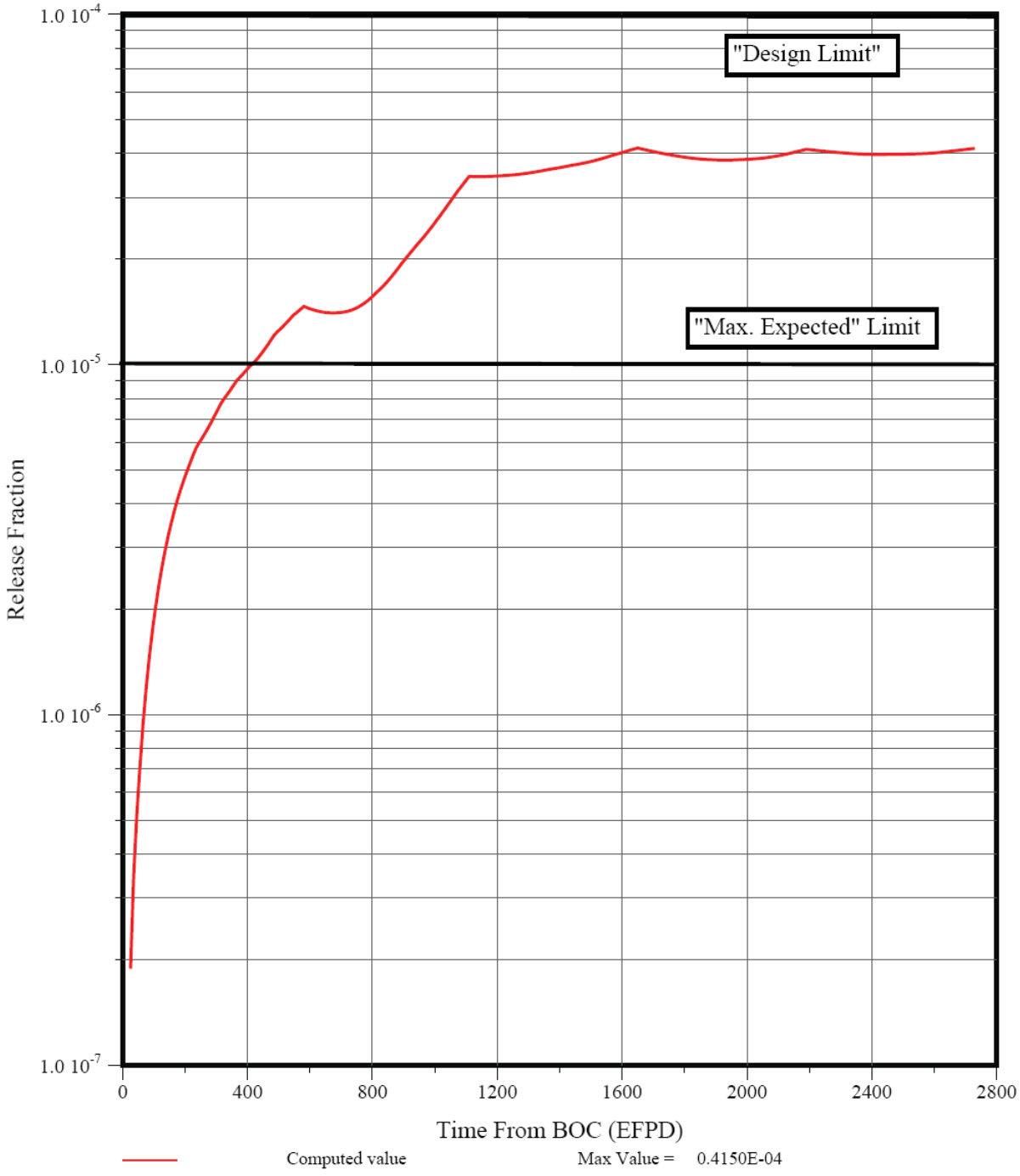

Figure 3-2. Cumulative Fractional Release of Cs-137 (Case 7.9)

FDDM/F does not include diffusive release from intact TRISO particles. There is also some holdup of Cs-137 by the fuel compact matrix and the graphite. Like the Ag-110m release fraction, the cumulative Cs-137 release fraction peaks at the end of cycle 2, but unlike the Ag-110m release fraction, the Cs-137 release fraction remains relatively constant throughout the subsequent cycles. The peak cumulative fractional release of Cs-137 exceeds the limit of 1 x 10^{-4} by about a factor of four.

The excessive localized, but short-term temperatures (see Table 3-3) calculated for Case 7.9 (and all other binary-fuel-particle core design cases) at the bottom of the core in subcolumns adjacent to control rods are the result of fission density spikes caused by large incremental control rod movements associated with the 10-day time steps used in DIF3D. Based on the assumption that these very-high temperatures are responsible for much of the predicted in-pile SiC failure and resultant Cs-137 release, and at least some of the Ag-110m release; an effort was made to determine a means of reducing the impact of these control rod movements.

The first attempt to achieve this objective (Case 7.9.1) was not effective [GA 2009b]. Subsequent to issuance of [GA 2009b], Case 7.9.4 was developed and run over the initial core and cycles 2 and 3 as a further effort to eliminate the fission density spikes. In this design iteration, the Keff "bandwidth" in the GAUGE calculation to determine control rod bank position was reduced to 0.00002 ΔK_{eff} in each cycle, which is the minimum allowed by the code. The very-tight bandwidth required a considerable increase in calculation time. Next the time points at which a fully inserted control bank withdrawal was started were selected in each of the three cycles, and the burnup calculation time step at, and immediately after that point, was reduced first to fit into a standard time point and then to 1-day intervals over about a 10-day period. The intent was to minimize the size of the axial control bank motion in these 10-day burnup intervals when a rod bank was first being withdrawn from the fully-inserted position.

The results are summarized in Table 3-5, which compares the change in rod bank position as a fraction of axial block distance over the short time-step intervals for the three cycles. The results show that the change in rod bank motion is considerably reduced when both the allowable change in reactivity and the time step are reduced; and the rod motion is much smoother over the corresponding full 10-day time period. However, Case 7.9.4 did not provide the anticipated improvement. The maximum fuel temperature decreased only from 1488°C to 1447°C and there was essentially no change in the in-service SiC failure fraction or in the Ag-110m and Cs-137 cumulative release fractions.

Table 3-5. Comparison of Control Rod Bank Withdrawals, Case 7.9.1, Cycles 1 through 3

Cycle 1 (Keff band = 0.00002)			Cycle 2 (Keff band = 0.00002)			Cycle 3 (Keff band = 0.00002)		
Time step, days	Axial Bank Change, Block.Fraction	No of Rod Banks.Fractions Inserted	Time step, days	Axial Bank Change, Block.Fraction	No of Rod Banks.Fractions Inserted	Time step, days	Axial Bank Change, Block.Fraction	No of Rod Banks.Fractions Inserted
1	-0.4	8.0	6	-0.20	6	9	-0.20	6
1	-0.4	7.96	1	0.00	5.98	1	-0.20	5.98
1	-0.6	7.9	1	-0.60	5.98	1	-0.40	5.96
1	-0.6	7.84	1	-0.60	5.92	1	-0.40	5.92
1	-0.4	7.8	1	-0.60	5.86	1	-0.20	5.88
1	-0.4	7.76	1	-0.60	5.8	1	-0.20	5.86
1	-0.4	7.72	1	-0.40	5.74	1	-0.40	5.84
1	-0.4	7.0	2	-0.2	5	9	-0.2	5
1	-0.2	6.98	1	-0.2	4.98	1	-0.4	4.98
1	-1.0	6.88	1	-0.8	4.96	1	-1	4.94
1	-1.0	6.78	1	-0.8	4.88	1	-0.8	4.84
1	-0.8	6.7	1	-0.6	4.8	1	-0.6	4.76
1	-0.6	6.64	1	-0.4	4.74	1	-0.6	4.7
1	-0.4	6.6	1	-0.4	4.7	1	-0.4	4.64
1	-0.6	6.0	3	-0.2	4	1	0	4
1	-0.4	5.96	1	-0.8	3.98	1	-1	4
1	-0.8	5.88	1	-1	3.9	1	-1	3.9
1	-0.6	5.82	1	-1	3.8	1	-0.8	3.8
1	-0.6	5.76	1	-0.6	3.7	1	-0.8	3.72
1	-0.6	5.7	1	-0.6	3.64	1	-0.6	3.64
1	-0.4	5.66	1	-0.4	3.58			
1	-0.4	5.0	1	0	3	1	0	3
1	-0.6	4.94	1	-0.4	3	1	-0.4	3
1	-1.0	4.84	1	-1	2.96	1	-0.8	2.96
1	-1.0	4.74	1	-0.8	2.86	1	-0.4	2.88
1	-0.6	4.68	1	-0.6	2.78	1	-0.6	2.84
1	-0.6	4.62	1	-0.6	2.72	1	-0.4	2.78
1	-0.4	4.58	1	-0.6	2.66			
1	-0.2	4.0	2	-0.2	2	7	-0.2	2
1	-0.8	3.92	1	0	1.98	1	0	1.98
1	-1.2	3.8	1	-1	1.98	1	-0.6	1.98
1	-1.0	3.7	1	-0.8	1.88	1	-1	1.92
1	-0.6	3.64	1	-0.8	1.8	1	-0.8	1.82
1	-0.6	3.58	1	-0.6	1.72	1	-0.8	1.74
1	-0.6	3.52	1	-0.4	1.66	1	-0.6	1.66
1	-0.4	3.0	1	-0.6	1	1	0	1
1	-0.6	2.94	1	-0.6	0.94	1	-2.2	1
1	-0.8	2.86	1	-1.2	0.88	1	-1.2	0.78
1	-0.6	2.8	1	-1	0.76	1	-1	0.66
1	-0.4	2.76	1	-0.8	0.66	1	-0.8	0.56
1	-0.4	2.72	1	-0.8	0.58	1	-0.6	0.48
1	-0.6	2.66	1	-0.4	0.5			

To fully resolve the “problem” would require a combination of the smaller allowed variation in the calculated K_{eff} from time step to time step over all cycles, and the use of even smaller time step intervals where necessary to minimize the size of the control bank motion. In turn, this would require considerable iteration between the 2D and 3D burnup models, and perhaps the use of separately generated control rod bank worth curves for each operating condition during each cycle. There was insufficient time available to go to this level of detail in the CPA. However, based on the results for Case 7.9.4 it doesn’t appear likely that these efforts would have a significant impact on predicted fuel failure and fission product release even if they are effective in reducing the localized, but short-term temperature spikes.

Another approach would be to investigate alternative control rod operating patterns aimed at reducing these fission density spikes. One scheme that could be considered would be a scheme in which all the operating rod groups are initially inserted approximately half way into the core rather than having 6 of the 12 banks fully inserted and the other 6 withdrawn, as in the present scheme. This would minimize rod withdrawal for a required reactivity change and help to maintain an axial power shape tilted toward the top of the core. In addition, a change to the DIF3D package that would allow a control rod position search to maintain a given core K_{eff}, plus a variable burnup time step, would minimize control bank motion and provide a simpler solution to eliminate the spikes.

4 SINGLE-FUEL-PARTICLE CORE DESIGN

The focus of the single-fuel-particle core design work was to achieve an acceptable core design for a single fissile fuel particle having a single U-235 enrichment. This work involved a series of design iterations that primarily investigated fuel loading zoning and fixed burnable poison zoning to achieve a design that meets the PF and cycle-length requirements, and which has predicted fuel performance and fission product release approximately equivalent to that predicted for binary-fuel-particle core design Case 7.9. These iterations resulted in design Case 8.9.3, which is the best single-fuel-particle/single U-235 enrichment design that was achieved within the PF limits, cycle-length requirement, and time constraints of the CPA. The physics design for Case 8.9.3 is described in Section 4.1 and the design iterations that led to Case 8.9.3 are described in Section 4.2. Additional details of the physics design work are documented in [Ellis 2009c]. The fuel performance/fission product release assessment for Case 8.9.3 is presented in Section 4.3.

The single-fuel-particle core design work also included an evaluation of core designs utilizing a single fissile particle having multiple U-235 enrichments. In these cases, two identical UCO fuel particles (i.e., same kernel diameter, same coating layer properties, etc.) having two different U-235 enrichments were considered. Such a core design is considered a potential fall back if an acceptable core design cannot be achieved with a single fuel particle and single U-235 enrichment. This is because use of a single fuel particle with two U-235 enrichments should still require qualification of only one fuel particle because the irradiation and accident condition performance of the fuel particle having the higher U-235 enrichment should be bounding for the fuel particle having the lower U-235 enrichment. The single-fuel-particle/two-enrichment cases (8.1 and 8.5) are discussed in Section 4.2.

4.1 Core Physics Design – Single-Fuel-Particle/Single-Enrichment (Case 8.9.3)

The potential to achieve an acceptable core physics design using a single fissile fuel particle having a single U-235 enrichment was evaluated based on the results of the binary-fuel-particle core design work completed in the first part of Phase 2. Core/block optimization strategies included particle PF zoning, B_4C burnable poison zoning, and other optimization strategies were evaluated for the binary-fuel-particle core design. The U-235 enrichment selected for the core design was the effective U-235 enrichment for the equilibrium binary-fuel-particle core design, which was 15.5%.

4.1.1 Fuel Cycle Description

The fuel cycle uses two reload segments, so that 51 of the 102 columns core (half of the core) are replaced each reload. The control rod pattern (12 control rods in the core and 36 control rods in the outer reflector) allows refueling by 1/6 core sectors. The refueling operation is performed one sector at a time. Each refueling sector thus contains 17 core columns, with 10

fuel elements per column. In refueling each of the six refueling core sectors, the sector elements are removed one layer at a time until all of the core elements in the sector have been removed. Fresh reload elements and one-cycle-old elements are then reloaded into the sector. Thus, all 1020 core elements are removed from the reactor each reload, and the 510 two-cycle-old elements are reinserted with 510 fresh reload elements. As noted in Table 1-1, a minimum fuel cycle length of 540 EFPD (startup to shutdown) was specified as a design goal for the CPA.

The fuel cycle design is summarized in Table 4-1, and was determined after several design iterations from two-dimensional analysis. As shown in Table 4-1, this cycle length was achieved for all cycles except cycles 2 and 3, which ran for 530 EFPD. Note that in Table 4-1 (and in subsequent tables in this section), two fuel particles are identified, TRISO#1 and TRISO#2. This is because the DIF3D code is set up for a binary-fuel-particle system and it was easier to "trick" the code by defining the two fuel particles to be identical rather than to modify the code to handle only one fuel particle. Therefore, each compact for each Segment of all cycles contains two fissile particles that have the same design (a 425-micron diameter kernel of $UC_{0.5}O_{1.5}$ having the coating layer thicknesses and densities shown in Table 2-4) and the same U-235 enrichment (15.5 weight % U-235).

Table 4-1. Fuel Cycle Design

	Cycle Time		Fuel Loading (kg)		FBP Loading (kg)	EOC GAUGE K_{eff}
Reload	EFPD	Months	TRISO#1 (15.5%)	TRISO#2 (15.5%)		
0	540	18	2187.017	2187.017	2.297	1.024
1	530	17.7	1518.424	1518.424	1.5	1.019
2	530	17.7	1518.424	1518.424	1.5	1.020
3	540	18	1518.424	1518.424	1.5	1.021
Equilibrium	540	18	1518.424	1518.424	1.5	1.019

In the binary-fuel-particle core design, the fertile fuel particle loading in Segment A of the initial core is much larger than in the reload segments. Therefore, in order to keep the same total uranium loading using a smaller fuel kernel (425 micron vs. 500 micron), more fuel particles would be needed resulting in a higher PF. Rather than have unacceptably high PFs, the initial core was shortened to 540 EFPD by removing 10% of the total uranium loading from Segment A only. The impact on approach-to-equilibrium cycle length is minimal; only reducing the second reload length by 10 days. The optimization strategy used for the fuel cycle keeps the fissile loadings constant for every reload, but allows the cycle time to vary to obtain the required

K_{eff} at the end of each cycle. For the initial cycle, Segments A and B contain 0.606 kg and 1.691 kg of FBP, respectively. The advantages of this strategy are:

1. The fuel loadings for all reloads are identical. This will greatly simplify core nuclear analysis and fuel production, and will make reload fuel blocks much more interchangeable.
2. A reasonable ΔK_{eff} over each cycle can be achieved. This allows the maximum control rod worth requirement to be a small as possible.

Based on the fuel loadings for each cycle in Table 4-1, the heavy metal loadings (Table 4-2) and average GAUGE core region atom densities (Table 4-3) were calculated for the initial core and reload segments. Table 4-3 includes atom densities for B-10 resulting from burnable and non-burnable impurities in the graphite. Table 4-3 also includes the beginning-of-initial-cycle (BOIC) and reload-atom densities for B-10 resulting from the FBP compacts.

Table 4-2. Heavy Metal Loading Design

Particle	Nuclide	BOIC Segment A (kg)	BOIC Segment B (kg)	Reload Segments[1] (kg)
TRISO#1 (15.5%)	U-235	137.304	201.683	235.356
	U-238	748.530	1099.5	1283.068
TRISO#2 (15.5%)	U-235	137.304	201.683	235.356
	U-238	748.530	1099.5	1283.068
Total Heavy Metal		1771.668	2602.366	3036.848
[1]Segment A is the first reload segment				

Table 4-3. Average Core Region Atom Densities

Nuclide	Atom Densities (atoms / barn-cm)		
	BOIC Segment A	BOIC Segment B	Reload Segments
U-235 (TRISO#1)	7.70793×10^{-6}	1.13220×10^{-5}	1.32123×10^{-5}
U-238 (TRISO#1)	4.14898×10^{-5}	6.09436×10^{-5}	7.11185×10^{-5}
U-235 (TRISO#2)	7.70793×10^{-6}	1.13220×10^{-5}	1.32123×10^{-5}
U-238 (TRISO#2)	4.14898×10^{-5}	6.09436×10^{-5}	7.11185×10^{-5}
B-10 (FBP)	7.67929×10^{-7}	2.14285×10^{-6}	1.90081×10^{-6}
B-10 (burnable impurities)	2.18693×10^{-8}	2.18957×10^{-8}	2.17240×10^{-8}
B-10 (non-burnable impurities)	7.54112×10^{-10}	7.55024×10^{-10}	7.49103×10^{-10}
Carbon (in fuel)	1.59863×10^{-2}	1.59239×10^{-2}	1.55338×10^{-2}
Carbon (in moderator)	5.22318×10^{-2}	5.23767×10^{-2}	5.22311×10^{-2}
Oxygen	1.47593×10^{-4}	2.16797×10^{-4}	2.52992×10^{-4}
Silicon	2.91959×10^{-4}	4.28852×10^{-4}	5.00452×10^{-4}

The discharge fuel burnup in each cycle is given in Table 4-4 in megawatt-days per initial metric ton (MWd/MT) of fissile uranium in each reload segment. The denominator term in the calculation of the fissions per initial metal atom (FIMA) includes all heavy metal atoms in the reload segment, and was taken from SURVEY output. The denominator term in the calculation of the fissions per initial fissile atom (FIFA) includes all U-235 atoms in the reload segment. This table shows that the average FIMA in the fissile particles in the equilibrium cycle is 0.118, and the peak FIMA in the fissile particles in the equilibrium cycle is 0.165.

Table 4-4. Discharge Fuel Burnup for Each Cycle

Reload	EFPD	Burnup (MWd/MT)	Average				Peak	
			TRISO#1		TRISO#2		TRISO#1	TRISO#2
			FIMA	FIFA	FIMA	FIFA	FIMA	FIMA
0	540	74,074	0.084	0.539	0.084	0.539	0.135	0.135
1	530	104,714	0.131	0.837	0.131	0.837	0.176	0.176
2	530	104,714	0.121	0.771	0.121	0.771	0.164	0.164
3	540	106,690	0.119	0.762	0.119	0.762	0.165	0.165
Equilibrium	540	106,690	0.118	0.755	0.118	0.755	0.165	0.165

4.1.2 Fuel and FBP Zoning

Power distributions are controlled to limit fuel temperature, to limit fuel element stress, and to assure axial power stability. The principal means of power distribution control is the use of axial and radial zones of differing concentrations of LEU and FBP. The current zoning scheme consists of three radial zones (Table 4-5 for fuel and Table 4-6 for FBP) and three axial zones (Table 4-7 for fuel and FBP.) The three radial zones correspond to the three annular core rings containing 30, 36, and 36 columns per ring as seen in Figure 2-2. The three axial zones correspond to the top two layers, bottom two layers, and the remaining middle six layers.

Fuel radial zoning is given another level of detail with buffer zoning factors. These regions apply along all sides directly adjacent to a reflector (both inner and outer) element and extend to only the first 4-rows of fuel compacts at the outer boundaries facing the reflector. This thin buffer layout is shown in Figure 4-1 and is identical to layout used for the binary-fuel-particle core design. These factors reduce the relative fuel loading to help minimize and fine tune power peaking typically seen at these interfaces.

An important consideration related to fuel zoning factors is the fuel particle PF in the fuel compacts. These PFs are shown in Figure 4-2 for the segment reloads only, and at the middle axial zone where the zoning is a uniform 1.0. The current zoning factors and fuel loadings result in acceptable particle PFs, i.e., an average of 20% for the initial core and 27.7% for reloads. The maximum PF is calculated to be 38.3% for segment A of the core reloads. The maximum (goal) total PF of fuel particles in a fuel compact assigned for this NGNP core performance analysis is 35%, with an allowance for localized zoning ranging from 35% to 40% not to exceed 5% of the total core compact volume. Maximum initial cycle PF is only 32.6% and therefore under the localized zoning requirement. This design has localized zoning ranging from 35% to 38.3% in the reloads (which occupies 5.9% of the total core compact volume.) Therefore the design exceeds the requirement by 0.9%.

Table 4-5. Radial Fuel Zoning Factors

Cycle	Segment	Region	Compacts	Compact Fraction	Unbuffered Blocks		Buffered Blocks					
					Relative TRISO#1	Relative TRISO#2	TRISO#1 Buffer	Relative TRISO#1 (Standard Portion)	Relative TRISO#1 (Buffered Portion)	TRISO#2 Buffer	Relative TRISO#2 (Standard Portion)	Relative TRISO#2 (Buffered Portion)
Initial	A	Radial Row 1	447300	0.292	*1.033*	*1.033*	0.707	1.078	0.762	0.707	1.078	0.762
		Radial Row 2	562680	0.368	0.994	0.994		1.047	0.740		1.047	0.740
		Radial Row 3	519480	0.340	*0.979*	*0.979*		1.102	0.779		1.102	0.779
		Average:			1.000	1.000						
	B	Radial Row 1	447300	0.288	*0.831*	*0.831*	0.645	1.096	0.707	0.645	1.096	0.707
		Radial Row 2	541080	0.349	1.060	1.060		-	-		-	-
		Radial Row 3	562680	0.363	*1.076*	*1.076*		1.116	0.720		1.116	0.720
		Average:			1.000	1.000						
Reloads 1,3	A	Radial Row 1	447300	0.292	*0.708*	*0.708*	0.671	1.089	0.730	0.671	1.089	0.730
		Radial Row 2	562680	0.368	1.125	1.125		1.053	0.706		1.053	0.706
		Radial Row 3	519480	0.340	*1.116*	*1.116*		1.116	0.749		1.116	0.749
		Average:			1.000	1.000						
Reloads 2,4	B	Radial Row 1	447300	0.288	*0.721*	*0.721*	0.645	1.096	0.707	0.645	1.096	0.707
		Radial Row 2	541080	0.349	1.145	1.145		-	-		-	-
		Radial Row 3	562680	0.363	*1.082*	*1.082*		1.116	0.720		1.116	0.720
		Average:			1.000	1.000						

note: values in *italics* indicate value is only used to calculate/verify the average is 1.0 - block type in that region doesn't exist.

Table 4-6. Radial FBP Zoning Factors

Cycle	Segment	Region	Compacts	Compact Fraction	Relative FBP
Initial	A	Radial Row 1	12600	0.294	1.020
		Radial Row 2	15120	0.353	1.040
		Radial Row 3	15120	0.353	0.943
		Average:			1.000
	B	Radial Row 1	12600	0.294	1.077
		Radial Row 2	15120	0.353	1.040
		Radial Row 3	15120	0.353	0.896
		Average:			1.000
Reloads 1,3	A	Radial Row 1	12600	0.294	0.918
		Radial Row 2	15120	0.353	1.040
		Radial Row 3	15120	0.353	1.028
		Average:			1.000
Reloads 2,4	B	Radial Row 1	12600	0.294	1.020
		Radial Row 2	15120	0.353	1.040
		Radial Row 3	15120	0.353	0.943
		Average:			1.000

Table 4-7. Axial Zoning Factors

Cycle	Axial Layer	Relative TRISO#1	Relative TRISO#2	Segment A Relative FBP	Segment B Relative FBP
Initial	1 (top)	1.15	1.15	1.05	1.05
	2	1.15	1.15	1.05	1.05
	3	1.00	1.00	1.00	1.00
	4	1.00	1.00	1.00	1.00
	5	1.00	1.00	1.00	1.00
	6	1.00	1.00	1.00	1.00
	7	1.00	1.00	1.00	1.00
	8	1.00	1.00	1.00	1.00
	9	0.85	0.85	0.95	0.95
	10 (bottom)	0.85	0.85	0.95	0.95
	Average:	1.00	1.00	1.00	1.00
Reloads	1 (top)	1.10	1.10	0.94	0.94
	2	1.10	1.10	0.94	0.94
	3	1.00	1.00	1.00	1.00
	4	1.00	1.00	1.00	1.00
	5	1.00	1.00	1.00	1.00
	6	1.00	1.00	1.00	1.00
	7	1.00	1.00	1.00	1.00
	8	1.00	1.00	1.00	1.00
	9	0.90	0.90	1.06	1.06
	10 (bottom)	0.90	0.90	1.06	1.06
	Average:	1.00	1.00	1.00	1.00

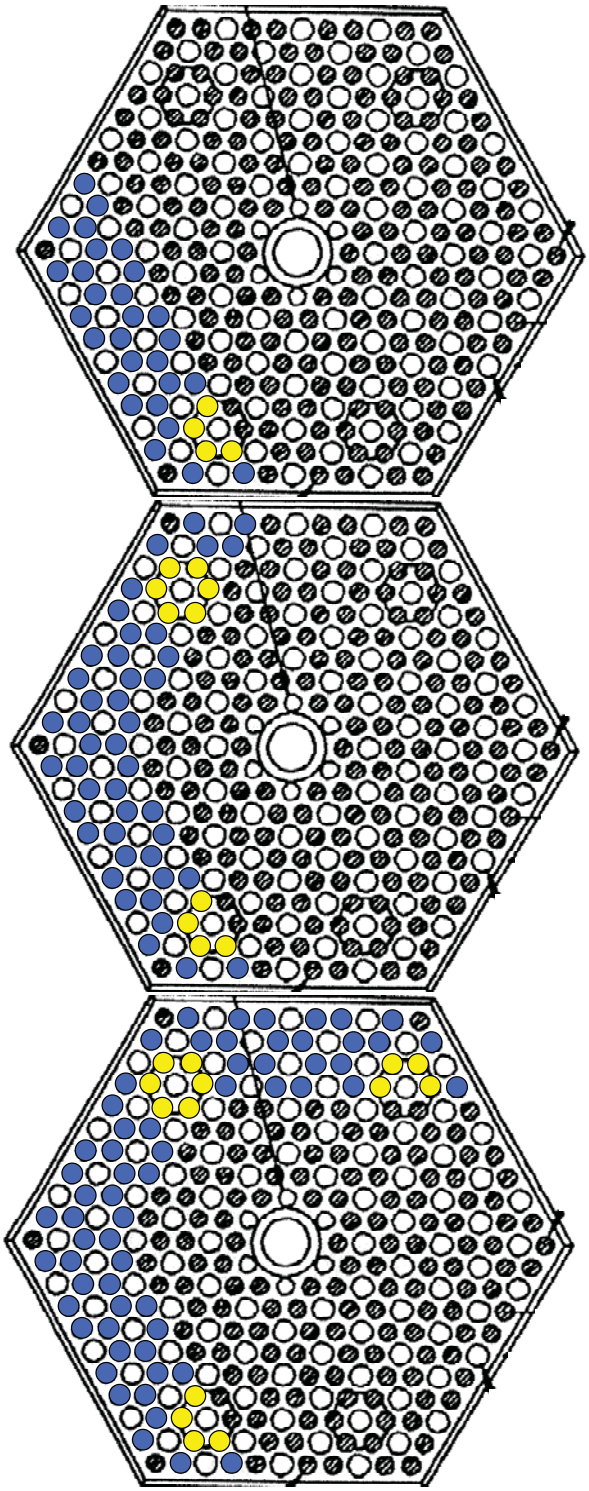

Figure 4-1. 1, 2, and 3-sided Buffered Standard Fuel Element Example

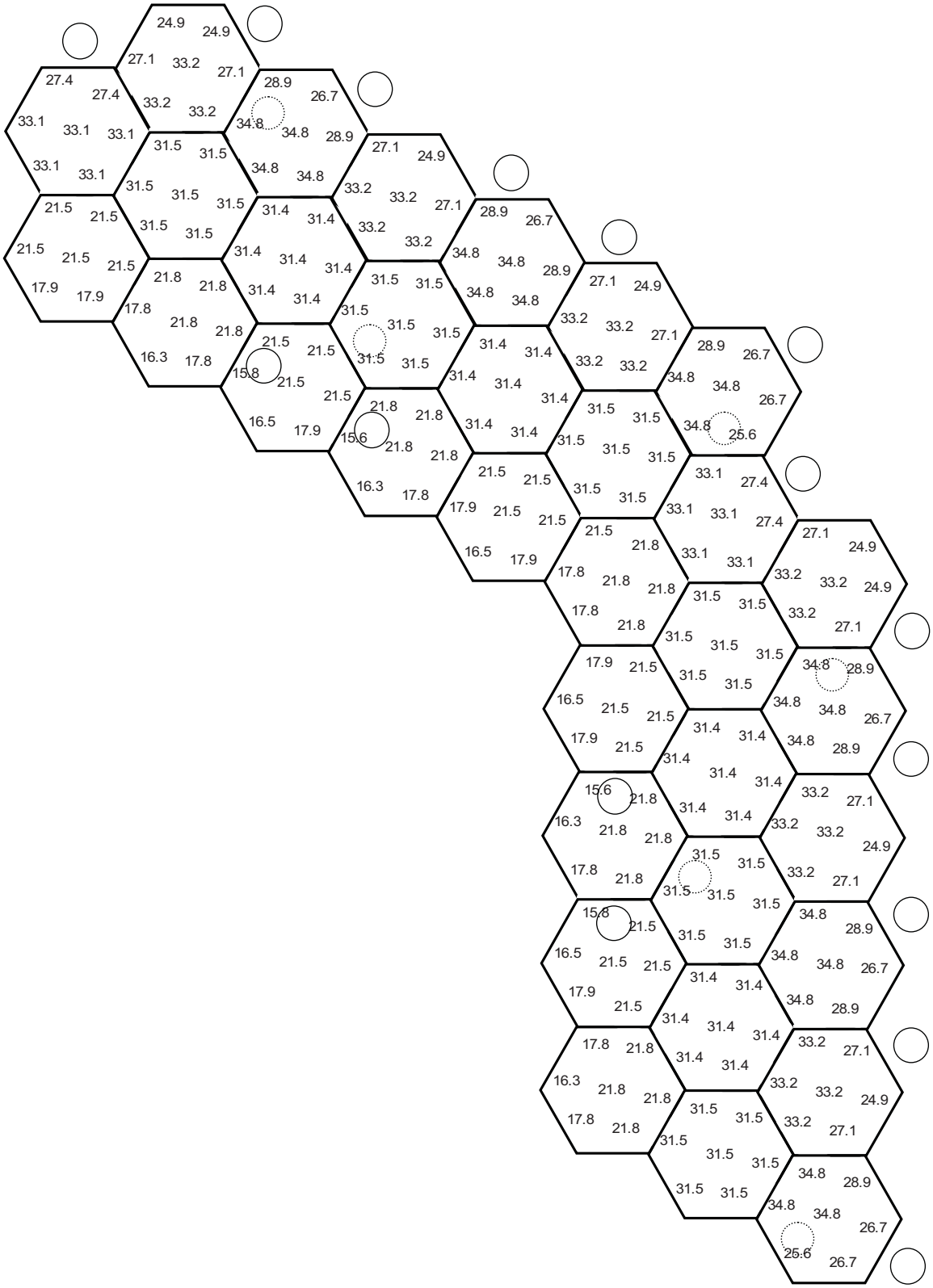

Figure 4-2. Radial Fuel Particle PF (%) – Segment Reloads

4.1.3 Steady State Power Distributions

Results of the 3-dimensional DIF3D hexagonal mesh diffusion calculations were used to create power distributions as a function of burnup. DIF3D results (as opposed to GAUGE) were chosen because the input to the fuel performance analysis comes directly from DIF3D output.

Table 4-8 summarizes the radial power history data for the equilibrium cycle from the DIF3D fuel depletion calculation with control rod banks moved to maintain criticality over the fuel cycle. Data is given for each time point during the equilibrium cycle, and includes the core ring (row) peaking factor and the radial peaking factor (RPF) for the maximum subcolumn region normalized by the number of fuel compacts within the subcolumn (column and subcolumn numbering is shown in Figure 2-10, and discussed in Section 2.2). Also given is the number of inserted control rod groups needed for a near-critical reactor and the K_{eff} obtained with those rods inserted. Each control rod group includes three control rods spaced symmetrically around the core. The 'Col_Sub' column displays two pieces of information. Using Figure 2-10 as a guide, 'Col' refers to the core column number in a 1/3 core sector ranging, in a clockwise direction, from 1 to 10 for row 1, 11 to 22 for row 2, and 23 to 34 for row 3. 'Sub' refers to the subcolumn number also shown in Figure 2-10. The order of subcolumns 2 through 7 rotates 60° for every 1/6 core sector as indicated in the figure. This 'Col_Sub' numbering scheme is also used in the SORT3D and SURVEY codes.

The subcolumn model in DIF3D limits the calculation of the power peaks to that averaged over the fuel compacts in the subcolumn. Power peaking within individual compacts in the subcolumn area may be higher, depending on the power distribution through that region. However, this power peaking is due to a higher fission density in the compact and this tends to burn down fairly quickly to the subcolumn average.

The zero day power and critical rod group data are based on a hypothetical 100% power level, but with no xenon buildup. Since this condition is unrealistic, the data given for the 3.0 day burnup is actually more representative of the expected beginning of equilibrium cycle conditions, and is used for the zero day data in Table 4-8. The middle region of fuel columns has been zoned to run at higher than average power density, while the inner and outer zones run at somewhat lower power density to minimize power peaking at the two core-reflector interfaces.

The radial power distribution and operating control rod pattern for the beginning, middle and end of the equilibrium cycle (BOEC, MOEC and EOEC, respectively) calculated in the DIF3D depletion are given in Figures 4-3, 4-4, and 4-5. These figures give the RPF for each of the seven hexagonal subcolumn regions. The calculated RPF is for each entire subcolumn region, and varies over the cycle due to the effects of fuel depletion and movement of the control rods.

Table 4-8. DIF3D Radial Power Results for Equilibrium Cycle

Time Point	Delta EFPD	Total EFPD	Control Rod Banks Inserted	K-eff	Row Peaking Factor			Max. Sub Power	
					Row 1	Row 2	Row 3	Col_Sub	RPF[1]
1	-	0	6.1	1.023	1.072	1.132	0.808	10_5	1.48
2	3	3	6.1	1.009	1.017	1.109	0.877	10_5	1.48
3	7	10	6.0	1.008	1.016	1.110	0.877	10_5	1.48
4	10	20	6.0	1.007	1.015	1.111	0.877	10_5	1.47
5	10	30	6.0	1.007	1.014	1.111	0.877	10_5	1.47
6	10	40	6.0	1.007	1.013	1.112	0.877	20_5	1.48
7	10	50	6.0	1.007	1.011	1.113	0.877	20_5	1.48
8	10	60	6.0	1.007	1.010	1.115	0.878	20_5	1.49
9	10	70	6.0	1.007	1.008	1.116	0.878	20_5	1.49
10	10	80	6.0	1.006	1.006	1.117	0.878	20_5	1.5
11	10	90	6.0	1.006	1.003	1.118	0.879	20_5	1.5
12	10	100	6.0	1.006	1.001	1.119	0.880	20_5	1.5
13	10	110	5.7	1.008	0.983	1.117	0.897	20_5	1.51
14	10	120	5.7	1.008	0.987	1.118	0.893	20_5	1.51
15	10	130	5.4	1.010	0.970	1.115	0.910	20_5	1.52
16	10	140	5.4	1.009	0.972	1.117	0.907	20_5	1.52
17	10	150	5.3	1.010	0.963	1.116	0.915	20_5	1.53
18	10	160	5.3	1.010	0.961	1.117	0.915	20_5	1.53
19	10	170	5.3	1.009	0.958	1.119	0.916	20_5	1.54
20	10	180	5.2	1.009	0.953	1.118	0.920	20_5	1.54
21	10	190	5.2	1.008	0.949	1.120	0.923	20_5	1.54
22	10	200	5.1	1.008	0.945	1.120	0.926	20_5	1.55
23	10	210	5.1	1.007	0.942	1.122	0.927	20_5	1.55
24	10	220	5.0	1.006	0.938	1.122	0.930	20_5	1.55
25	10	230	5.0	1.005	0.934	1.124	0.931	20_5	1.55
26	10	240	5.0	1.004	0.931	1.125	0.932	20_5	1.55
27	10	250	4.6	1.006	0.914	1.122	0.950	20_5	1.5
28	10	260	4.4	1.008	0.906	1.118	0.959	20_5	1.48
29	10	270	4.2	1.008	0.897	1.117	0.969	14_5	1.49
30	10	280	4.2	1.007	0.894	1.119	0.969	14_5	1.49
31	10	290	4.1	1.006	0.889	1.119	0.973	14_5	1.5
32	10	300	4.0	1.005	0.885	1.120	0.976	14_5	1.5
33	10	310	4.0	1.003	0.881	1.121	0.978	14_5	1.5
34	10	320	3.4	1.008	0.858	1.120	0.998	14_5	1.46
35	10	330	3.2	1.007	0.857	1.119	1.000	14_5	1.46
36	10	340	3.1	1.006	0.848	1.121	1.005	14_5	1.45
37	10	350	3.0	1.005	0.845	1.121	1.008	14_5	1.44
38	10	360	3.0	1.003	0.840	1.124	1.009	14_5	1.45
39	10	370	2.6	1.009	0.816	1.116	1.037	14_5	1.5
40	10	380	2.4	1.010	0.809	1.113	1.046	14_5	1.5
41	10	390	2.2	1.010	0.799	1.112	1.056	14_5	1.52
42	10	400	2.2	1.008	0.797	1.114	1.056	14_5	1.51
43	10	410	2.1	1.008	0.791	1.112	1.062	14_5	1.52
44	10	420	2.1	1.006	0.787	1.115	1.063	14_5	1.52
45	10	430	2.1	1.004	0.784	1.115	1.065	14_5	1.52
46	10	440	2.0	1.003	0.779	1.117	1.067	25_7	1.53
47	10	450	1.7	1.005	0.765	1.114	1.082	23_1	1.49
48	10	460	1.4	1.007	0.754	1.109	1.095	23_1	1.46
49	10	470	1.3	1.006	0.748	1.109	1.102	23_1	1.45
50	10	480	1.1	1.006	0.744	1.107	1.107	23_1	1.44
51	10	490	1.1	1.004	0.738	1.109	1.109	23_1	1.43
52	10	500	1.0	1.003	0.737	1.108	1.111	23_1	1.43
53	10	510	1.0	1.001	0.731	1.111	1.113	23_1	1.42
54	10	520	0.4	1.004	0.714	1.111	1.127	14_5	1.36
55	10	530	0.4	1.002	0.715	1.112	1.126	25_1	1.37
56	10	540	0.1	1.002	0.707	1.111	1.133	25_1	1.36

[1] Fuel rod per subcolumn normalized relative powers.

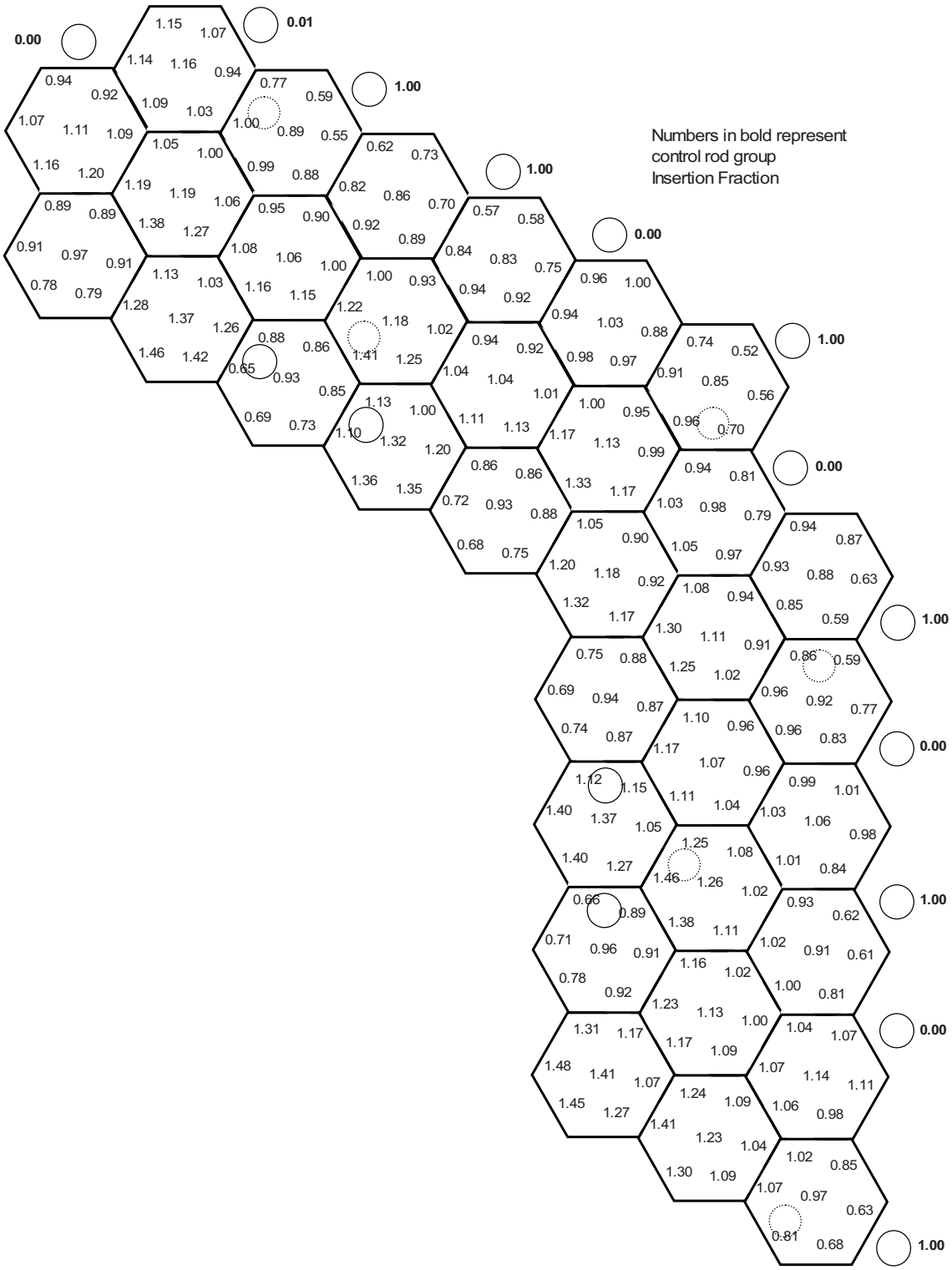

Figure 4-3. Cycle 5 Radial Power Distribution - BOEC (3 EFPD)

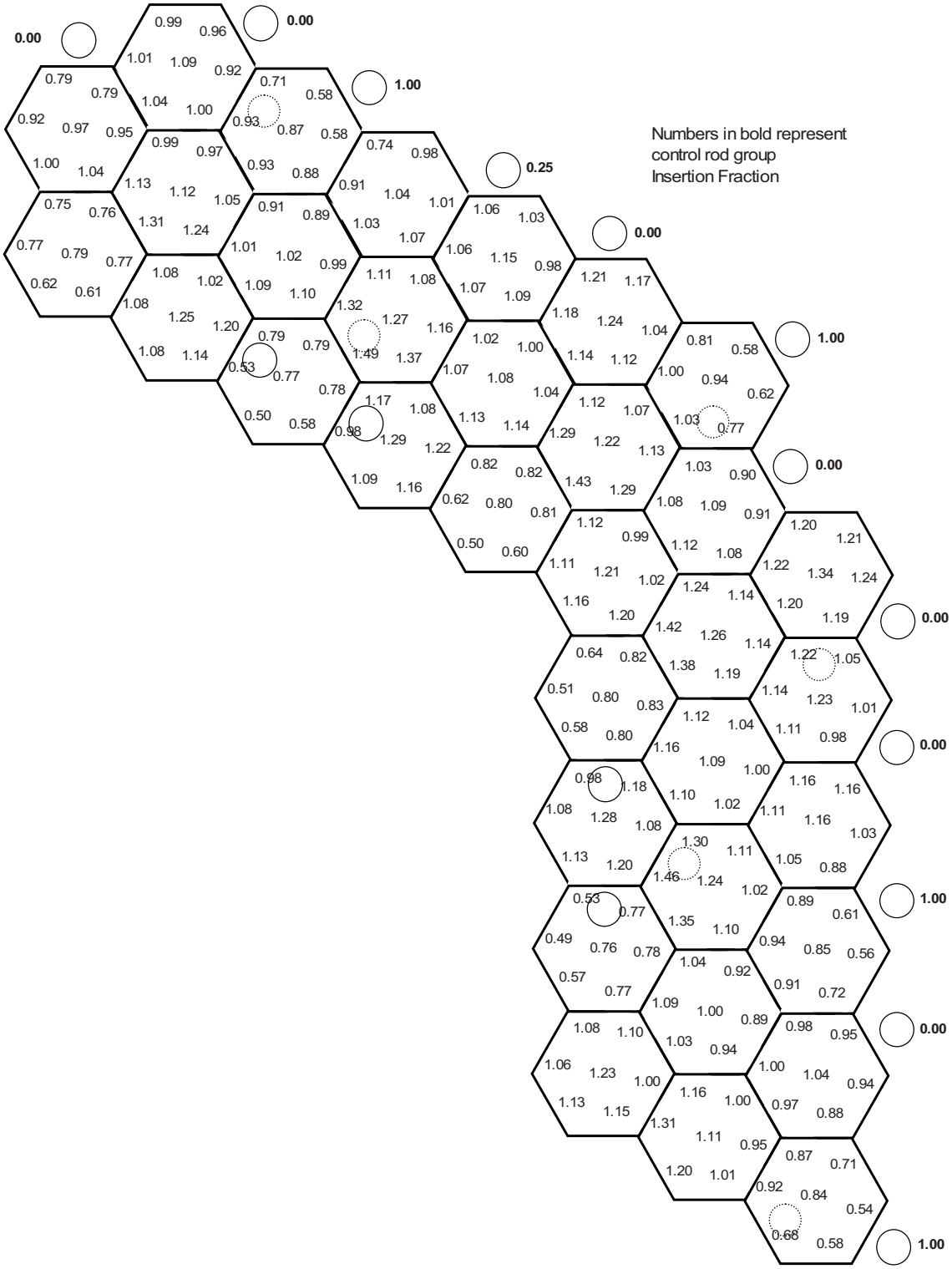

Figure 4-4. Cycle 5 Radial Power Distribution - MOEC (270 EFPD)

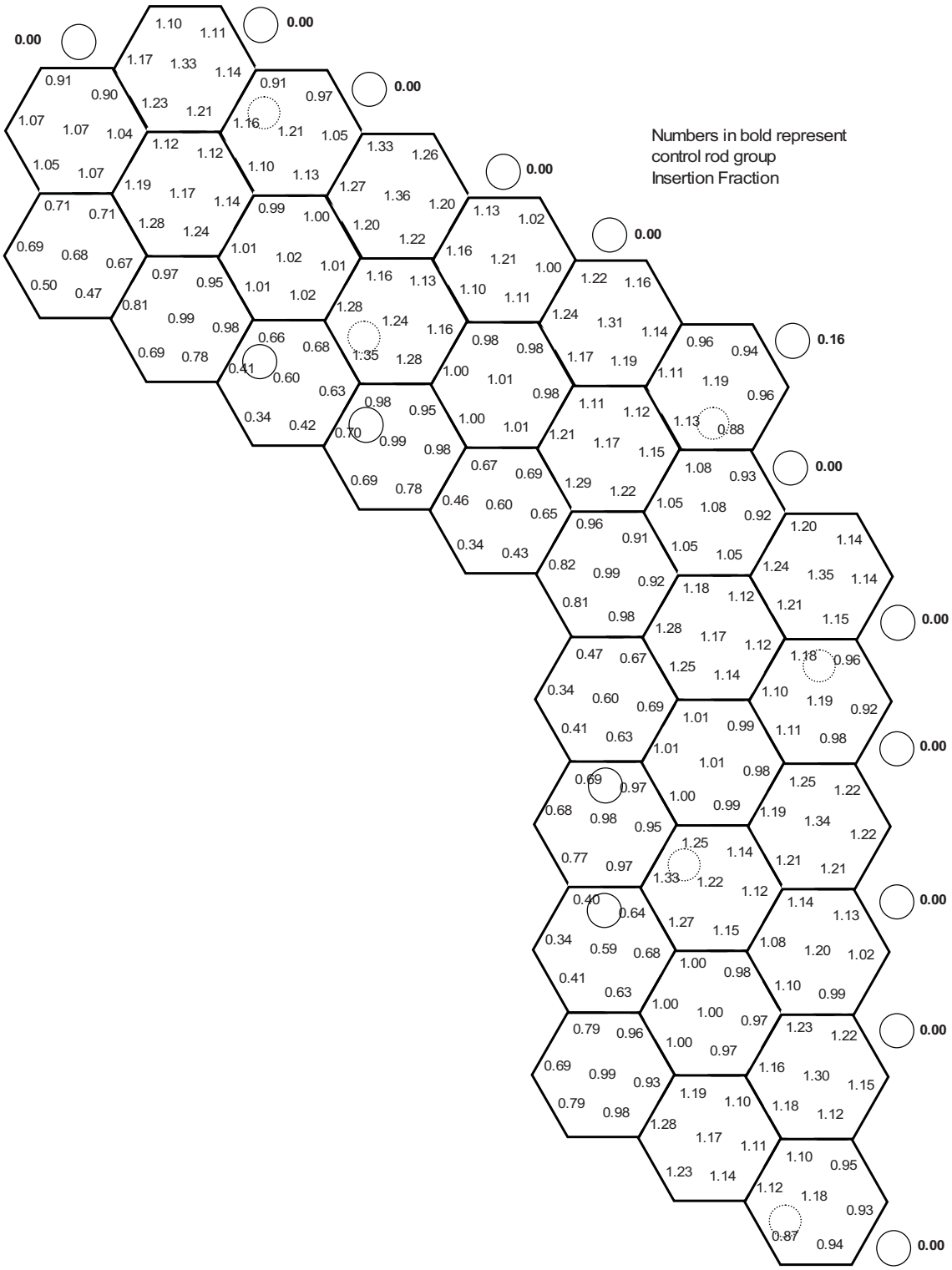

Figure 4-5. Cycle 5 Radial Power Distribution - EOEC (540 EFPD)

As for the axial power factors (APF) for each DIF3D axial region, or 1/5th core layer, they are generally kept below 1.4. The axial power profiles (core average, not column specific) and operating control rod pattern for every burnup time point of the equilibrium cycle calculated in the DIF3D depletion are given in Figures 4-6 through 4-12.

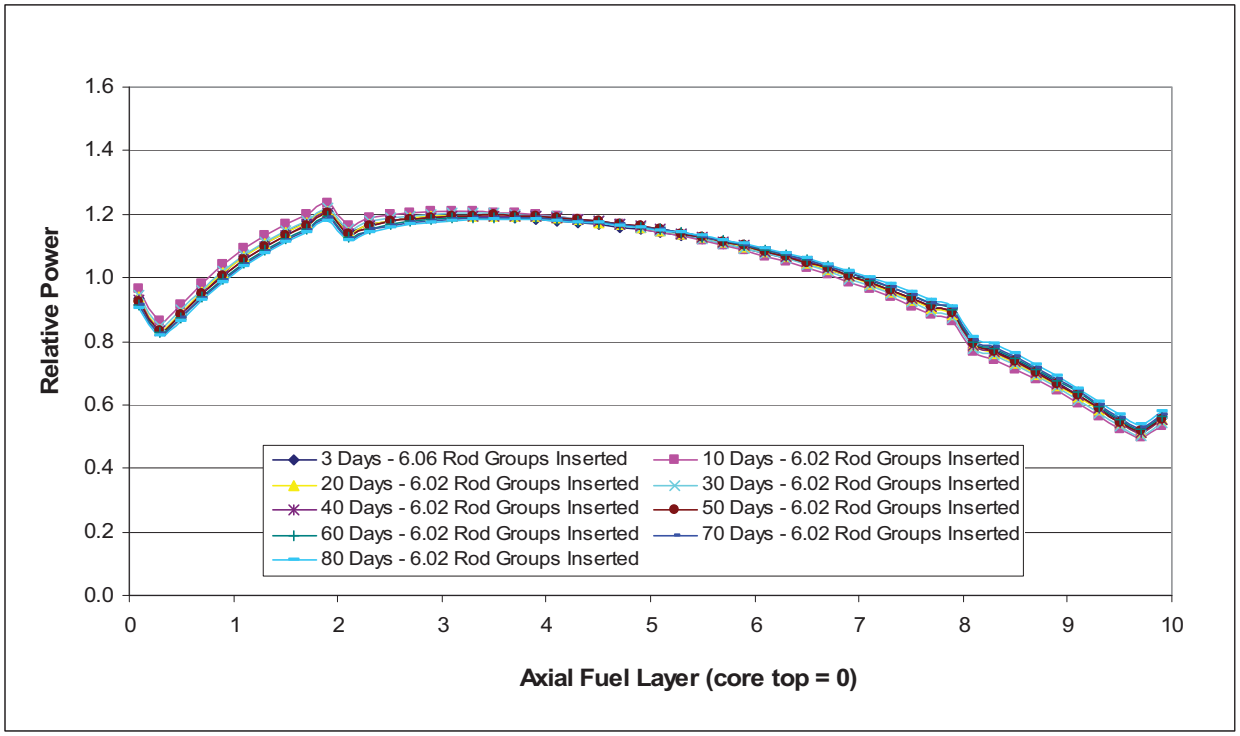

Figure 4-6. Cycle 5 Axial Power Profiles – BOEC to 80 EFPD

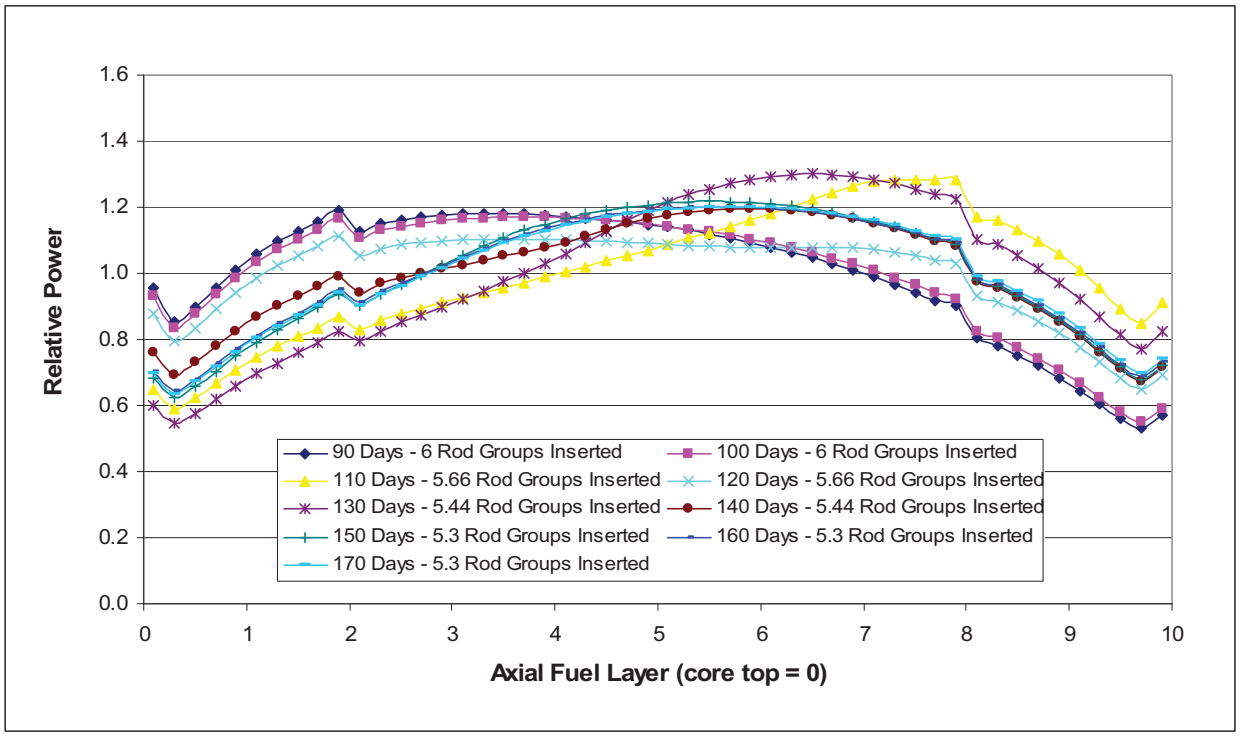

Figure 4-7. Cycle 5 Axial Power Profiles – 90 EFPD to 170 EFPD

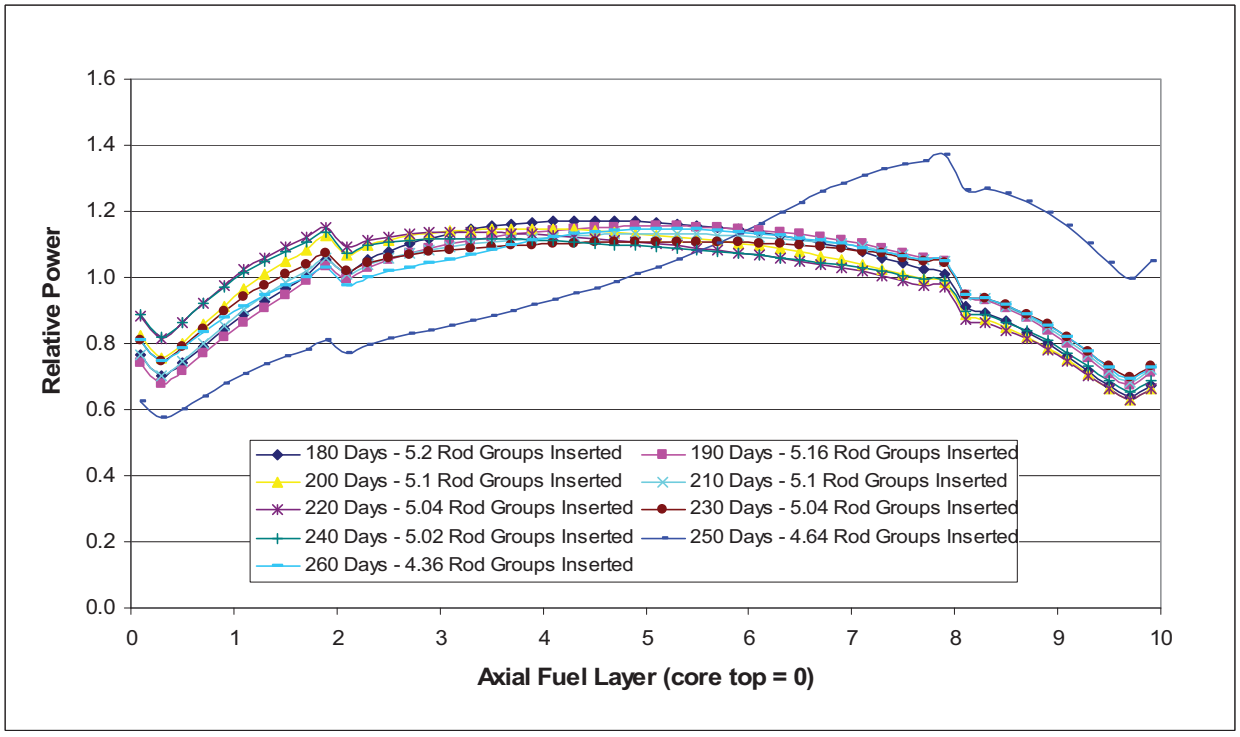

Figure 4-8. Cycle 5 Axial Power Profiles – 180 EFPD to 260 EFPD

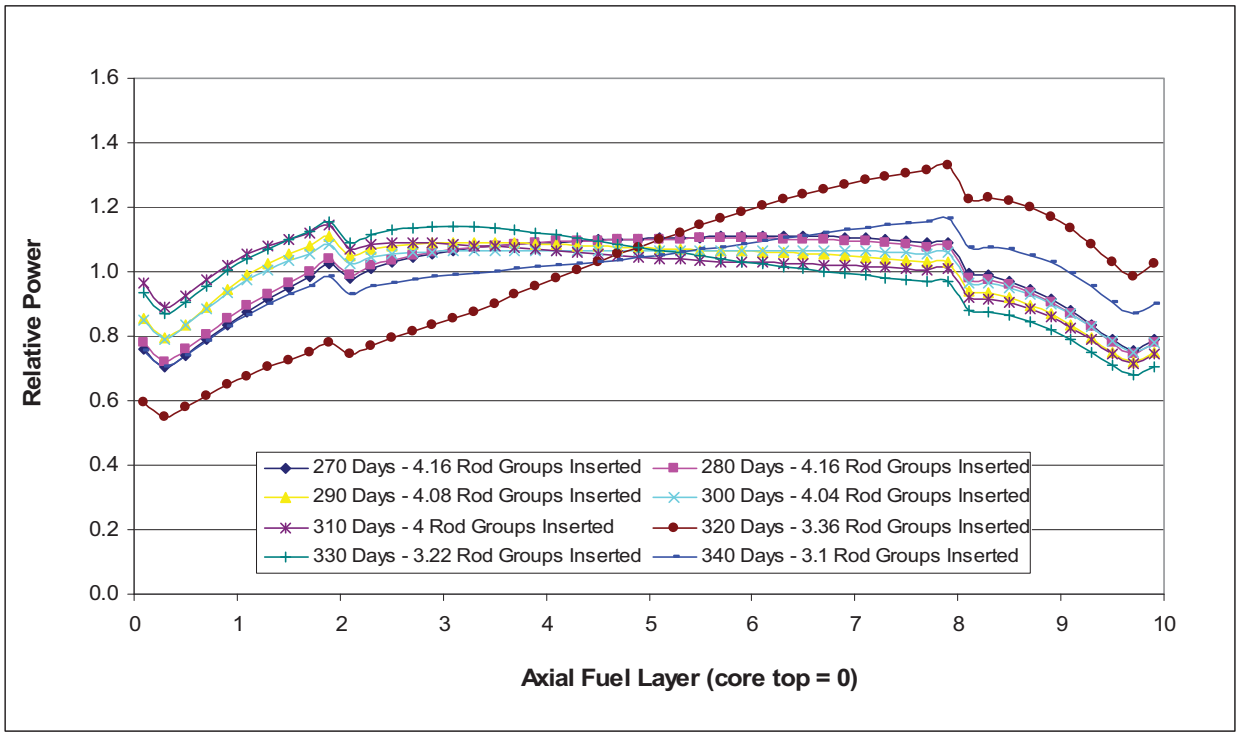

Figure 4-9. Cycle 5 Axial Power Profiles – 270 EFPD to 340 EFPD

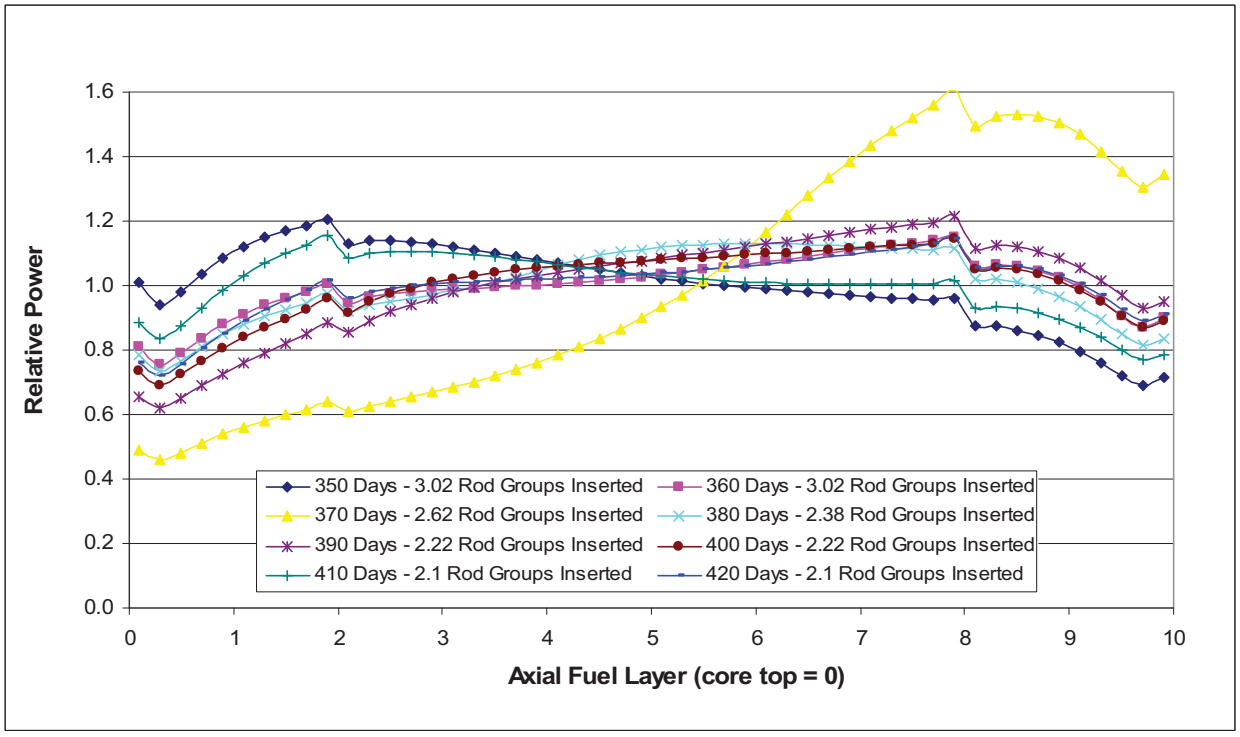

Figure 4-10. Cycle 5 Axial Power Profiles – 350 EFPD to 420 EFPD

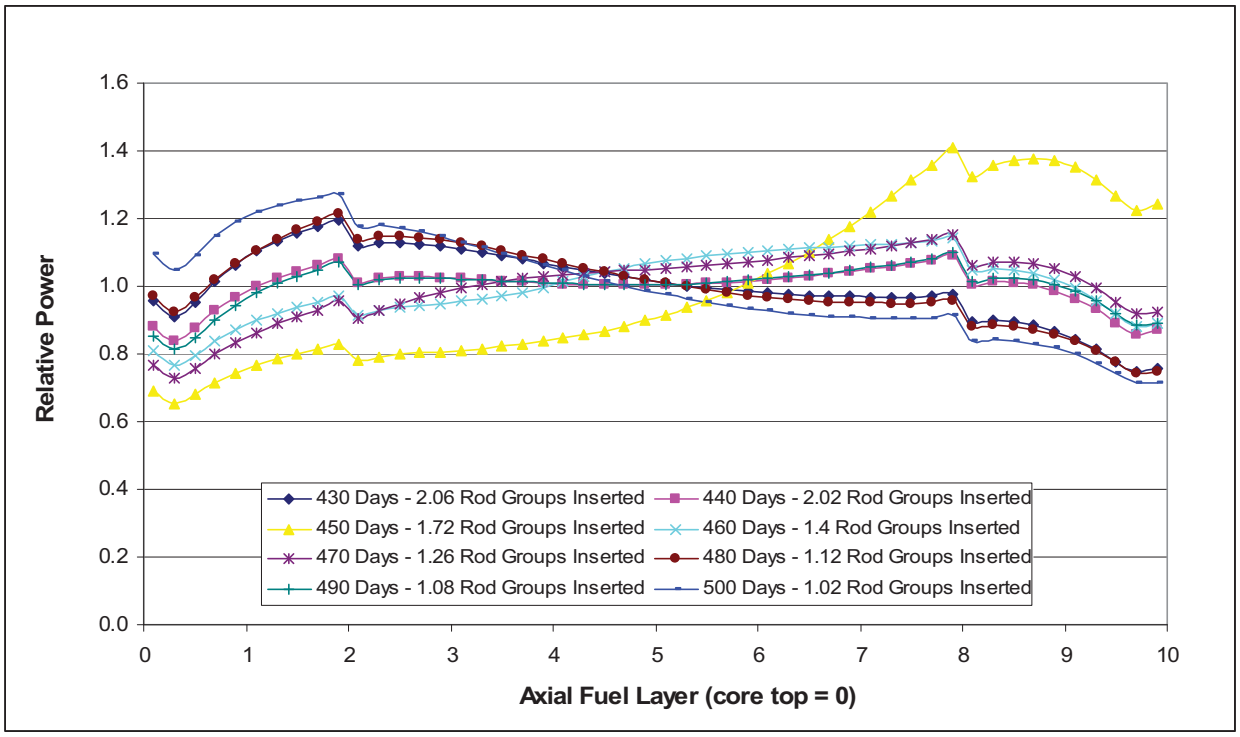

Figure 4-11. Cycle 5 Axial Power Profiles – 430 EFPD to 500 EFPD

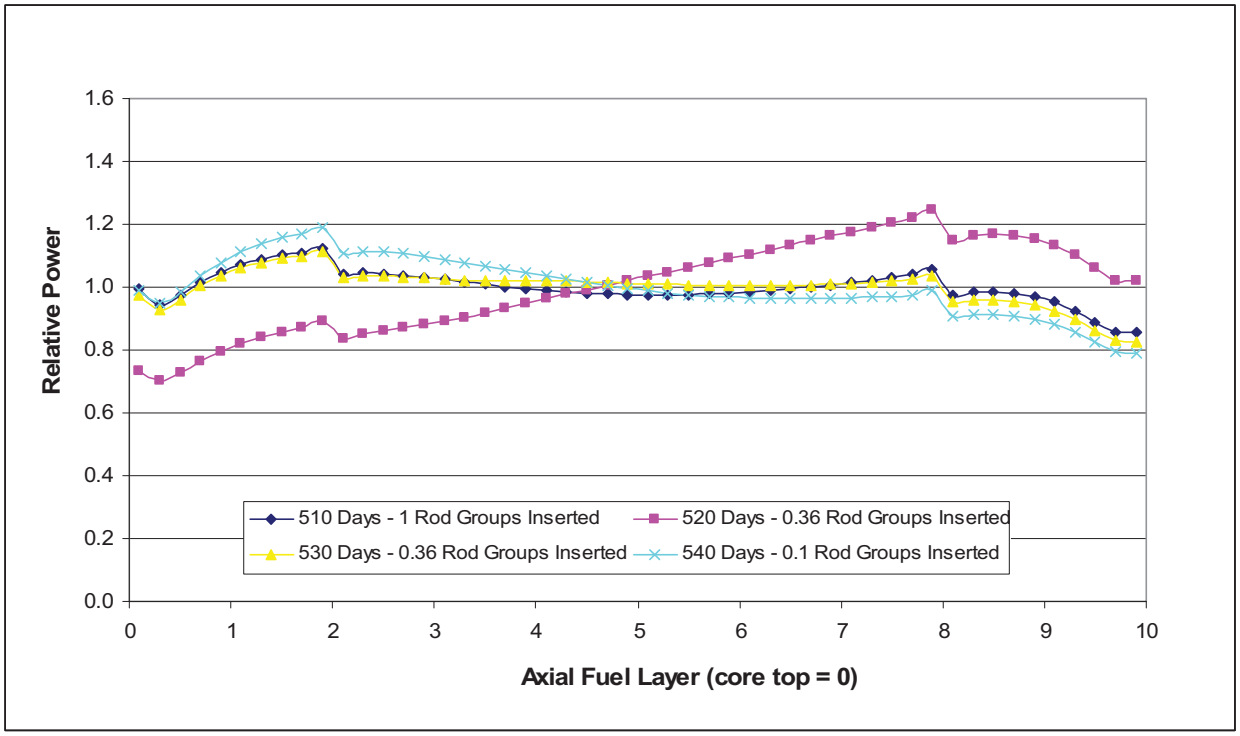

Figure 4-12. Cycle 5 Axial Power Profiles - 510 EFPD to 540 EFPD

4.1.4 Core Temperature Coefficients

The core temperature coefficient for design Case 8.9.3 is always negative, as shown in Figure 4-13 for the equilibrium core for BOEC (3 EFPD), MOEC (270 EFPD) and EOEC (540 EFPD). The main contribution to the negative temperature coefficient in the active core over the operating temperature range is made by the Doppler broadening effect of the U-238 capture resonances. Neutron capture in the Pu-240 resonance at 1.05 eV yields a strong negative coefficient at temperatures exceeding operating conditions. At the time of this writing, the overall reactor temperature coefficient, which is typically most conservative (more positive) because it includes the reactivity effects of temperature changes in the inner and outer reflectors, has not been calculated. However, the least negative value of the EOEC core temperature coefficient (-4.8×10^{-5}) is slightly more negative than the reference GT-MHR design value of -4.1×10^{-5}. The core temperature coefficient calculations were performed using full power Xe-135, an important contributor to temperature coefficient, and with constant "hot" (100% power) reflector cross sections with all control rods fully withdrawn.

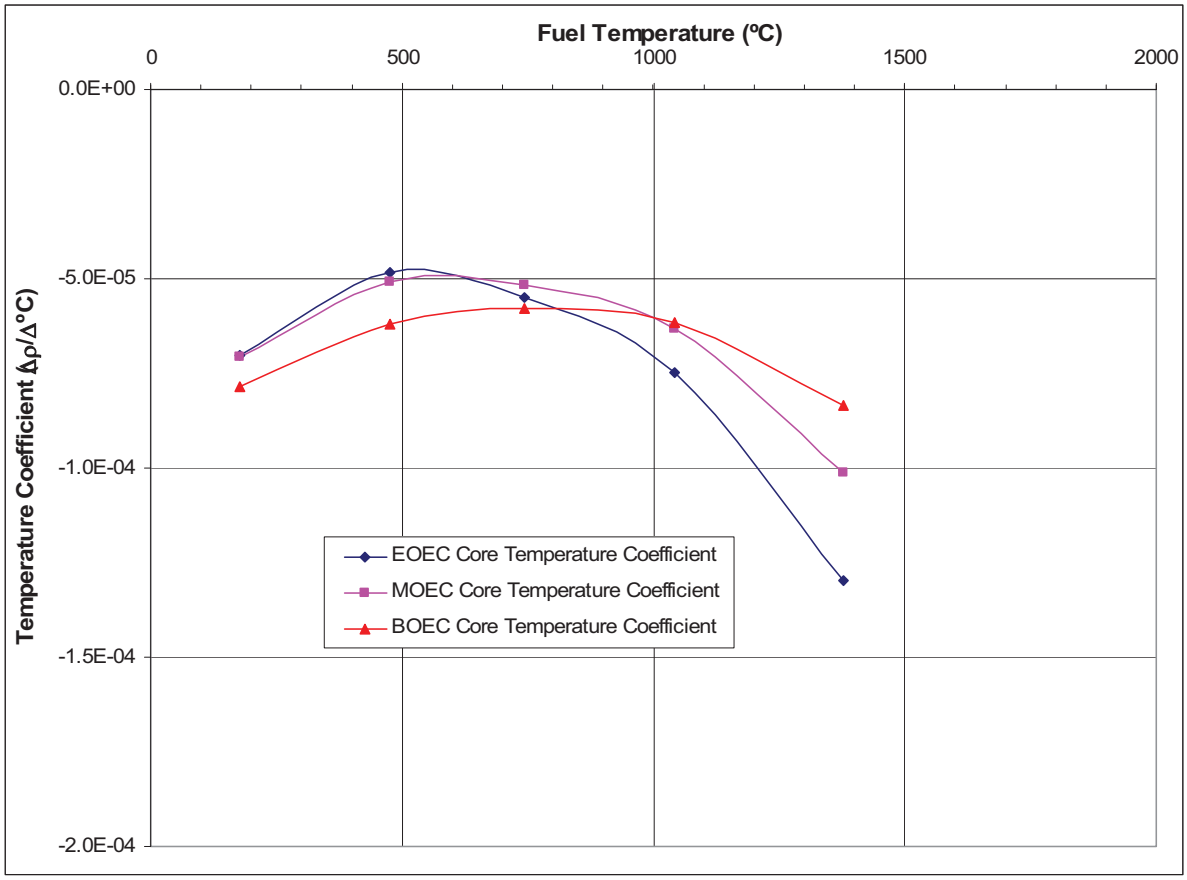

Figure 4-13. Core Temperature Coefficients for Equilibrium Cycle (Case 8.9.3)

4.2 Summary of Single-Fuel-Particle Design Iterations

A series of design iterations were carried out to transition from the binary-fuel-particle core design (Case 7.9, as summarized in Section 3) to a core design utilizing a single fuel particle and a single U-235 enrichment. The initial iterations evaluated core designs utilizing two identical fuel particles having two different U-235 enrichments. These design iterations, which included Cases 8.1 and 8.5, are referred to as single-fuel-particle/two-enrichment designs. The subsequent iterations evaluated designs utilizing a single fuel particle and a single U-235 enrichment. All of these design iterations are discussed in the following sections, and the results are summarized in Tables 4-9 and 4-10.[12]

4.2.1 Case 8.1

In the first single-fuel-particle/two-enrichment case, the fertile and fissile particles in binary-fuel-particle design Case 7.9 were redefined to have the same design (425-micron diameter UCO kernel and fissile-particle coating properties), but the U-235 enrichments were kept at 19.8% for the fissile particle and 0.72 (natural uranium) for the fertile particle. SURVEY and TRAFIC-FD were run for this case and, not surprisingly, the fuel performance and fission product release results were comparable to Case 7.9. However, due to the high fertile-particle uranium loading in the initial core, retaining the same uranium loading with the smaller fertile particles (425 microns vs. 500 microns) had a significant impact on PF, increasing the maximum PF to 42.1% with a large fraction of the compacts (36%) having a PF above 35%. However, in the reloads, the PFs decreased relative to Case 7.9 because of the larger fissile particles and the reduced fertile particle uranium loading.

The impact on PFs from using a single-fuel-particle design with a 350-micron kernel for both the fissile and fertile particles was also calculated, and was found to be prohibitive. Specifically, the maximum PF in the initial core increased to 57% with 53% of the compacts having a PF greater than 35%. The maximum PF in the reload segments increased to 40% with 38% of the compacts having a PF greater than 35%.

4.2.2 Cases 8.2 through 8.4

These cases were run as part of the investigation to resolve the power and fuel temperature spikes in localized regions of the core as a result of the large incremental control rod movements associated with the 10-day time steps used in the DIF3D core depletion analysis. This phenomenon was more fully evaluated in binary-fuel-particle core design Case 7.9.1, which is discussed in Section 4.6 of [GA 2009b] and in Case 7.9.4, which is discussed in Section 3.2

[12] In these Tables, IC = initial core, RL = reload(s), and ARO = all rods out.

of this report. Cases 8.2 through 8.4 did not contribute to the development of the final single-fuel-particle core designs, so they will not be discussed further herein.

4.2.3 Case 8.5

This design case involved using two identical fuel particles having two different U-235 enrichments in the initial core (cycle 1). However, only one of these fuel particles was used in the reloads. The enrichment of the fuel particle used in the initial core and in the reloads was selected to be 15.5% such that the U-235 enrichment in the reloads is the same as the effective enrichment in binary-fuel-particle core design Case 7.9. The enrichment of the second particle used in the initial core was selected to be 7.9% so that the effective enrichment of the initial core would be 10.9%, which is the same as the effective enrichment in the initial core in Case 7.9. The 7.9% enriched fuel particle was used only (and exclusively) in the first fuel load of Segment 1, which was removed after cycle 1. To limit the increase in PFs in the initial core (relative to Case 7.9) resulting from replacing the larger fertile particle and the more-highly-enriched fissile particle, the Segment 1 first-core uranium loading was reduced by 10% relative to Case 7.9. This resulted in a reduction of the initial core cycle length from 580 EFPD to 540 EFPD. The maximum PF in the initial core for this case is 40.6% with about 10% of the compacts having a PF greater than 35%. This does not meet the PF guidelines for the CPA, but it is a considerable improvement over Case 8.1. The PF guidelines are satisfied in the reloads, which have a maximum PF of 35% with only about 1% of the compacts having a PF greater than 35%.

In view of the large power and temperature spikes noted in the binary-fuel-particle core design cases, a new control rod s-curve was calculated to more accurately reflect the current design and to replace the old GT-MHR s-curve used throughout the binary-fuel-particle core design iterations. A series of 50 static DIF3D calculations in which rod group #5 was moved through every fuel block axial point of the fine axial mesh model was performed for the Case 8.1 design. This was done with the core atom densities at 310 EFPD into the initial cycle to represent a typical core fuel loading. The new s-curve is shown in Figure 4-14 and compared with the old reference GT-MHR s-curve. The worths of the bottom three layers (insertion fraction from 0.7 to 1) are very similar for both s-curves. Layers 6 and 7 from the top (insertion fraction 0.5 to 0.7) display the largest difference between the two s-curves, with the new worths being almost half of what they were before. Layers 4 and 5 from the top (insertion fraction 0.3 to 0.5) have very similar worths. The top three layers (insertion fraction 0 to 0.3) have almost doubled in worth with the new s-curve.

The direct impact of this new s-curve on Case 8.5 (or any of the subsequent single-fuel-particle design cases, all of which used the new s-curve) cannot be determined because other design changes were also made for each case. However, as discussed in [GA 2009b], the largest spikes occurs when a control rod group is first withdrawn because the rod group typically

withdraws from about half the core in just a couple of time steps. Because the bottom-half of the core is now worth less with the new s-curve, it is expected that for a given required reactivity insertion starting from a fully inserted rod group, more DIF3D regions would see poison removal and could contribute to more power and temperature spikes.

Although local power peaking at the location of maximum fuel temperature (which increased to 1522°C from 1462°C in Case 8.1) increased about 20%, the fuel performance was essentially unchanged relative to Case 8.1. The Ag-110m cumulative release fraction decreased by about a factor of two relative to Case 8.1, but there was a modest increase in the Cs-137 cumulative release fraction.

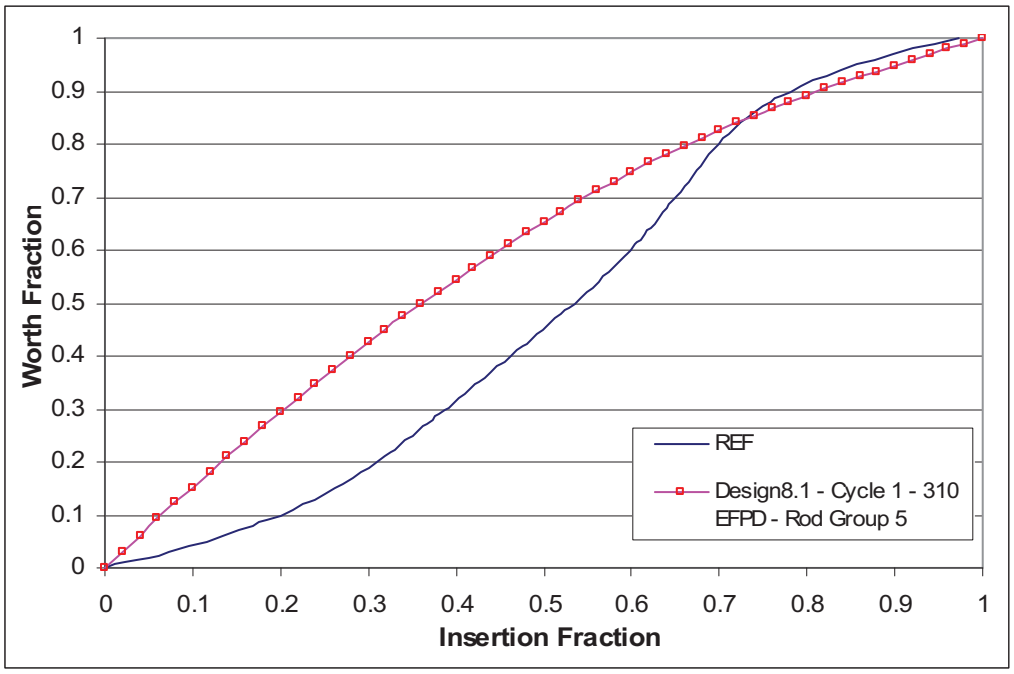

Figure 4-14. New Control Rod S-Curve versus REF (old)

4.2.4 Case 8.6.1

The third and last step in transitioning to a single-fuel-particle/single-enrichment design was to use only a single enrichment of 15.5% for all segments and all cycles. Keeping the same initial core U-235 loadings in Case 8.5 in order to preserve its cycle length, it was observed that the amount of excess reactivity of the initial core was substantial since the neutron absorptions in U-238 have been reduced and the effective core enrichment is now 15.5%. To bring down this reactivity to a manageable level, the FBP within segment-A of the initial core was increased by a

factor of four. Adding this amount of poison resulted in it being necessary to increase U-235 loadings in all reloads by 10% to sustain cycle lengths of 540 EFPD, and maintain constant segment fuel loadings. Reload cycles also used BOC2 atom density cross sections until the transition from initial core to reloads in a single enrichment core is better understood. This case was run with the coarse axial mesh model (with one axial node per fuel block).

4.2.5 Case 8.6.2

Case 8.6.2 was the same as Case 8.6.1 except that it was run with the fine-axial-mesh model (with five nodes per fuel block). Although the local power peaking at the location and time step of the maximum fuel temperature increased slightly relative to Case 8.6.1, there was a significant improvement in fuel performance and fission product release relative to Case 8.6.1 as shown in Table 4-9. However, the gaseous and metallic fission product release results for Case 8.6.2 exceed the “maximum expected” limits in Table 2-10 by a considerable amount and are also significantly worse than the results achieved for the final binary-fuel-particle core design (Case 7.9). Thus, it was decided that additional fuel zoning and FBP zoning be evaluated as a means of achieving improved fuel performance in a single-fuel-particle/single enrichment core design.

4.2.6 Case 8.7.5

A series of five 2D GAUGE iterations were performed leading up to this case. These iterations focused on using fuel and FBP radial zoning to better optimize the radial power distribution and reduce the highest RPFs. The general approach was to move a fraction of power from the middle fuel row (where fuel temperatures were the highest in Case 8.6.1) to the non-buffered portions of the inner and outer fuel rows, while staying within PF requirements. This case was run using the coarse-axial-mesh model for 3 cycles only due to time constraints. This case included the following changes relative to Case 8.6.1:

- halved FBP in initial core of segment A only
- moved 5% FBP in initial core of segment B only from middle row to inner row
- same initial core thin-buffer zoning as reloads
- moved 3% fuel in initial core of segment B from inner and middle rows to outer row
- moved 10% fuel in segment-A reloads from middle row to outer row
- reduced segment-A reload thin-buffer zoning by 5%

The maximum local fuel temperature for this case increased by 60°C relative to Case 8.6.1, but the highest time-averaged maximum fuel temperature (in Segment A, fuel load 2) decreased from 1284°C to 1224°C. The time-averaged maximum fuel temperatures for the other fuel loads also decreased slightly. The reductions in the time-averaged maximum fuel temperatures are

an indication that the fuel and FBP zoning scheme used in this design case was effective in improving the design by reducing age-peaking effects. This conclusion is confirmed by the somewhat better exposed kernel fraction, SiC defect fraction, and fission product release results for Case 8.7.5 relative to Case 8.6.1. The fuel zoning used in this case resulted in the maximum PF in the reloads increasing from 38.8% in Case 8.6.1 to 41.2%, but the percentage of compacts having a PF greater than 35% decreased from 11.9% to 6.4%.

4.2.7 Case 8.8.1

To take advantage of the low initial core PFs in Cases 8.6.1 and 8.7.5, a 3-4-3 axial zoning scheme was considered to allow significantly more fuel to be moved from the bottom part of the core to the top part of the core. For the initial core, the top zone had 138% more fuel per layer and the bottom zone had 38% less fuel per layer relative to the nominal middle zone. For the reloads, the top zone had 105% more fuel per layer and the bottom zone had 5% less fuel per layer relative to the nominal middle zone. Also, 5% of the segment A reload fuel loading was moved from the outer row to the middle row. The SURVEY results for this case show that too much fuel was moved towards the top of the core in the initial cycle, resulting in some very high temperatures occurring in layers 6 and 7. The maximum local temperature for this case increased to 1690°C and the highest time-averaged maximum temperature increased to 1271°C. Given the higher fuel temperatures for this case, it is not surprising that the fuel performance and fission product release results are considerably worse than for Case 8.7.5. Consequently, the design changes evaluated in Case 8.8.1 were not used in subsequent design iterations.

4.2.8 Case 8.8.2

This case also evaluated the benefit of moving fuel from the bottom to the top of the core (i.e., axial fuel zoning), but the 3-4-3 axial zoning evaluated in Case 8.8.1 was abandoned in favor of the 2-6-2 axial zoning used in previous cases. For the initial core, the top zone had 115% more fuel per layer and the bottom zone had 15% less fuel per layer relative to the nominal middle zone. For the reloads, the top zone had 110% more fuel per layer and the bottom zone had 10% less fuel per layer relative to the nominal middle zone. The fuel performance and fission product release results for this case were comparable to those for Case 8.7.5, but the modified axial zoning had the benefit of decreasing maximum PFs in the reloads relative to Case 8.7.5. Specifically, the maximum PF was reduced from 41.2% to 38.3%. The percentage of compacts having a PF greater than 35% was also decreased slightly (from 6.4% to 5.9%). The maximum PF in the initial core increased from 29.7% to 32.6%.

4.2.9 Case 8.9.1

More FBP zoning was considered in this case in an attempt to further improve fuel performance. Specifically, 10% of the FBP in Segment A at BOC2 was moved from the inner row to the outer row, and 15% FBP in all reload segments was moved from the top axial fuel zone to the bottom axial fuel zone. The goal of the axial zoning was to push more of the segment power towards the top of the core. As shown in Table 4-10, these changes resulted in a modest improvement in the predicted fuel performance and fission product release relative to Case 8.8.2.

4.2.10 Case 8.9.2

To determine the influence of the extra FBP added in Case 8.6.1, the FBP in segment A of the initial core was halved again back down to Case 7.9 levels. In addition, 10% of FBP in all initial core segments was moved from the top axial zone to the bottom axial zone of the core. These FBP changes resulted in an increase of about 30°C in the maximum local fuel temperature relative to Case 8.9.1 and also a very slight increase in the predicted fuel failure and fission product release. Consequently, the design changes evaluated in Case 8.9.2 were not used in subsequent design iterations.

4.2.11 Case 8.9.3

Given that the changes evaluated in Case 8.9.2 had a negative impact on fuel performance and fission product release, Case 8.9.1 was selected as the final coarse-axial-mesh case to run with the fine-axial-mesh model. The fine-axial-mesh version of Case 8.9.1 is designated as Case 8.9.3.

Case 8.9.3 is considered the best single-fuel-particle/single enrichment core design (without fuel shuffle) that was achieved within the PF constraints and cycle-length goal imposed on the CPA, and within the time constraints of the CPA. The current zoning factors and fuel loadings result in acceptable PFs, i.e., an average PF of 20% for the initial core and an average PF of 27.7% for reloads. Case 8.9.3 has a maximum PF of 32.6% for the initial core and 38.3% for the reloads, with 5.9% of the fuel compact volume in the reloads having a PF greater than 35%. This is within the maximum PF limit of 40%, but slightly exceeds the limit of 5% on the total core fuel compact volume having a PF greater than 35%. The minimum fuel cycle length goal of 540 EFPD (startup to shutdown) was achieved for all cycles except cycle 2 and cycle 3, which ran for 530 EFPD. Again, it is important to note that, as in the binary-fuel-particle core design effort, the PF constraints combined with the fuel cycle length goal of 540 EFPD (which requires relatively heavy fuel loadings) significantly limited the flexibility to fuel zone the core.

The details of the physics design for Case 8.9.3 are presented in Section 4.1. The temperature, fuel performance, and fission product release predictions for this case as obtained from

SURVEY and TRAFIC-FD are presented in Section 4.3.

4.2.12 Case 8.10

Table 1-1 indicates that the U-235 enrichment for the fuel particles in the single-fuel-particle/single enrichment core design is supposed to be ~14%. This is consistent with the U-235 enrichment of the fuel particle that is currently being developed and qualified by the NGNP/AGR Fuel Program [Plan 2007]. However, it was determined during the binary-fuel-particle core design work that a U-235 enrichment of 14% is not compatible with the PF limits and the cycle length goal adopted for the CPA. Consequently, as previously noted, a U-235 enrichment of 15.5% was selected for the fuel particles in the single-fuel-particle/single enrichment design iterations based on the effective enrichment for the reloads in the binary-fuel-particle design case 7.9.

Case 8.10 was performed to determine the cycle length that can be achieved within the PF constraints of the CPA using a single 14% enriched fissile particle. This case involved performing a 2D GAUGE calculation through equilibrium cycle with the same radial zonings as Case 8.9.1. Burnup was simulated with all control rods out (no rod search) to determine the maximum fuel cycle length that could be achieved. This analysis showed that a cycle length of 486 EFPD (equivalent to 90% availability over a 540 calendar day cycle) should be achievable (with some reactivity margin) using only 14% LEU particles. A DIF3D/SURVEY/TRAFIC-FD analysis was not performed for this case.

Table 4-9. Summary of the Optimization Design Studies and Results

Parameter	Case							
	7.9	**8.1**	**8.2**	**8.3**	**8.4**	**8.5**	**8.6.1**	**8.6.2**
Sequence (1=first)	1	2	3	4	5	6	7	8
Design based on	N/A	7.9	8.1	8.1	8.3	8.1	8.5	8.6.1
Description	Binary particle final design (no shuffling)	Single particle design, 2 particles, 2 enrichments (LEU/NU)	1-day ΔEFPD @ 280 EFPD, small K-band during 1-day ΔEFPD, 1 cycle	Small K-band, custom K-search, new s-curve, 1 cycle	An order of magnitude tighter DIF3D fission source (point wise & avg.) convergence	SegA-IC-7.9% enrich, SegB-IC & all reloads 15.5% enrich, 10% less HM in SegA-IC, IC only 540 EFPD, new s-curve	Single enrichment of 15.5% (all segments & cycles,) 4x more FBP in SegA-IC, 10% more U-235 in reloads, coarse axial mesh	Fine axial mesh
Conclusion	N/A	Worse Perfor/metal release	Power and temperature "spiking" investigations do not contribute to single particle design			Alternate single particle design	RPF*APF increased 11%	Better Perfor/metal release
Time-averaged max. fuel temp. (°C) Segment 1 - Load1 Segment 1 – Load 2 (Segment 2 - Load1	 1115 1213 1137	 1113 1216 1137	 1115 - -	 1114 - -	 1114 - -	 1248 1253 1148	 1199 1284 1185	 1185 1275 1173
Max. fuel temp. (°C)	1480	1462	Only 1 cycle – results not comparable			1522	1560	1563
RPF at max. fuel temp.	1.54	1.56				1.61	1.63	1.63
APF at max. fuel temp.	1.16	1.01				1.20	1.29	1.31
RPF*APF	1.79	1.58				1.90	2.10	2.14
Max. fuel temp. location (col/sub/layer/point) (time (cycle#-EFPD))	11/7/10/5 (C2-430)	11/7/10/5 (C2-450)	25/7/10/5 (C1-491)	25/7/10/5 (C1-490)	25/7/10/5 (C1-490)	19/5/10/5 (C4-250)	19/5/10/1 (C2-210)	19/5/10/5 (C2-210)
Max Initial cycle PF (%) (% compacts >35%)	35.5 (3.3)	42.1 (36)	42.1 (36)	42.1 (36)	42.1 (36)	40.6 (9.9)	27.1	27.1
Max Reloads PF (%) (% compacts >35%)	38.5 (6.1)	29.9	29.9	29.9	29.9	35.2 (1)	38.8 (11.9)	38.8 (11.9)
Max SiC Fail Fract.	1.1×10^{-4}	1.4×10^{-4}	Only 1 cycle – results not comparable			1.5×10^{-4}	3.5×10^{-4}	2.3×10^{-4}
Max Exposed kernel Fail Fract (lim=5×10^{-5})	1.3×10^{-5}	1.5×10^{-5}				1.4×10^{-5}	2.2×10^{-5}	1.7×10^{-5}
Max Ag-110m Cumulative Rel. Frac. (lim=5×10^{-4})	1.3×10^{-3}	3.6×10^{-3}				1.7×10^{-3}	9.3×10^{-3}	6.7×10^{-3}
Max Cs-137 Cumulative Rel. Frac. (lim=1×10^{-5})	4.2×10^{-5}	5.6×10^{-5}				8.6×10^{-5}	2.0×10^{-4}	1.3×10^{-4}

Table 4-10. Summary of the Optimization Design Studies and Results (continued)

Parameter	Case						
	8.7.5	**8.8.1**	**8.8.2**	**8.9.1**	**8.9.2**	**8.9.3**	**8.10**
Sequence (1=first)	9	10	11	12	13	14	15
Design based on	8.6.1	8.7.5	8.7.5	8.8.2	8.9.1	8.9.1	8.9.1
Description	Half FBP in SegA-IC, same IC buf-zoning as reloads, move 3% SegB-IC fuel from rows1&2 to row3, move 10% SegA-RL from row2 to 3, 5% lower SegA-RL buff, move 5% SegB-IC FBP from row3 to row1, 3 cycles	3-4-3 axial zoning (top-zone rel nom: IC=138%,RL=105%), move 5% SegA-RL from row3 to row2	2-6-2 axial zoning (top-zone rel nom: IC=115%, RL=110%)	move 10% SegA-RL2 FBP from row1 to row3, move 15% all RLs FBP from top-zone to bottom-zone	Half FBP in SegA-IC, move 10% all IC FBP from top to bottom zone	Fine axial mesh, 5 cycles	Single enrichment of 14% (all segments & cycles,) ARO burn, 90% availability
Conclusion	RPF*APF decreased 2%	RPF*APF increased 34%	RPF*APF decreased 28%	Better performance & metal release	RPF*APF increased 4%	Single particle final design (no shuffling)	Single particle backup design (no shuffling)
Time-averaged max. fuel temp. (°C) Segment 1 - Load1 Segment 1 – Load 2 Segment 2 – Load 1	 1193 1224 1168	 1186 1271 1128	 1179 1259 1154	 1179 1253 1151	 1184 1253 1153	 1171 1243 1139	DIF3D/ BURP/ SURVEY/ TRAFIC-FD not run (2D GAUGE only)
Max. fuel temp. (°C)	1620	1690	1565	1563	1590	1529	
RPF at max. fuel temp.	1.73	1.74	1.65	1.58	1.60	1.62	
APF at max. fuel temp.	1.19	1.58	1.20	1.41	1.45	1.14	
RPF*APF	2.06	2.75	1.98	2.23	2.32	1.85	
Max. fuel temp. location (col/sub/layer/point) (time (cycle#-EFPD))	34/3/10/1 (C2-420)	15/5/10/1 (C2-70)	34/3/10/1 (C2-420)	31/6/10/1 (C1-500)	34/6/10/1 (C2-410)	34/6/10/5 (C2-410)	
Max Initial cycle PF (%) (% compacts >35%)	29.7	39.1 (3.9)	32.6	32.6	32.6	32.6	
Max Reloads PF (%) (% compacts >35%)	41.2 (6.4)	36.5 (3.5)	38.3 (5.9)	38.3 (5.9)	38.3 (5.9)	38.3 (5.9)	
Max SiC Fail Fract	2.2×10^{-4}	1.8×10^{-3}	2.5×10^{-4}	2.1×10^{-4}	2.3×10^{-4}	1.5×10^{-4}	
Max Exposed kernel Fail Fract (lim=5×10^{-5})	1.6×10^{-5}	8.3×10^{-5}	1.8×10^{-5}	1.6×10^{-5}	1.7×10^{-5}	1.4×10^{-5}	
Max Ag-110m Cumulative Rel. Frac (lim=5×10^{-4})	9.1×10^{-3}	1.6×10^{-2}	9.5×10^{-3}	8.2×10^{-3}	8.4×10^{-3}	5.7×10^{-3}	
Max Cs-137 Cumulative Rel. Frac (lim=1×10^{-5})	1.2×10^{-4}	1.4×10^{-3}	1.5×10^{-4}	1.2×10^{-4}	1.3×10^{-4}	7.7×10^{-5}	

4.3 Fuel Performance/Fission Product Release Analysis (Case 8.9.3)

The modified SURVEY code (version SURVEY_August_2009) was run for core design Case 8.9.3, the final single-fuel-particle/single-enrichment core design (without fuel shuffling), using the binary input data file generated by SORT3D from DIF3D output. Using the SURVEY output results as input, TRAFIC-FD was used to calculate Cs-137 and Ag-110m release.

4.3.1 SURVEY/THERM Results

The volume fast fluence distribution calculated by SURVEY/THERM for Segment 1 is shown in Figure 4-15. The fast fluences for Segment 2 are about the same as Segment 1 for the various core fuel loads (i.e., the fast fluences peak in cycles 3 and 5 for Segment 1 and in cycles 2 and 4 for Segment 2. The peak fast fluence is about 4.2×10^{25} n/m^2 (E >0.18 Mev), which is less than the design limit of $\leq 5 \times 10^{25}$ n/m^2. The core volume burnup distribution for Segment 2 is shown in Figure 4-16 (the burnups for Segment 1 are slightly lower). The peak burnup in Segment 2 is 17.6% FIMA in cycle 2. The peak burnup for Segment 1 is 16.5% FIMA in cycle 5.

The volume temperature distributions calculated by SURVEY are shown in Figures 4-17 through 4-24. With respect to the terminology used in Figures 4-15 through 4-22, SURVEY uses a different terminology than used in the physics analysis discussions in previous sections. The correspondence is defined below.

	Segment A (or 1)		Segment B (or 2)	
Cycle #	Fuel Load #	Reload #	Fuel Load #	Reload #
1	1	-	1	-
2	2	1	1	-
3	2	-	2	2
4	3	3	2	-
5	3	-	3	4

Figures 4-17 through 4-20 give maximum fuel temperature volume distributions for Segments 1 and 2. Plots are given for both the full-core volume and the hottest 5%. The maximum temperatures in each plot are listed numerically at the bottom of the figures. The maximum fuel temperature for Case 8.9.3 is 1534°C in both Segment 1, fuel load 2 and Segment 2, fuel load 1. Figures 4-21 through 4-24 provide time-average temperature volume distributions for the two segments. The maximum time-averaged fuel temperature for Case 8.9.3 is 1249°C[13] in segment 1, fuel load 2, which is below the design guideline “limit” of 1250°C.

[13] The maximum time-averaged fuel temperature for Segment 2, fuel load 3 is given as 1300°C in Figure 4-23, but this temperature is for one cycle rather than two (because DIF3D was run for only 5 cycles).

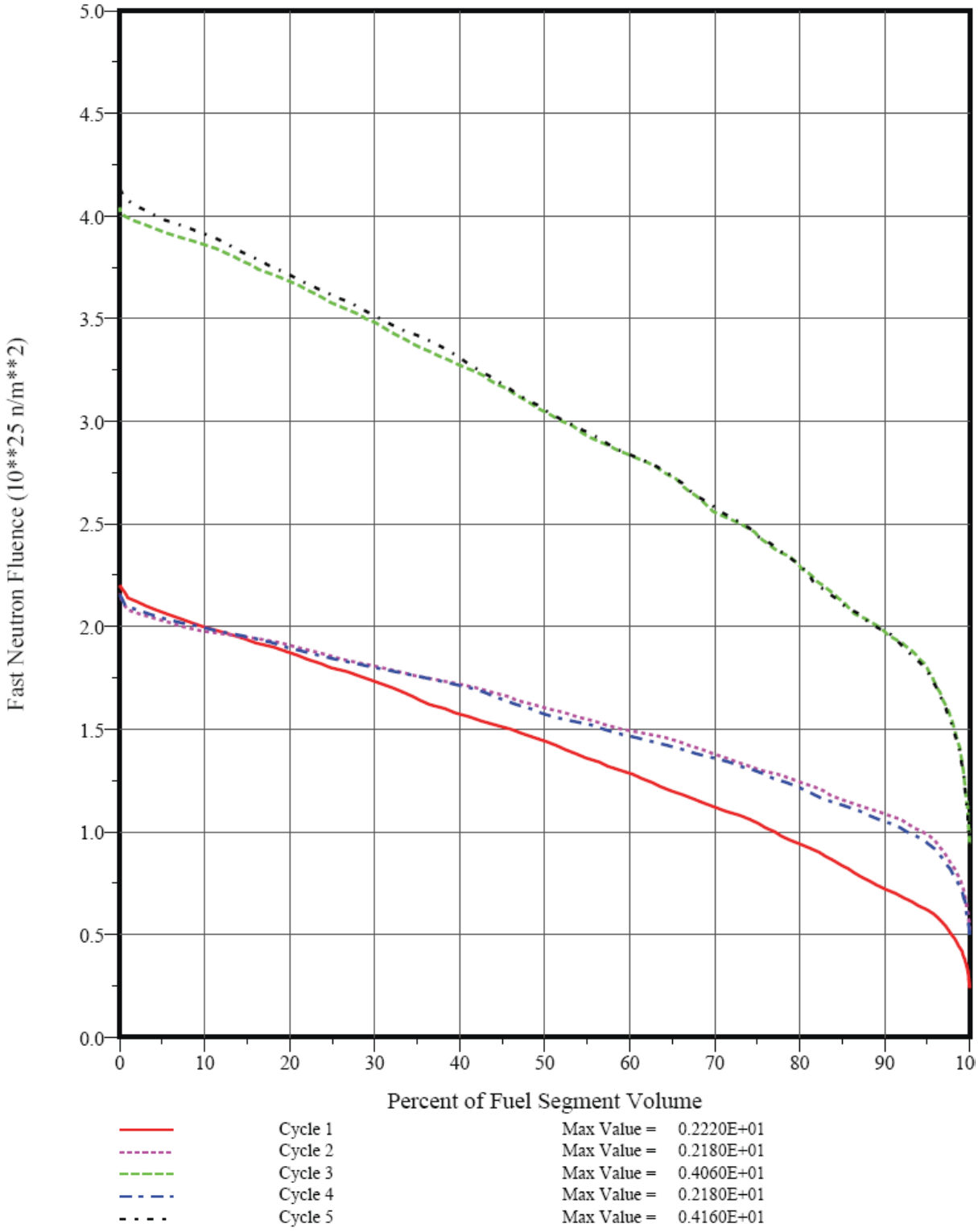

Figure 4-15. Fast Fluence Volume Distribution for Segment 1 (Case 8.9.3)

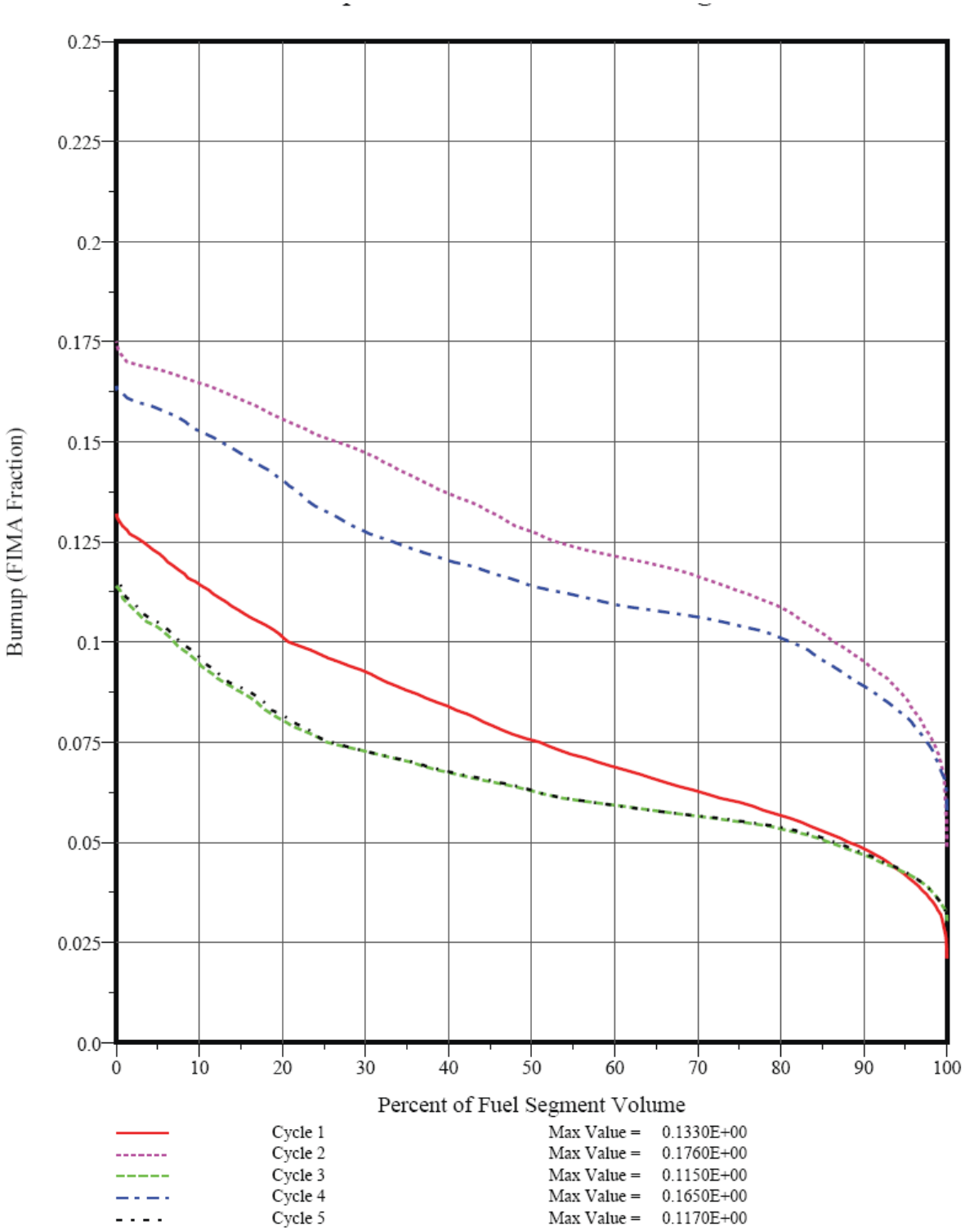

Figure 4-16. Fuel Particle Burnup Volume Distribution for Segment 2 (Case 8.9.3)

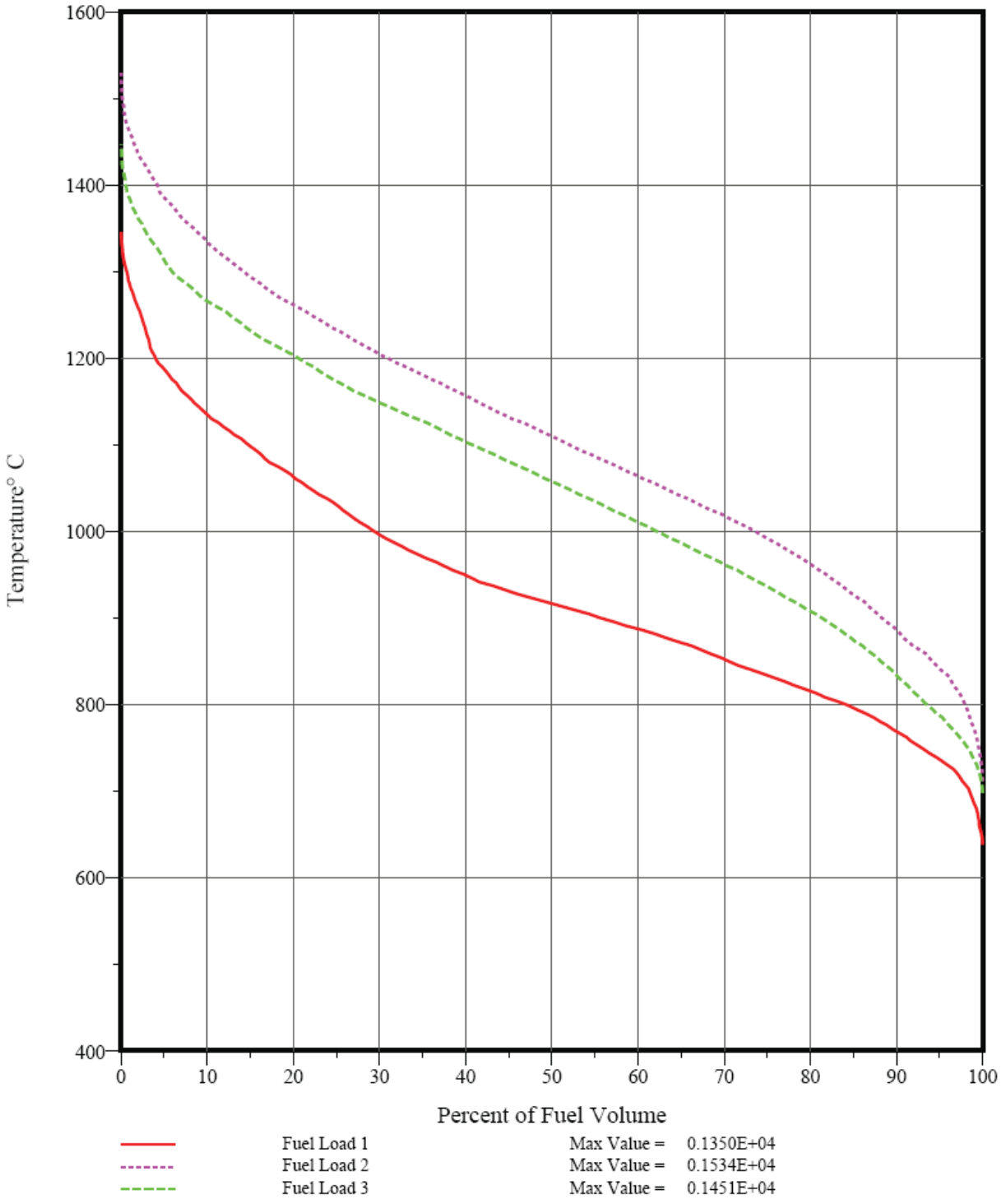

Figure 4-17. Peak Fuel Temperature Volume Distribution for Segment 1 (Case 8.9.3)

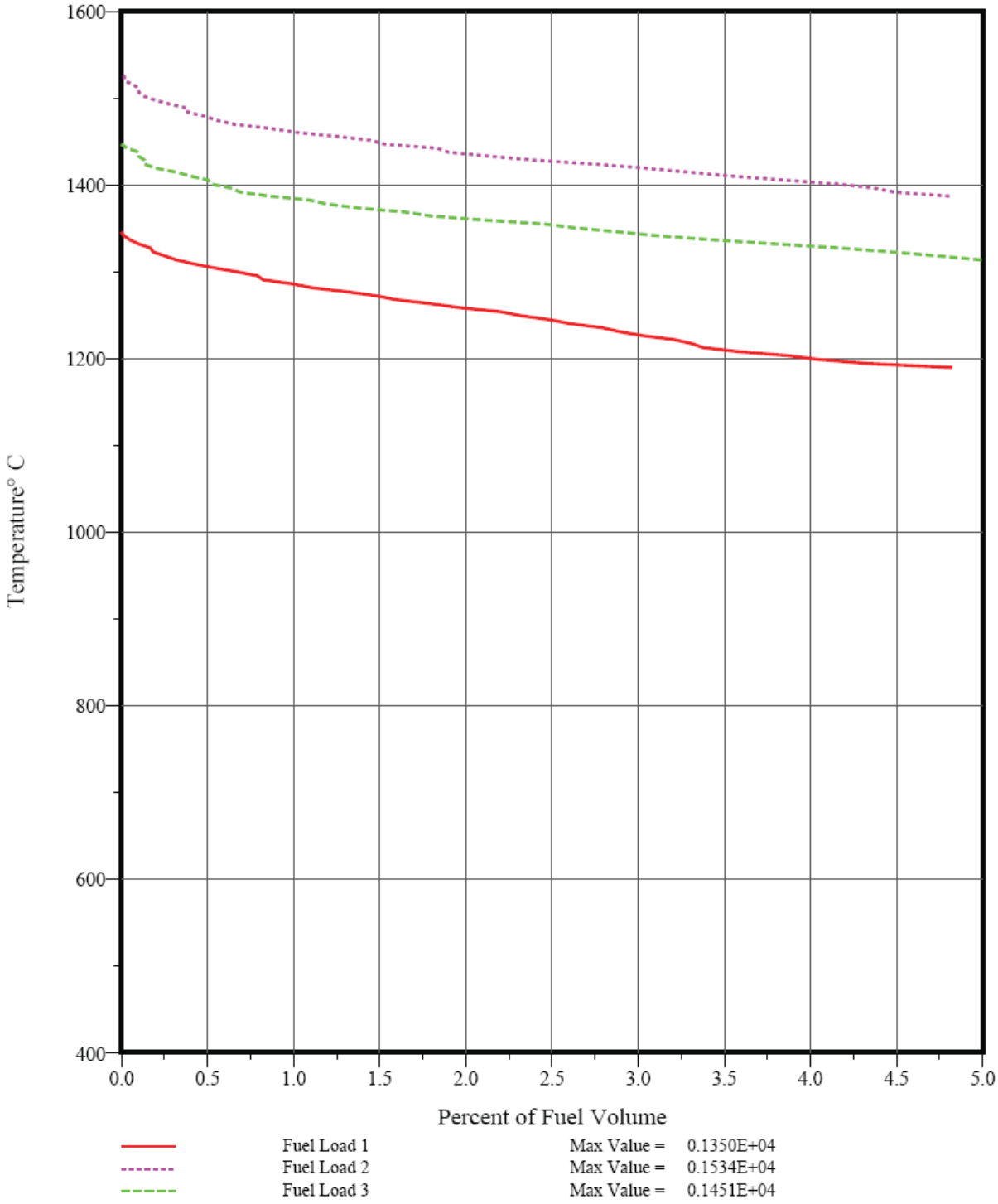

Figure 4-18. Peak Fuel Temperature Volume Distribution for Segment 1 (0-5%)

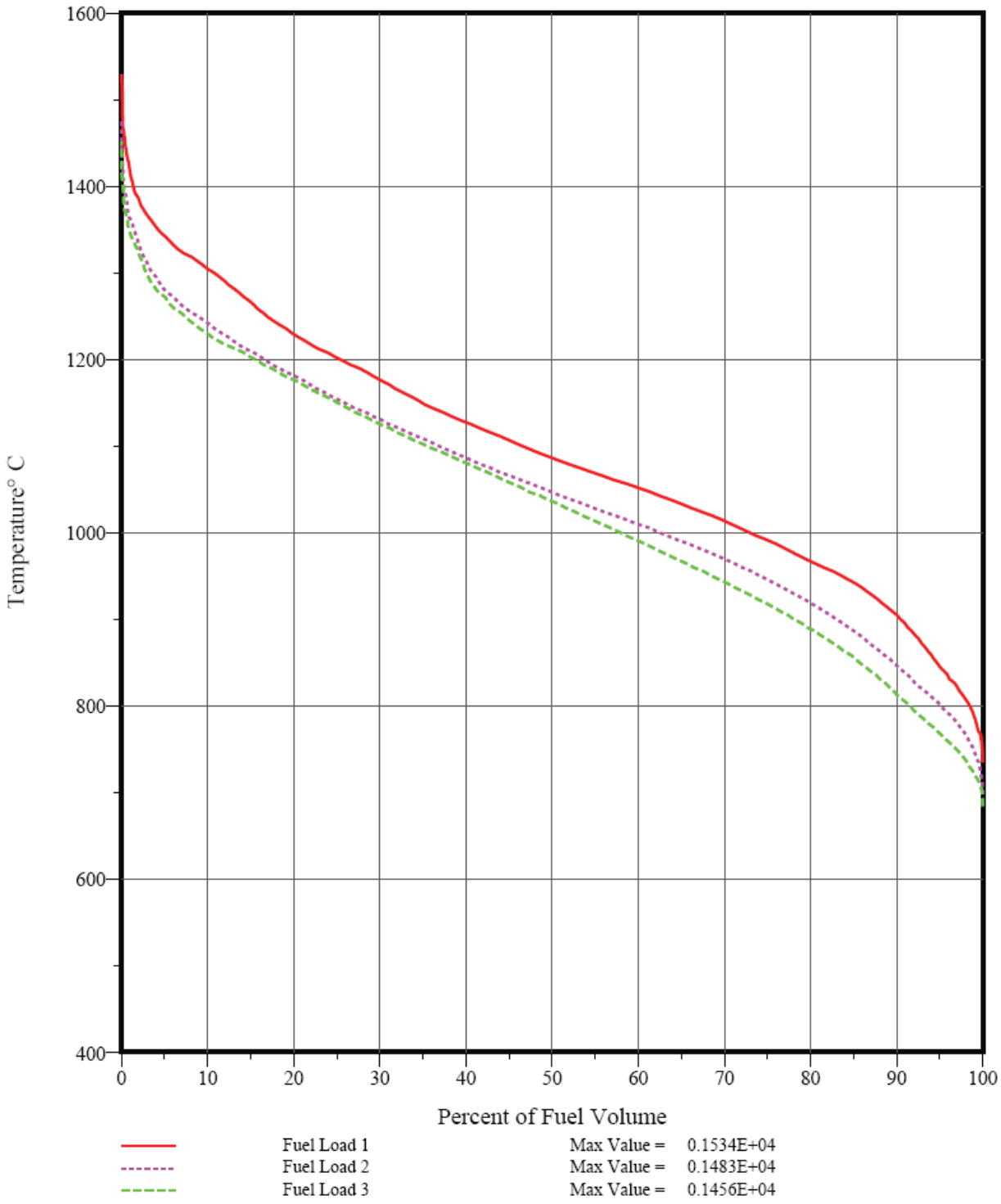

Figure 4-19. Peak Fuel Temperature Volume Distribution for Segment 2 (Case 8.9.3)

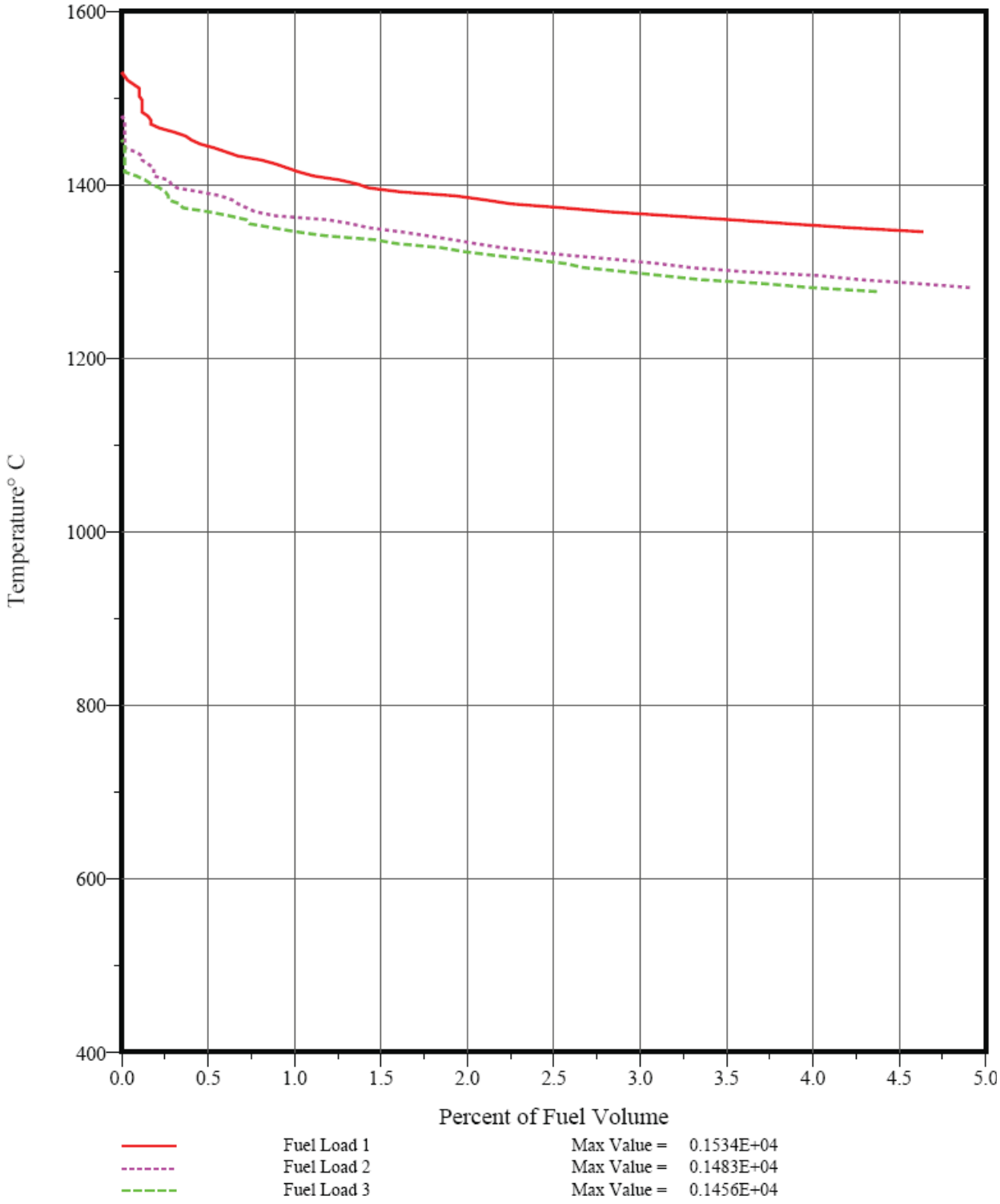

Figure 4-20. Peak Fuel Temperature Volume Distribution for Segment 2 (0-5%)

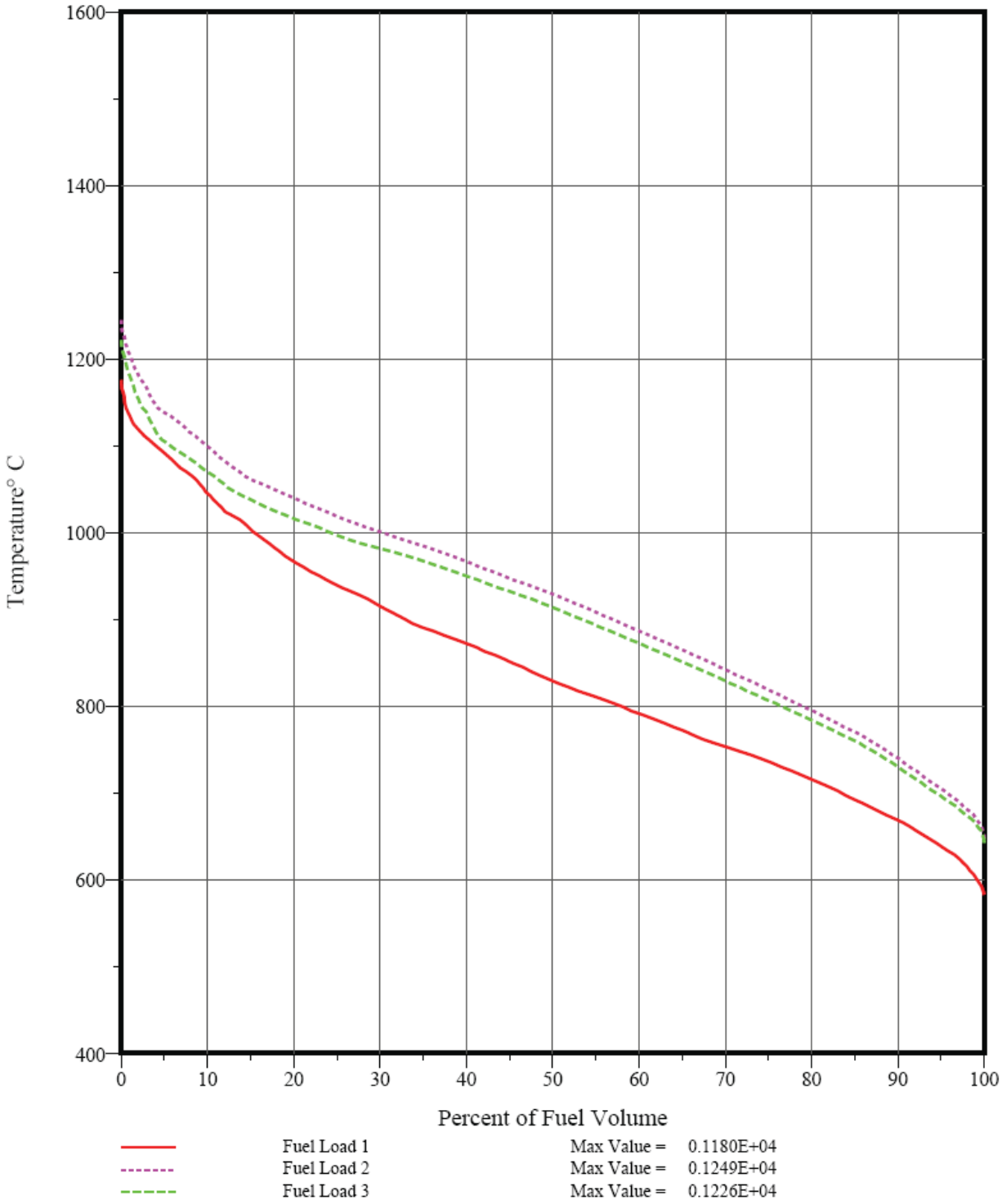

Figure 4-21. Time-Ave. Fuel Temperature Volume Distribution for Segment 1 (Case 8.9.3)

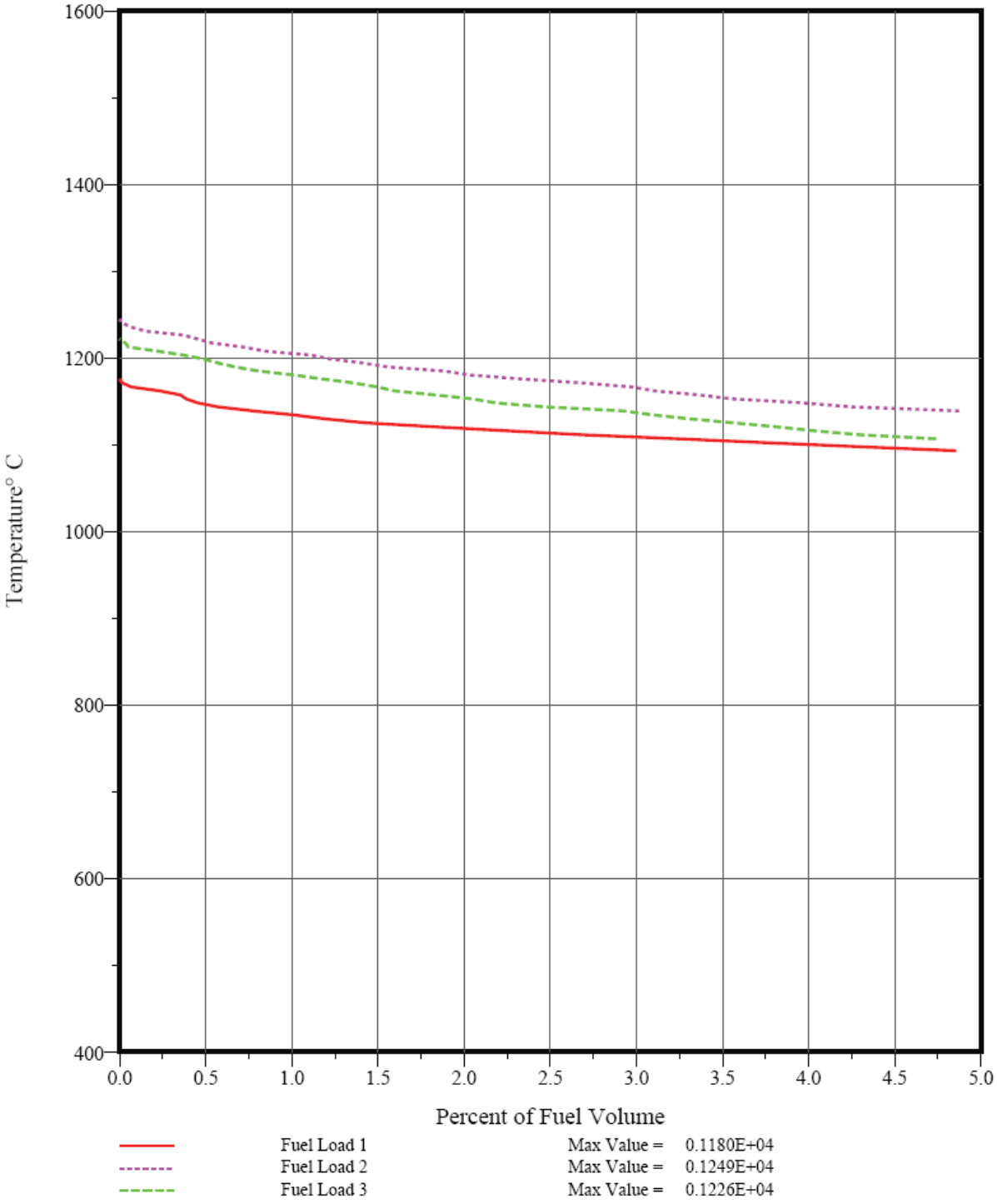

Figure 4-22. Time-Ave. Fuel Temperature Volume Distribution for Segment 1 (0-5%)

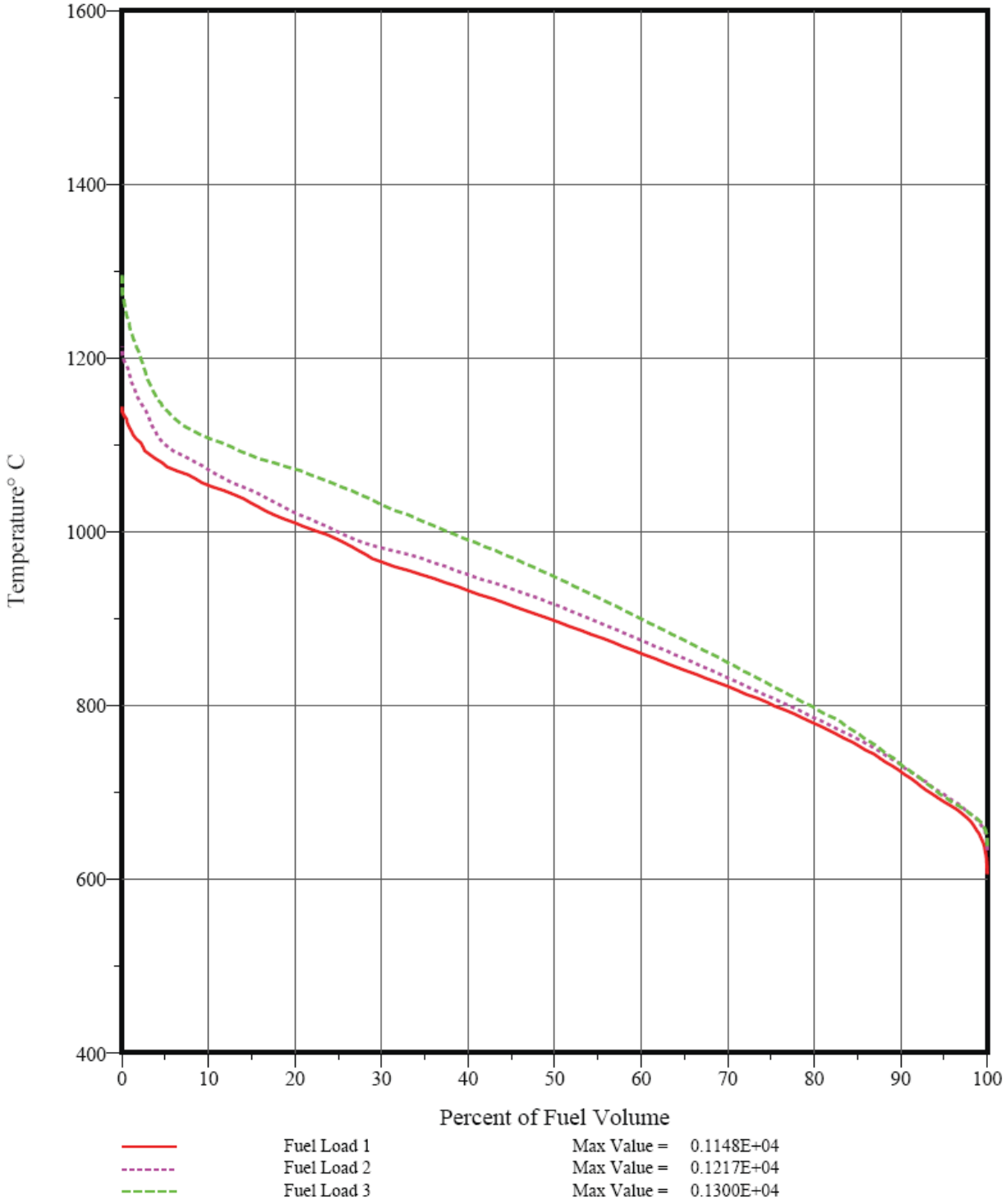

Figure 4-23. Time-Ave. Fuel Temperature Volume Distribution for Segment 2 (Case 8.9.3)

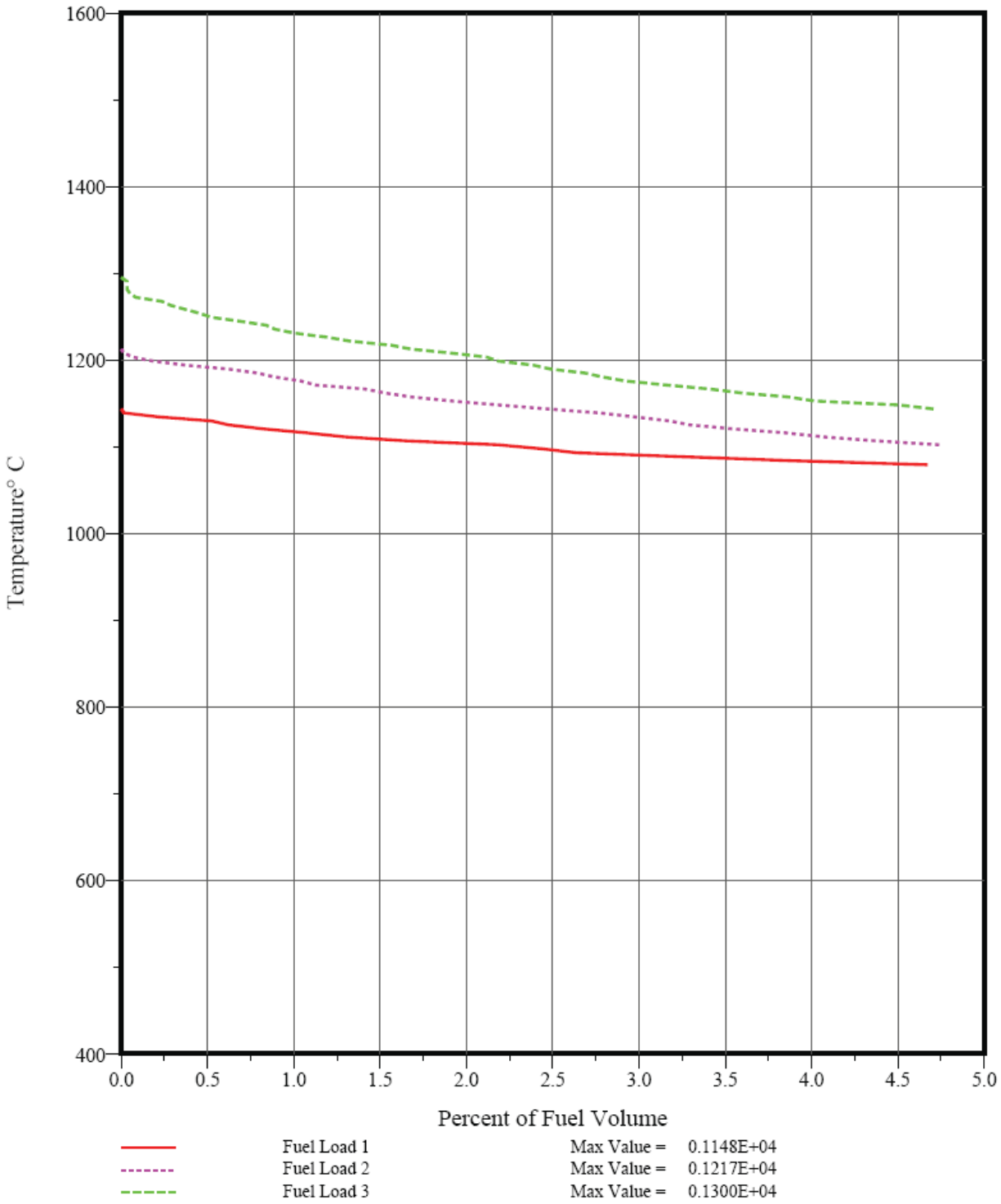

Figure 4-24. Time-Ave. Fuel Temperature Volume Distribution for Segment 2 (0 – 5%)

4.3.2 SURVEY/PERFOR Results

Based upon the burnups, fast fluences, and temperatures calculated by SURVEY/THERM, the fuel performance of core design Case 8.9.3 was calculated by SURVEY/PERFOR using the component models described in Section 2.3

The total core SiC failure fraction as a function of operating time is shown in Figure 4-25. The maximum SiC defect fraction is 1.5×10^{-4}. The plotted values are on the sum of the as-manufactured SiC defect fraction (f_M in the FDDM nomenclature) and the in-service SiC failure probability as a result of FP/SiC reactions (P_{SR}) plus kernel migration (P_{KM}) plus thermal decomposition (P_{SD}) plus heavy-metal dispersion as result of a defective IPyC layer. The in-service SiC failure is dominated by FP/SiC reactions; kernel migration and SiC thermal decomposition are negligible. The amount of in-service SiC failure peaks at the end of cycle 3 at about 1.0×10^{-4} and is less than the as-manufactured SiC defect fraction in cycles 4 and 5.

This SiC failure will primarily result in fission metal release. It will also contribute to a lesser degree to the exposed kernel fraction to the extent that OPyC layers are initially defective (the GT-MHR fuel product specification allows 1% defective OPyC layers) or fail in service (the FDDM/F model ramps up from zero to a constant 3% OPyC failure at a fast fluence of 2×10^{25} n/m^2).

The total core exposed kernel fraction as a function of operating time is shown in Figure 4-26. The maximum exposed kernel fraction is about 1.4×10^{-4}. Exposed kernels result from pressure-vessel (PV) failure of standard particles (i.e., particles without as-manufactured defects) and particles with a variety of as-manufactured defects. The initial value is very low because any exposed kernels in the as-manufactured fuel compacts would be counted as heavy-metal contamination. The contribution from PV failure of standard particles is insignificant because the failure probability is predicted to be extremely low. The dominant sources of exposed kernels are: (1) PV failure of particles with missing buffer layers, (2) PV failure of particles with defective or failed OPyC layers, and (3) OPyC failure on particles with defective or failed SiC layers. As stated above, 3% OPyC failure is predicted at a fast fluence of 2×10^{25} n/m^2. On a core-average basis, most of the fissile particles with missing buffers (~90%) are predicted to fail. The contribution from OPyC failure on particles with defective or failed SiC layers is about 0.03 times the SiC failure fractions given in Figure 4-26, which is a maximum of about 4.5×10^{-6}.

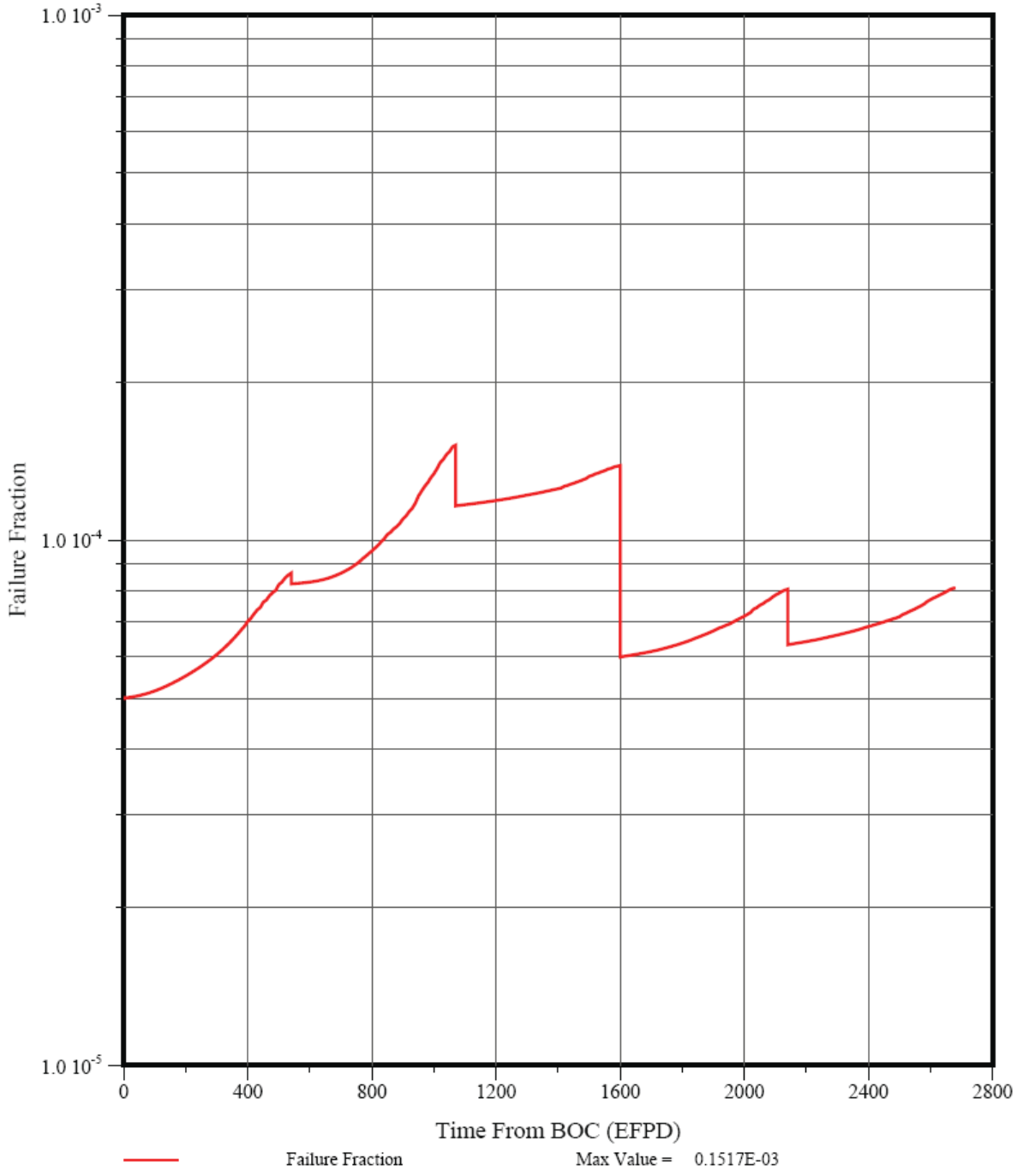

Figure 4-25. Total SiC Failure Fraction (Case 8.9.3)

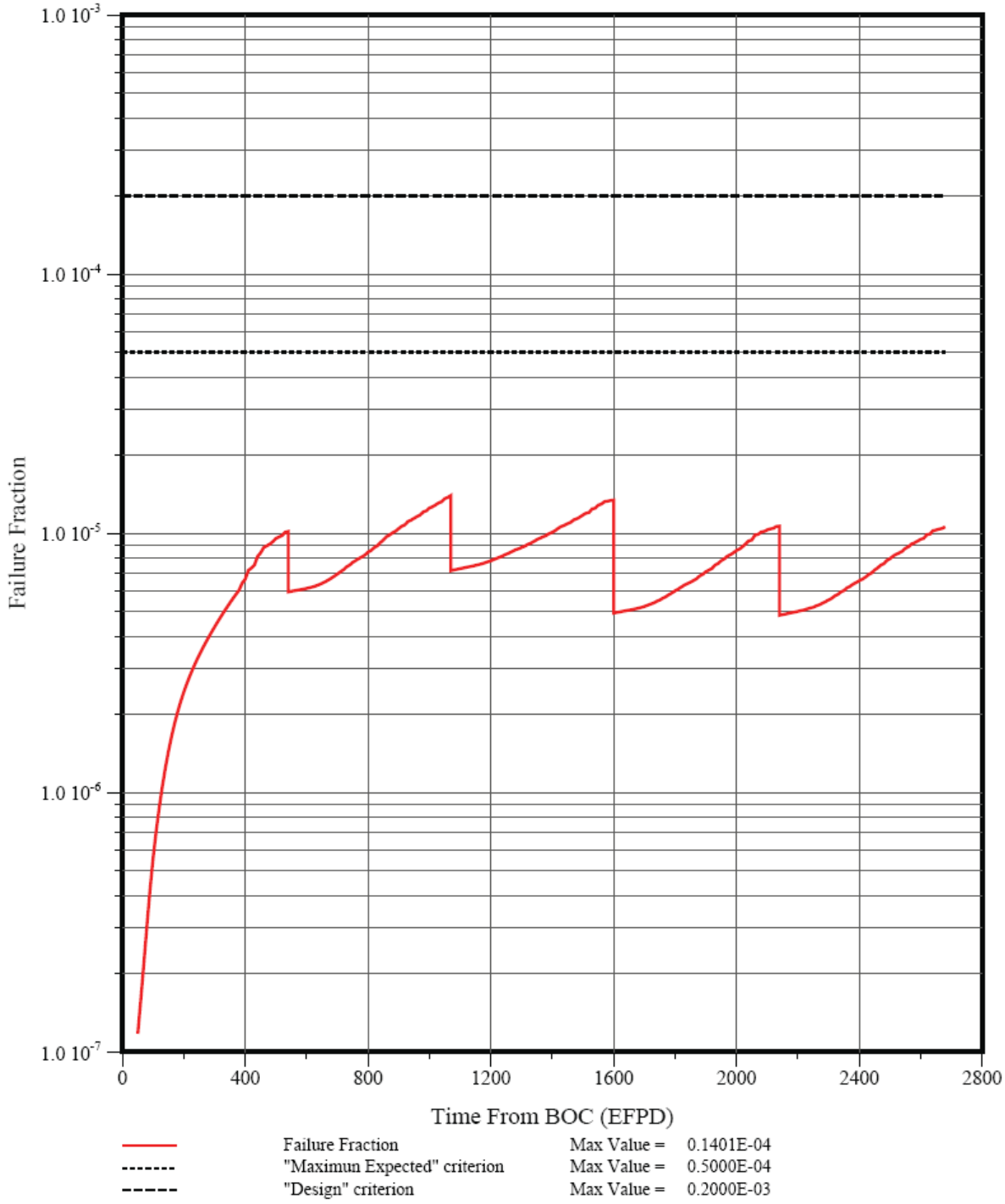

Figure 4-26. Exposed Kernel Fraction (Case 8.9.3)

For earlier MHR designs, including the 350-MWt steam-cycle MHTGR, the predicted exposed kernel fraction was dominated by the PV failure of fuel particles having a missing buffer layer [Jovanovic 1989]. The reasons were that the MHTGR fuel product specification allowed a missing-buffer fraction of 5×10^{-5}, and a minimal in-service FP/SiC corrosion failure was predicted (the MHGTR core outlet temperature was 687°C; hence, the fuel temperatures were considerably lower than predicted here). During the commercial GT-MHR program, the allowable missing-buffer fraction was reduced to 1×10^{-5} [Munoz 1995], and its contribution to in-service failure became less important.

The total core exposed kernel fraction is very low – about a factor of four lower than the "Maximum Expected" in-service failure limit of 5×10^{-5} (see Table 2-10). Exposed kernels result in release of both fission gases and fission metals. Given this low predicted value, the fission gas release (R/B) will be dominated by the contribution from heavy-metal contamination (see Eqn. (4-1)).

The release rate-to-birth rate (R/B) ratios (equivalent to the fractional release for steady-state calculations such as these) for 2.8-hr Kr-88 and 8-day I-131 were also calculated by SURVEY/PERFOR using the FDDM/F fission gas release models for hydrolyzed UCO fuel (Section 4.1.3). These R/Bs as a function of time are shown in Figures 4-27 and 4-28. These radionuclides were chosen because they are typically dominant contributors to off-site accident doses. The predicted core-average maximum R/B values are 1.1×10^{-6} for Kr-88 and 2.5×10^{-6} for I-131.

[FDDM/F 1987] contains fission gas release models for both unhydrolyzed and hydrolyzed UCO exposed kernels. The difference at steady-state is not particularly large (a factor of 1.7). The hydrolyzed model was chosen because the GA and AREVA preferred candidate prismatic NGNP configurations currently include a steam generator in the primary circuit. Under the present circumstances, the choice of gas release model is of little practical consequence because the predicted fission gas release is dominated by the contribution from heavy-metal contamination. The contribution from failed particles is low because the predicted exposed kernel fraction is very low as discussed above (primarily a result of the tight specification on allowable missing-buffer particles). Nevertheless, the peak predicted R/Bs are slightly above the "Maximum Expected" limits of 8.3×10^{-7} for Kr-88 and 2.0×10^{-6} for I-131 because of the high average fuel temperatures that are practically unavoidable with a 900°C core outlet temperature. The only effective way of reducing these R/Bs would be to tighten the specification on heavy-metal contamination.

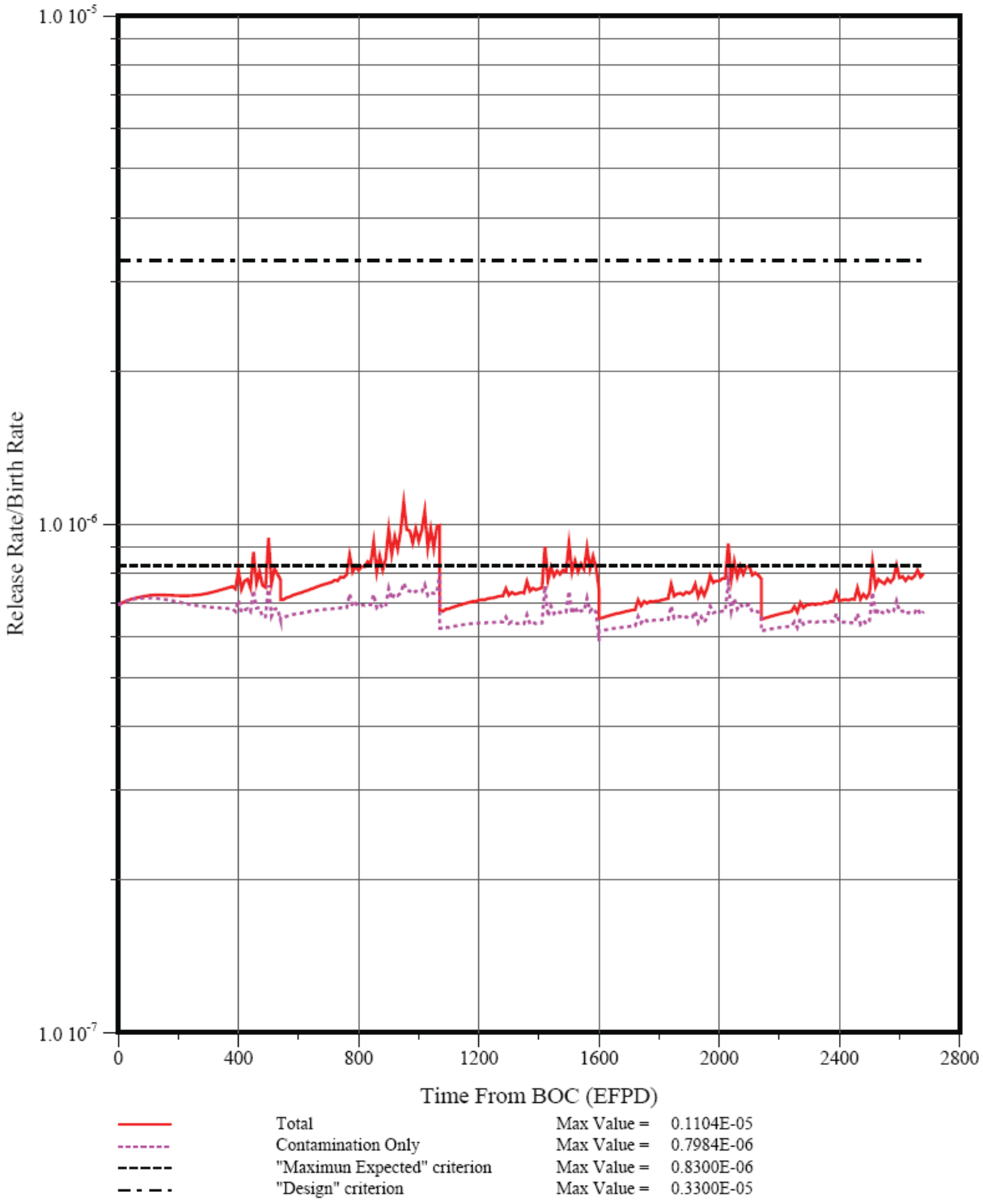

Figure 4-27. Core-Average R/B for Kr-88

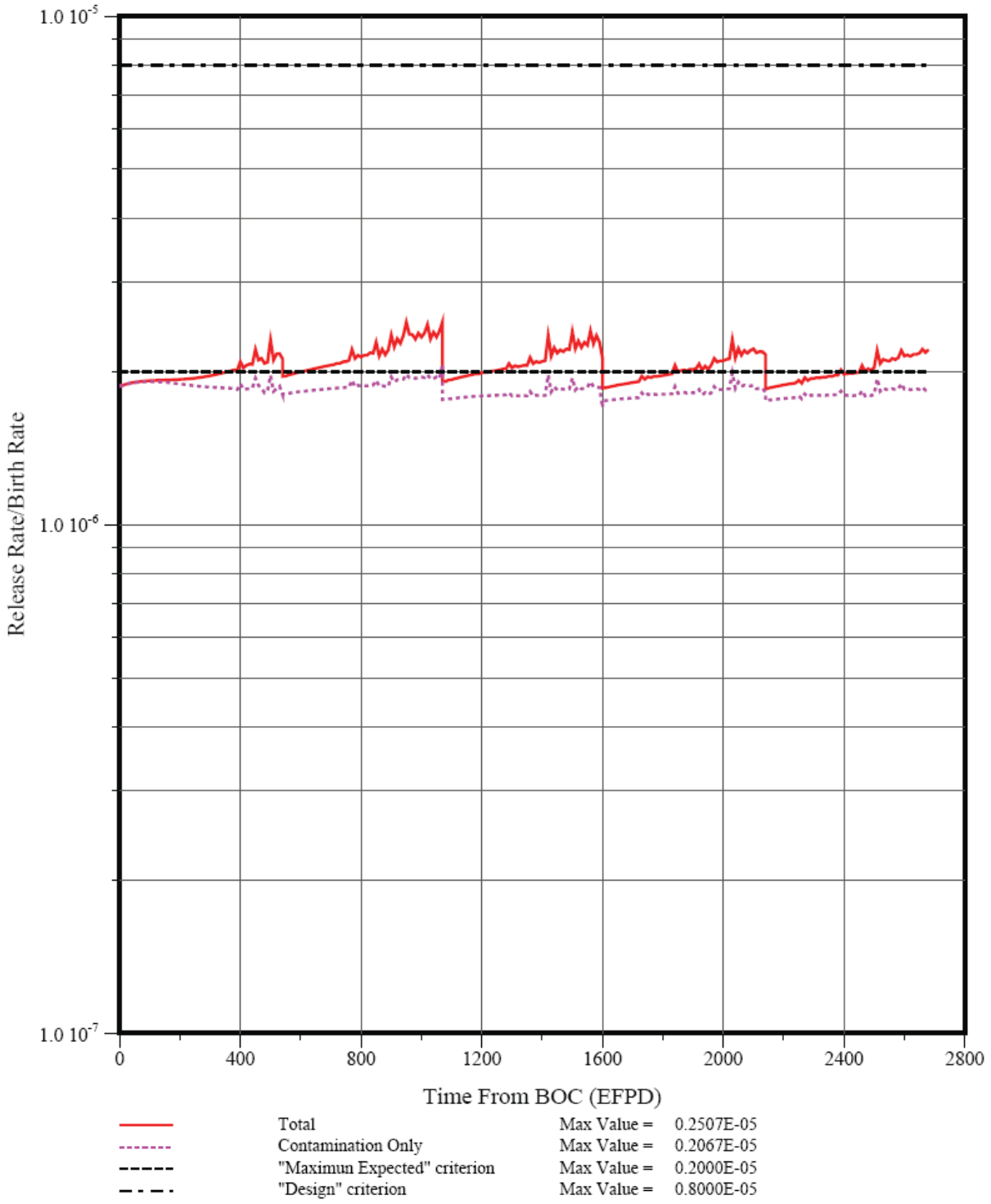

Figure 4-28. Core-Average R/B for I-131

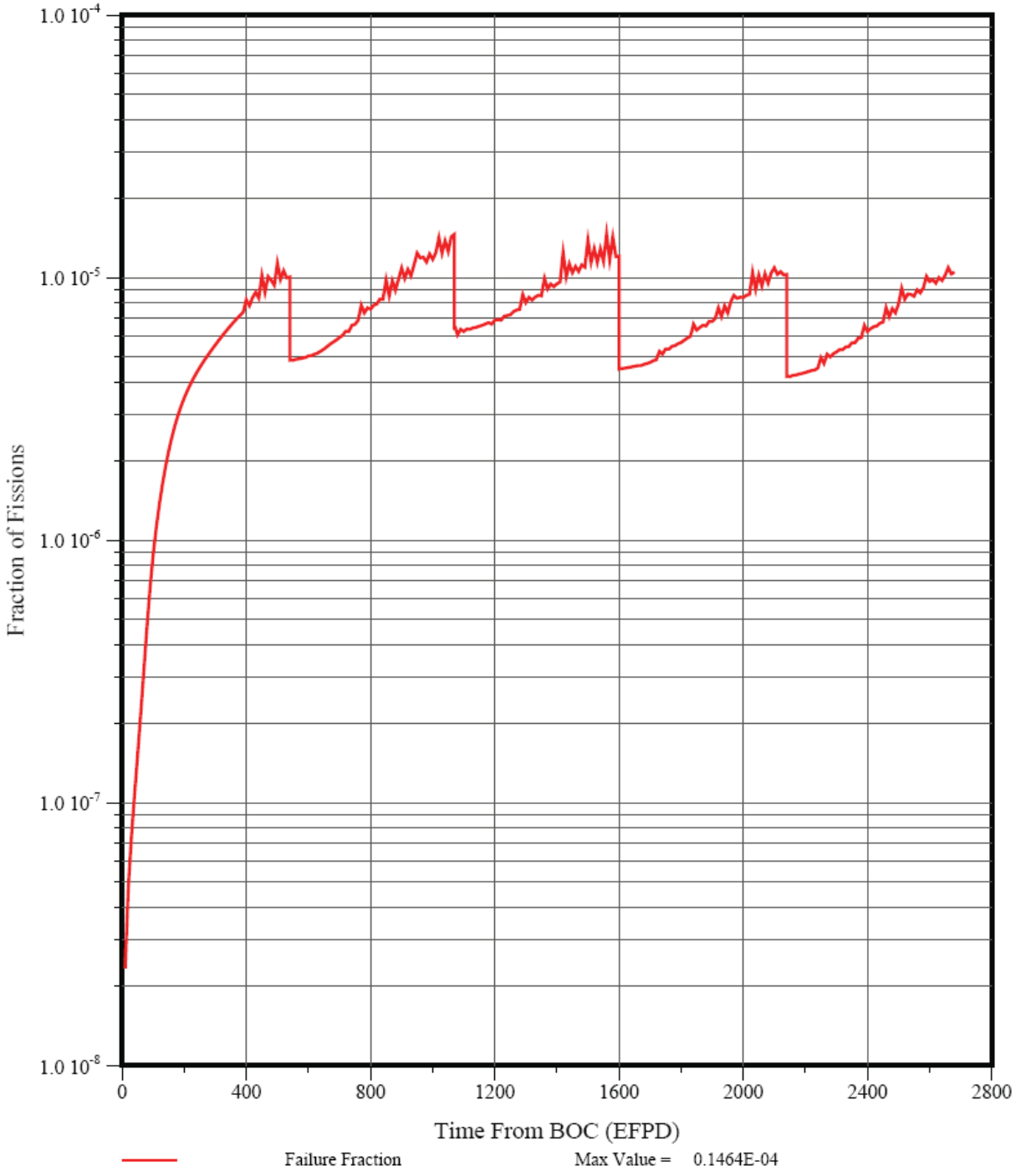

Figure 4-29. Fraction of Fissions in Failed Fissile Particles

The “spikes” in the calculated R/Bs were also evidenced in the calculated “fraction of fissions in failed particles” as shown in Figure 4-29 for the fissile particles. As discussed in Section 4.6 of [GA 2009b] and Section 3.2 of this report, these spikes are a manifestation of the fission density and temperature spikes in subcolumns adjacent to control rods that result from the large incremental control rod movements associated with the 10-day time steps used in DIF3D. A considerable effort was expended to eliminate or reduce the magnitude of this phenomenon based on the assumption that it is in large part responsible for the SiC failure and metallic fission product release predicted for the various core design iterations; however, as discussed in Section 3.2, these efforts resulted in only a modest reduction in the maximum fuel temperature for the case evaluated (Case 7.9) and had essentially no effect on the predicted fuel failure and fission product release. The significance of this is discussed further in Section 7.

4.3.3 TRAFIC-FD Results

The SURVEY/PERFOR results summarized in Section 4.3.2 were supplied as input to the TRAFIC-FD code which was used to predict the releases of Ag-110m and Cs-137 from the core for case 8.9.3.

The material property data (e.g., FP diffusivities in SiC coatings) required as input to TRAFIC-FD was taken from FDDM/F with two important exceptions. First, the KFA correlation for Ag diffusion in SiC coatings [Moormann 1987], [TECDOC 1997] was used instead of the FDDM/F correlation as recommended by a critical review of the Ag transport data in 1994 [Acharya 1994]. Use of the FDDM/F correlation would likely increase the calculated Ag-110m fractional release by a factor of five or more relative to the values reported herein based upon previous core analysis [PC-MHR 1994]. Secondly, no credit was taken for Cs retention in exposed kernels. The FDDM/F correlation for Cs diffusion in UCO kernels has an extremely large burnup dependence (i.e., FIMA to the fourth power]. This large burnup dependence for UCO kernels was inferred from the observed burnup dependence for Cs diffusion in ThO_2 kernels in the 1 - 6% FIMA range [Martin 1993]. This FDDM/F correlation was shown to grossly underpredict Cs release from UCO kernels at low burnups (2.5% FIMA) in the COMEDIE BD-1 test [Medwid 1993]; consequently, its use is not considered justified. An alternative would have been to use the German correlation for Cs diffusivity in LEU UO_2 which has no burnup dependence; however, this correlation would not necessarily be conservative for burnups greater than about 10% FIMA.

The predicted overall mass balance for 250-day Ag-110m is shown in Figure 4-30. The following “total” core (1/3 core because of symmetry) inventories are shown: (1) particle 1 (fissile), (2) particle (fertile), (3) matrix, (4) graphite, and (5) cumulative release into the coolant. The results are more easily interpreted by considering the corresponding inventories in each of the two core segments; the Ag-110m inventories in Segments 1 and 2 are shown in Figures 4-

31 and 4-32, respectively. When Segment 1 is reloaded after Cycles 1 and 3, the Ag-110m inventories in the particles, matrix, and graphite are reduced to zero as the irradiated fuel is replaced by fresh fuel; however, the inventory released into the coolant continues to accumulate. For Segment 2, the in-core inventories are zeroed out after Cycles 2 and 4 when that segment is reloaded.

The cumulative fractional release of Ag-110m into the coolant is shown in Figure 4-33. The cumulative fractional release at any time point is defined as the cumulative release into the He coolant from time zero to that time point divided by the cumulative birth in the core from time zero to that time point with both release and birth inventories corrected for decay (the cumulative birth includes the birth in the fuel in the core at any given time plus the birth in any previously discharged fuel loads). This cumulative fractional release for long-lived fission metals can be contrasted to the use of an instantaneous release rate-to-birth rate (R/B) for short-lived fission gases, including iodines. For noble gases, the action of the He purification system results in an effective upper-limit half life of about 4.5 hours (depending upon the fractional purification rate) [Hanson 2008]. Unlike the noble gases, the iodine and tellurium isotopes released from the core preferentially deposit ("plate out") in the primary circuit; however, the half lives of the radiologically important I and Te isotopes are short compared to the length of an irradiation cycle such that their plateout inventories approach equilibrium values corresponding to their R/B values throughout plant operation.

Figures 4-30 through 4-32 show that the total core Ag-110m inventory approaches an equilibrium value during each cycle since the cycle length of 540 EFPD is about two radioactive half lives. As seen in Figure 4-33, the cumulative fractional release of Ag increases rapidly during the first cycle even though the SiC failure and exposed kernel fractions are low. This is apparently because Ag is diffusing through the SiC layers of intact TRISO particles in the fuel that is operating at excessive temperatures in Segment 2 (see Figure 4-19). This conclusion is confirmed by Figures 4-31 and 4-32, which show that the inventory of Ag released to the coolant from Segment 2 in cycle 1 is approximately two orders of magnitude greater than released from Segment 1. In cycle 2, diffusive release from the fresh reload fuel in Segment 1 that is operating at excessive temperatures (see Figures 4-17 and 4-31) causes the cumulative Ag release to peak at 5.7×10^{-3}. This is about an order of magnitude greater than the "maximum expected" limit of 5.0×10^{-4}, and also exceeds the "design" limit of 5.0×10^{-3}.

The maximum fuel temperatures and, consequently, the SiC failure fractions and diffusive Ag release peak at the end of Cycle 2. Thus, during Cycle 3 and subsequent cycles, the cumulative Ag releases to the coolant decrease or go through minima during those time periods when the decay of the previously released Ag and the birth rate of "new" Ag exceed the release rate of "new" Ag from the core. By the end of cycle 5, the cumulative fractional release has

dropped to about 1.5 x 10^{-3}. During all cycles, the amount of Ag holdup by the matrix and graphite is minimal because almost all of the Ag released from the particles is released into the coolant (see Figures 4-30 through 4-32).[14]

[14] With lower core inlet and outlet temperatures, the matrix and graphite would be more effective release barriers.

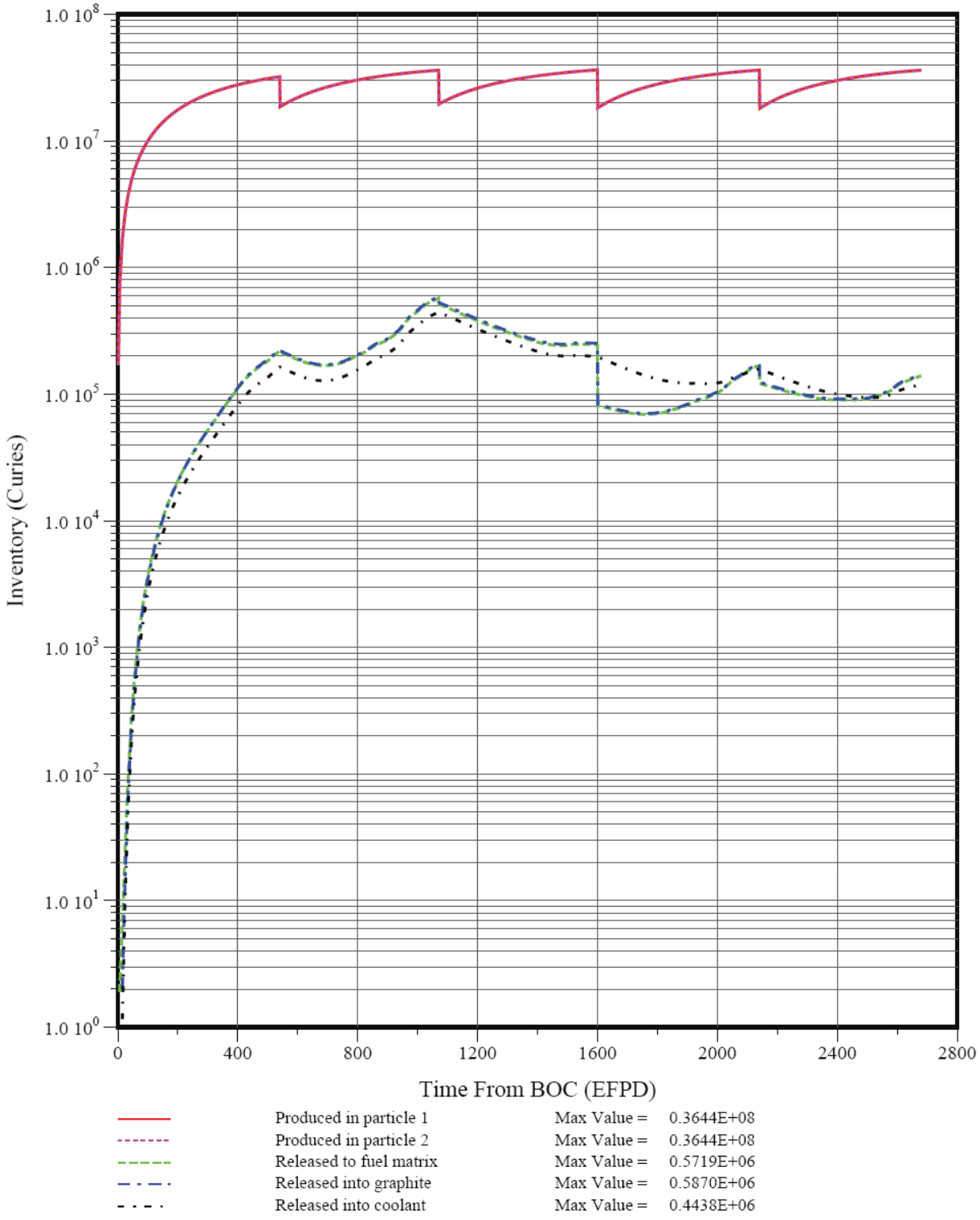

Figure 4-30. Full-core Ag-110m Inventories by Core Material Region (Case 8.9.3)

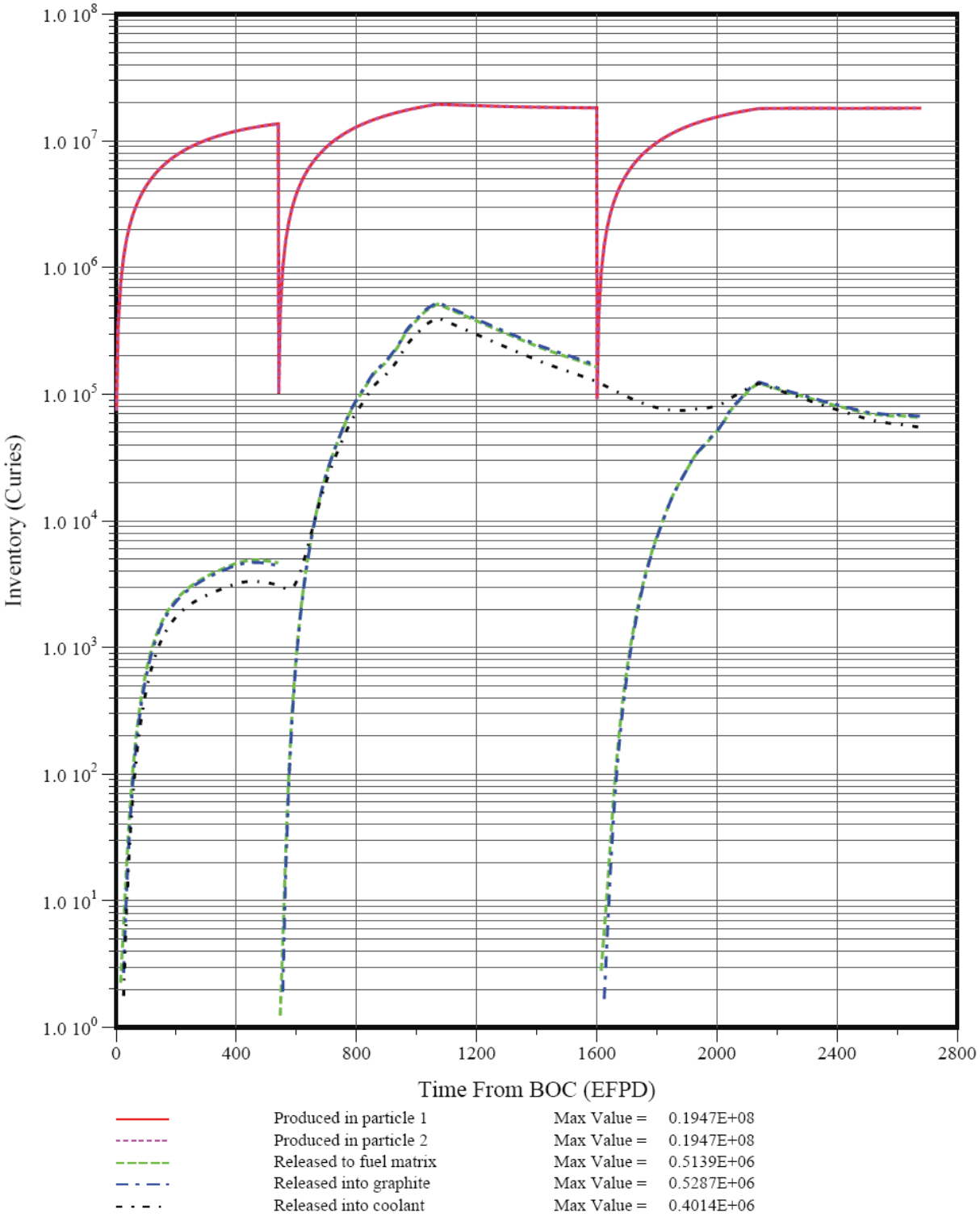

Figure 4-31. Ag-110m Inventories in Core Segment 1 (Case 8.9.3)

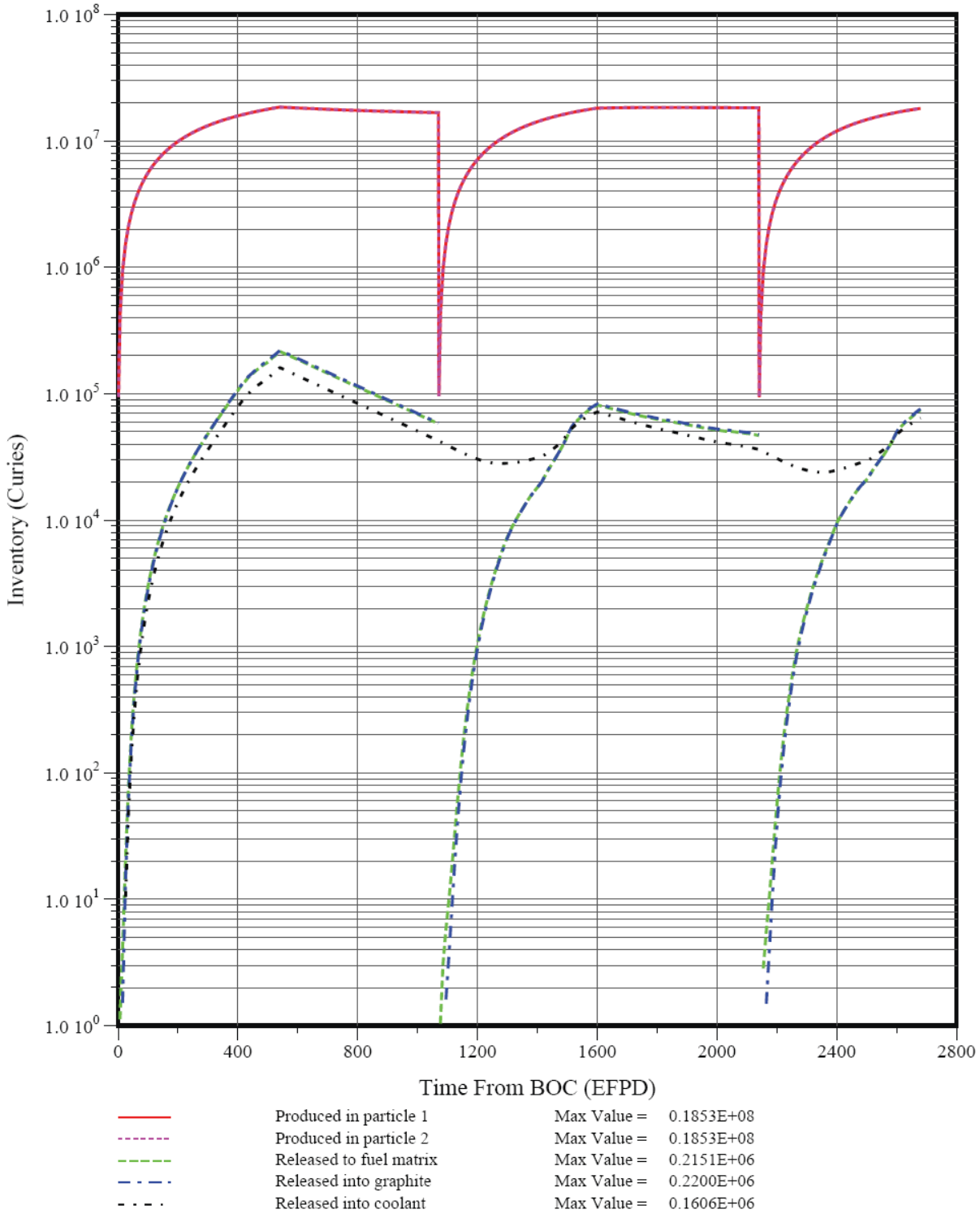

Figure 4-32. Ag-110m Inventories in Core Segment 2 (Case 8.9.3)

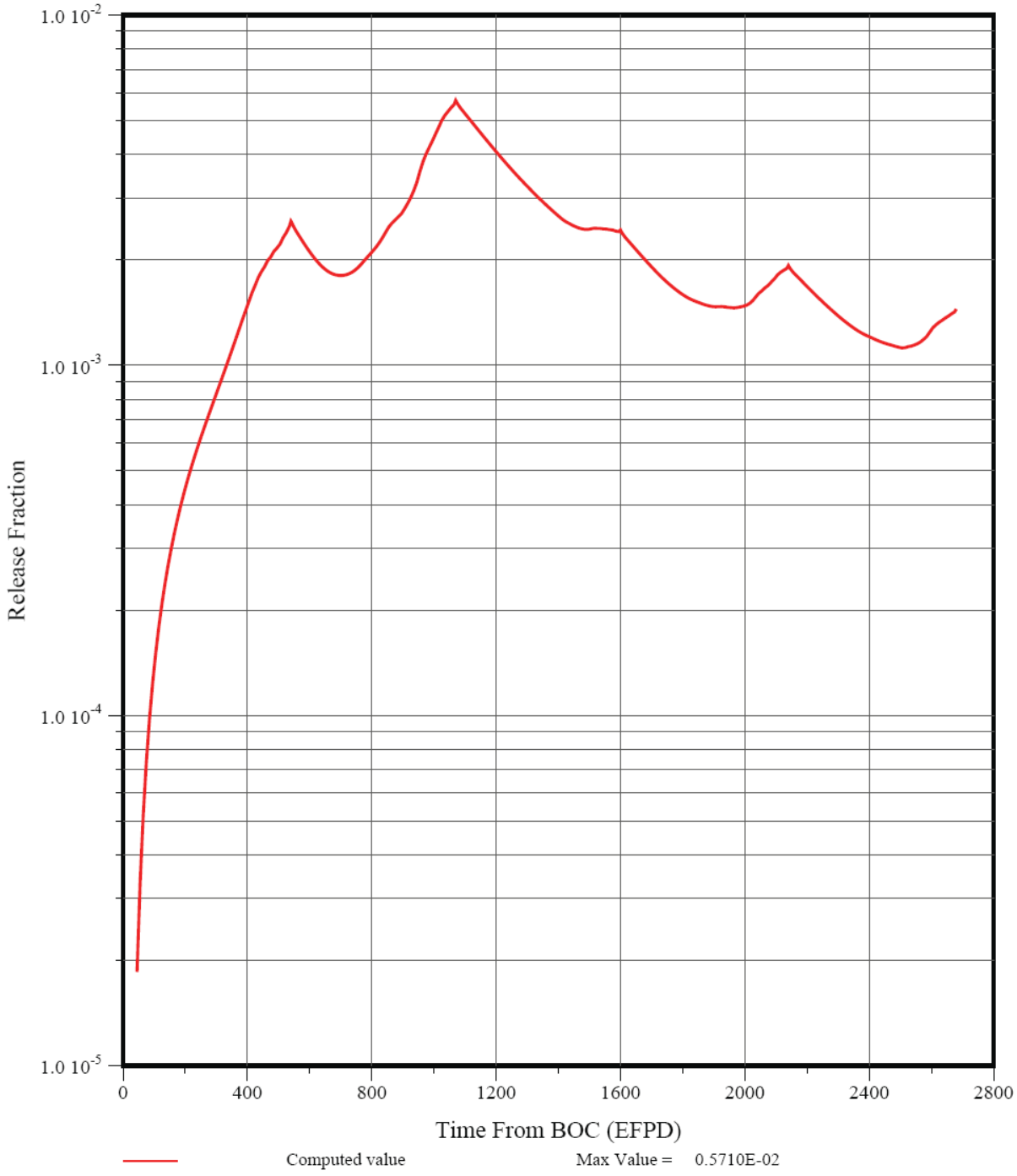

Figure 4-33. Cumulative Fractional Release of Ag-110m (Case 8.9.3)

The corresponding predicted transport behavior of 30.1-yr Cs-137 is shown in Figures 4-34 through 4-37. The predicted behavior Cs-137 is generally similar, but not identical to that of Ag-110m for two primary reasons. First, the half life of Cs-137 is much longer than that of Ag-110m (30.1 yr versus 0.68 yr) and much longer than an irradiation cycle; consequently, decay effects are insignificant during the five cycles analyzed. Secondly, there is no diffusive release from intact TRISO particles per the FDDM/F correlation.[15] Also, in contrast to the predicted Ag behavior, there is some Cs holdup by the matrix and graphite (see Figures 4-34 through 4-36).

The cumulative Cs-137 release fraction peaks at the end of cycle 3 at about 7.6×10^{-5}. During subsequent cycles, the fractional release of "new" Cs remains relatively constant, and the cumulative Cs release to the coolant is dominated by release during the first three cycles. In contrast to Ag-110m, this early Cs-137 release is not reduced because of its 30.1-yr half life.

The maximum predicted Cs cumulative fractional release exceeds the "Maximum Expected" limit of 1×10^{-5} by a factor of almost eight at the end of cycle 3 and about a factor of six by the end of cycle 5. As stated above, the predicted Cs release would likely be significantly reduced if the burnup-dependent FDDM/F correlation for Cs diffusion in UCO kernels were used; however, the use of that correlation is considered to be unjustified, given more recent experimental data [Medwid 1993].

[15] Per [FDDM/F 1987] and other GA documents of that vintage, Cs is not diffusively released from intact TRISO particles; rather Cs release from nominally intact TRISO particles at high temperatures (>~1600°C) is an indication of SiC degradation from fission product corrosion and/or thermal decomposition. This interpretation is not universally accepted (e.g., see discussion in [Martin 1993]).

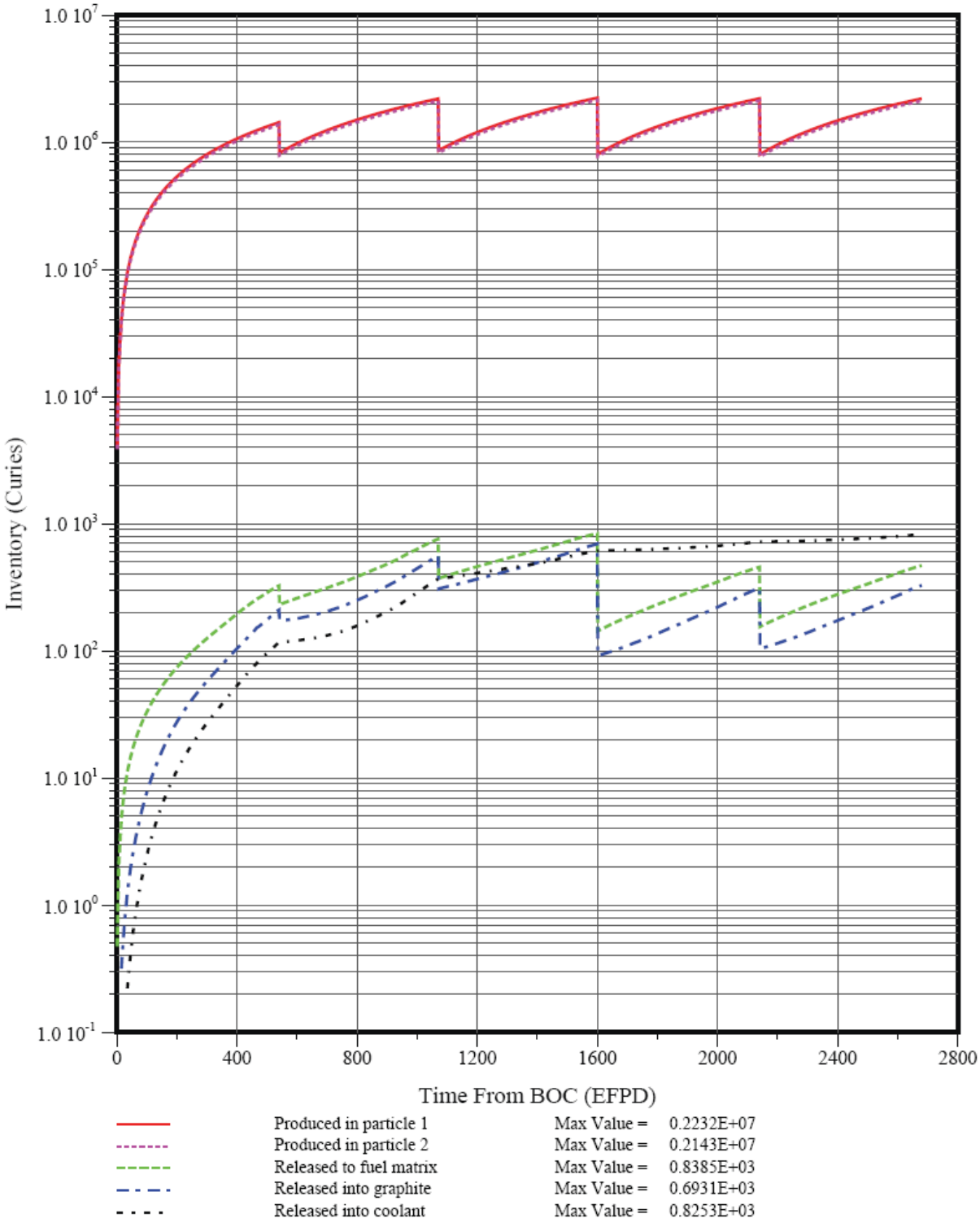

Figure 4-34. Cs-137 Inventories by Core Material Region (Case 8.9.3)

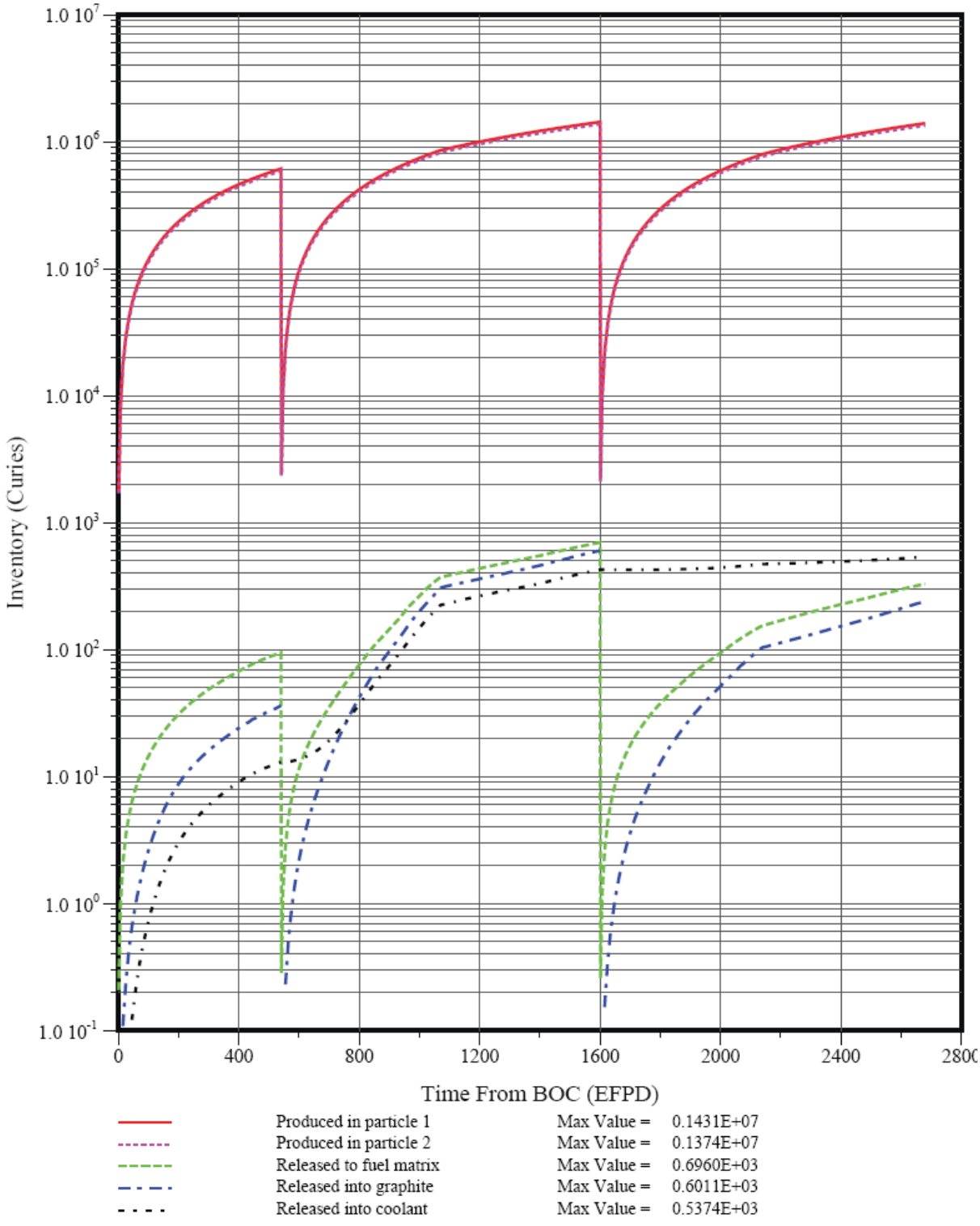

Figure 4-35. Cs-137 Inventories in Core Segment 1 (Case 8.9.3)

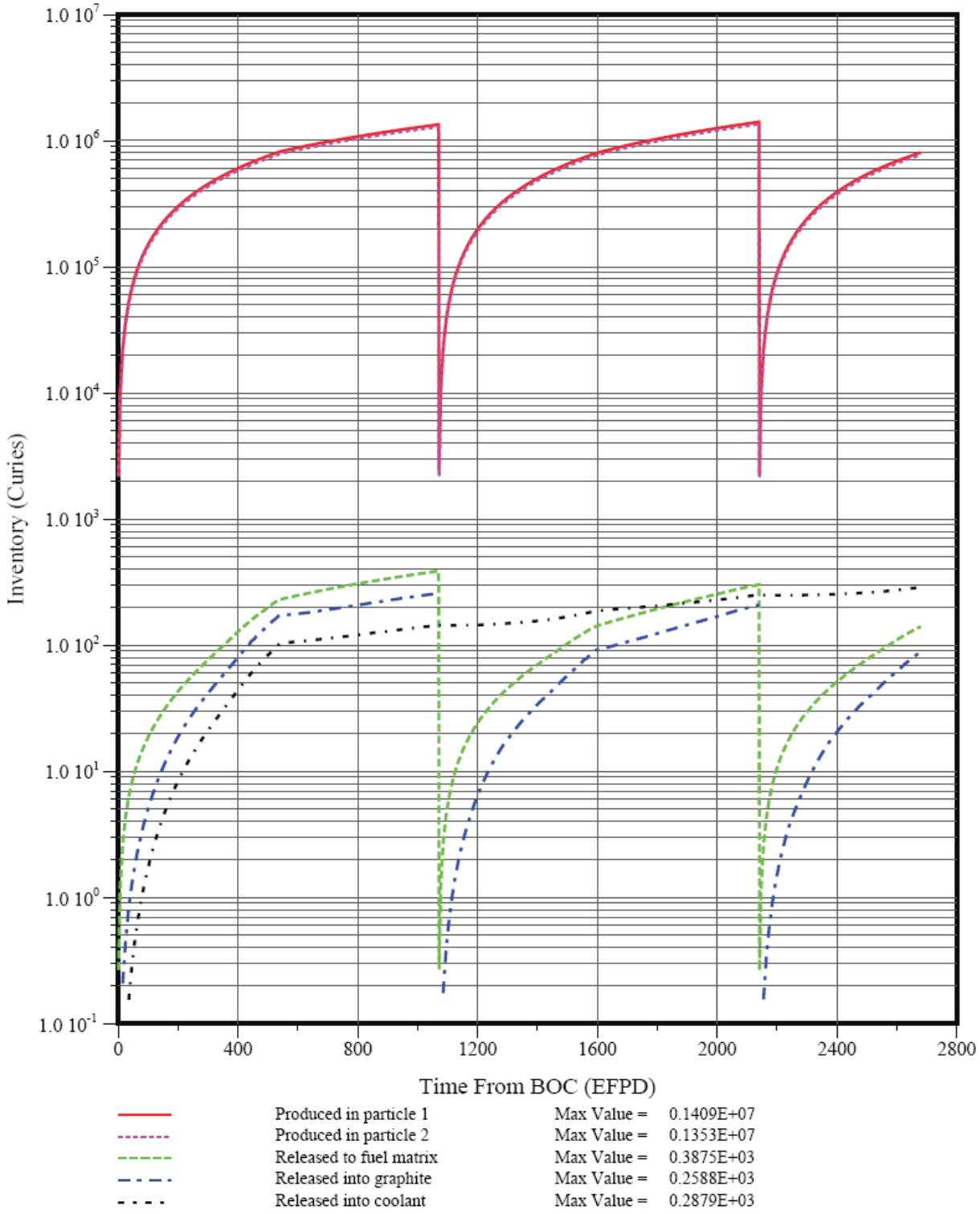

Figure 4-36. Cs-137 Inventories in Core Segment 2 (Case 8.9.3)

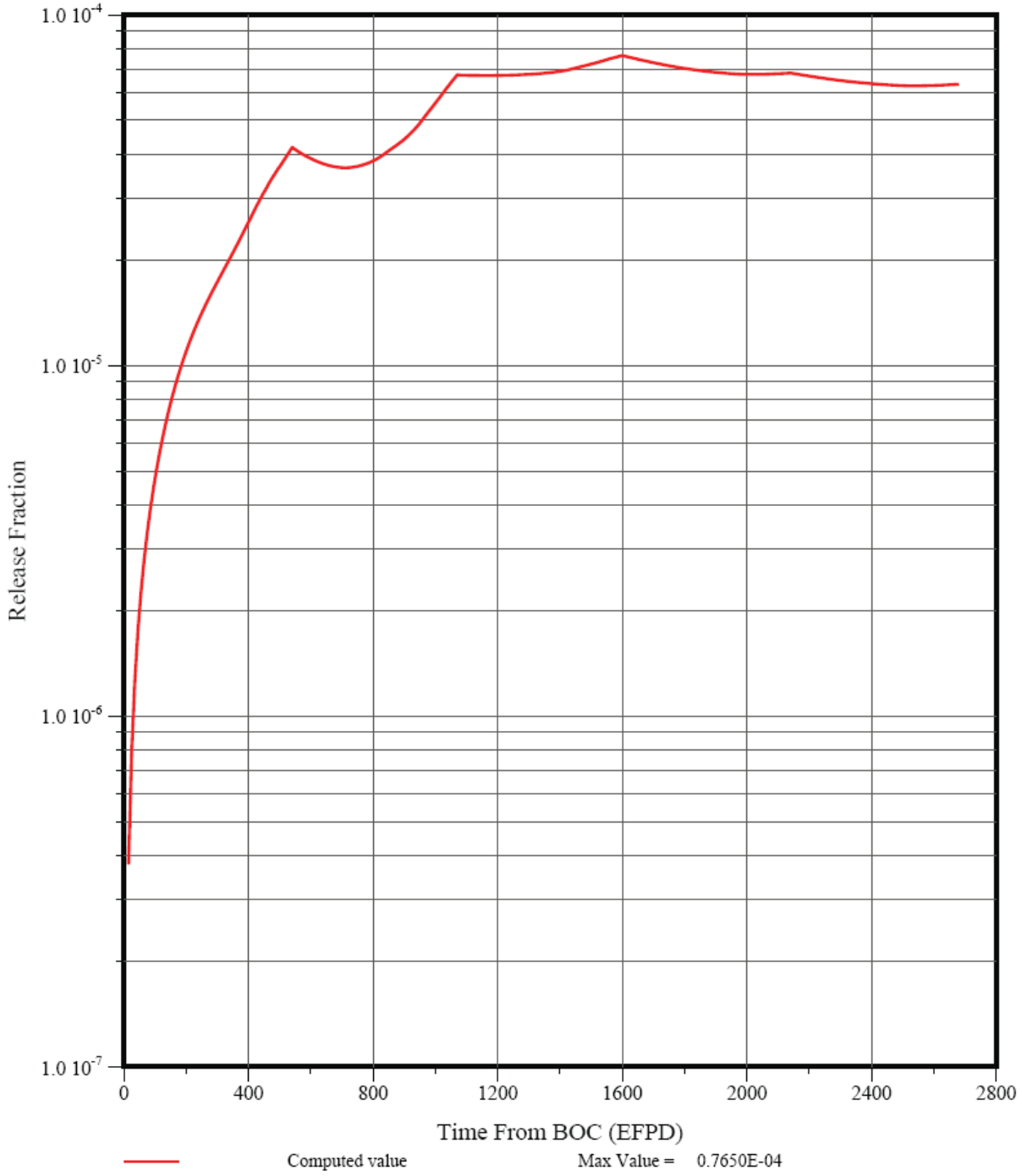

Figure 4-37. Cumulative Fractional Release of Cs-137 (Case 8.9.3)

4.3.4 Summary of Results for Case 8.9.3

Table 4-11 compares the predicted fuel failure and fission product release for Case 8.9.3 with the provisional fuel failure limits and fission product release limits from Table 2-10. The "Maximum Expected" criteria are the relevant figures-of-merit because the core performance results are best-estimate predictions.

Table 4-11. Comparison of Case 7.9 Results with Provisional Requirements

Parameter	"Maximum Expected" Limit	"Design" Limit	Case 8.9.3
Fuel failure during normal operation (exposed kernel fraction)	$\leq 5.0 \times 10^{-5}$	$\leq 2.0 \times 10^{-4}$	1.4×10^{-5}
Kr-88 R/B	$\leq 8.3 \times 10^{-7}$	$\leq 3.3 \times 10^{-6}$	1.1×10^{-6}
I-131 R/B	$\leq 2.0 \times 10^{-6}$	$\leq 8.0 \times 10^{-6}$	2.5×10^{-6}
Cs-137 fractional release	$\leq 1.0 \times 10^{-5}$	$\leq 1.0 \times 10^{-4}$	7.6×10^{-5}
Ag-110m fractional release	$\leq 5.0 \times 10^{-4}$	$\leq 5.0 \times 10^{-3}$	5.7×10^{-3}

A further comparison of the results for Case 8.9.3 with the corresponding results for the best binary-fuel-particle core design achieved in the CPA is presented in Section 7.

5 EVALUATION OF FUEL SHUFFLE

Part of the planned scope of the CPA was to evaluate the potential of fuel shuffling to improve on the binary-fuel-particle and single-fuel-particle core designs. The first activity in this subtask was to modify the SORT3D, SURVEY, and TRAFIC-FD codes to include fuel shuffle. It was also necessary to develop a utility program to support fuel shuffle in DIF3D/BURP. A software specification was prepared to define the fuel shuffle capability to be incorporated into the codes [Charman 2009] and all three codes were modified to include fuel shuffle capability. One fuel shuffle scheme for a binary-fuel-particle core design was analyzed and work was initiated to set up a fuel shuffle scheme for a single-fuel-particle design, but the fuel shuffle work was not completed within the time constraints of the CPA. The following sections describe the work that was performed on fuel shuffle for a binary-fuel-particle core design and a single-fuel-particle core design.

5.1 Binary-Fuel-Particle Core Design

Case 7.9 was chosen as the base design for investigating the potential benefits of fuel shuffling for a binary-fuel-particle core design. This fuel shuffle case was designated Case 7.9.2. The shuffling scheme selected for consideration is illustrated in Figure 5-1. Basically the approach is to shuffle all once-burned columns within each column (no radial shuffling) by flipping the top and bottom halves with each other as shown in Figure 5-1. In this shuffling scheme, 170 fuel blocks (1/3 core) are shuffled at the start of each cycle, excluding the initial core, resulting in a total of 680 fuel blocks being shuffled for 5 cycles.

Case 7.9.2 was run for 5 cycles (to equilibrium) with BURP and DIF3D. A SURVEY input file was generated using the new fuel-shuffle version of SORT3D, and the new fuel-shuffle version of SURVEY was successfully run. However, the SURVEY results for Case 7.9.2 were essentially the same as for Case 7.9 with respect to temperatures, fuel failure, and gaseous fission gas release. As of this writing, TRAFIC-FD has not been successfully run for Case 7.9.2.

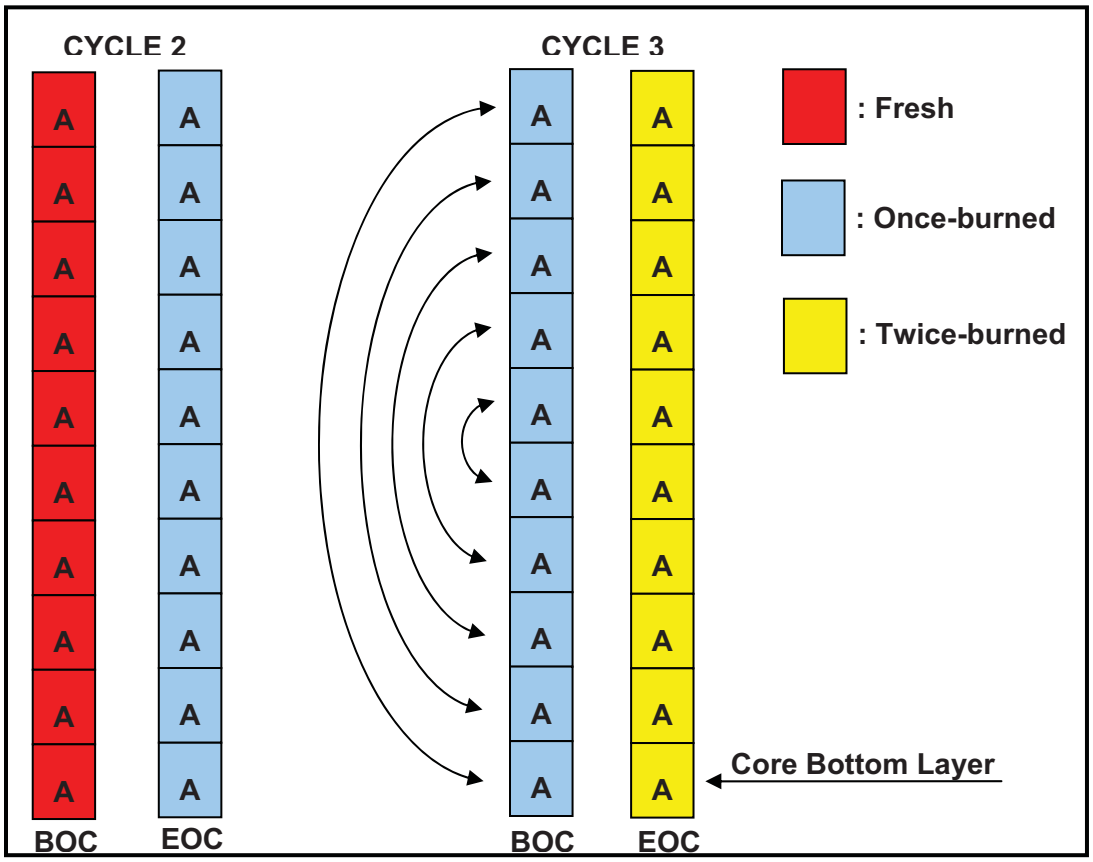

Figure 5-1. Example of "Column-Flip" Shuffling Scheme for Segment-A Column

5.2 Single-Fuel-Particle Core Design

Case 8.9.3 was chosen as the base design for investigating the potential benefits of fuel shuffling for a single-fuel-particle core design. This fuel shuffle case was designated Case 8.9.4.

Conceptually, an ideal fuel shuffling scheme for a two-batch core would be to shuffle the fuel such that the top-half of the core contains all fresh fuel and the bottom-half of the core contain once-burnt fuel at the beginning of each cycle. This would force the majority of the power to be generated in the top half of the core and minimize power peaking at the bottom of the core where gas temperatures are the highest. This scheme has been referred to as "axial-push-through". However, implementing this scheme with the current physics methods is not straight-forward and requires further description.

Essentially, setting-up the "axial-push-through" model requires starting from the current radial model, so additional radial shuffling is required for the methods. This isn't possible for the entire core but can be done for most of it. Figure 5-2 illustrates the required radial shuffling. Radial shuffling can only be between two columns of similar type; e.g., standard-column with standard-column; RSC-column with RSC-column; etc. For example, consider a single pair of shuffled columns. At BOC2, we want the bottom-half of a fresh segment-A column to switch places with the top-half of a once-burned segment-B column. After the shuffling is performed, for a 1/3 core sector, we're still left with two full segment-A control rod columns and two full segment-B standard columns.

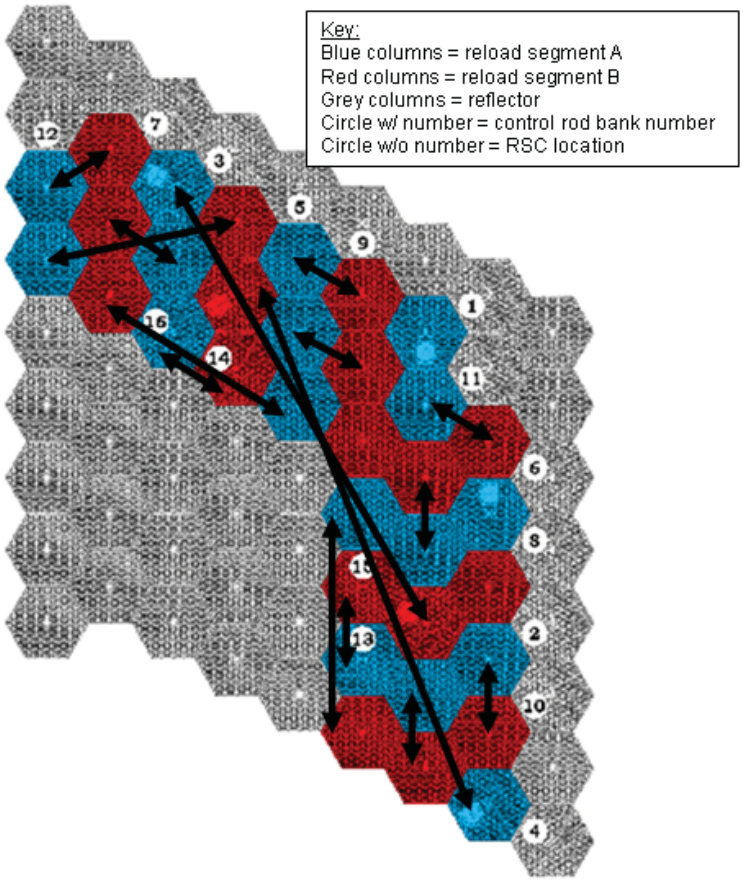

Figure 5-2. Radial Shuffling Required for "Axial-Push-Through" Shuffling Scheme

As of this writing, the input array that defines the fuel shuffle scheme for DIF3D/BURP has not been completed; thus, Case 8.9.4 has not been simulated with DIF3D/BURP.

6 CORE ACCIDENT ANALYSIS

The fuel performance and fission product release during a de-pressurized core conduction cooldown event for the final binary-fuel-particle core design (without fuel shuffle) discussed in Section 3 were calculated using the SORS code. The calculations were based on accident condition temperatures obtained using a TAC2D model and on steady state operating temperature and fuel performance input from SURVEY. An accident analysis was not performed for the single-fuel-particle core design because the single-fissile-particle core should have the same basic accident conditions behavior as the binary-fuel-particle core. This conclusion is based on the power distributions being similar for the two core designs.

6.1 Thermal/Hydraulics Analysis

Core accident-condition thermal/hydraulic calculations for the final binary-fuel-particle core design (without fuel shuffle), Case 7.9, were performed using an existing TAC2D model previously developed by GA for analysis of depressurized conduction cooldown (DCC) events in modular helium reactors. TAC2D [Boonstra 1976] is a thermal analysis code developed by GA.

The TAC2D model is a two-dimensional (R-Z) model that simulates one-third of a 102 column core and its surroundings, including the graphite reflectors, the core barrel, the reactor vessel, the RCCS, the shutdown cooling system, and the concrete and earth that surround the reactor system. The reactor core model consists of three fuel rings and ten axial positions in each ring. The model is axial-symmetric and is based on the mean parameters of each of the fuel rings. The following input to the existing model was modified to include the appropriate starting conditions for the DCC event as obtained from the DIF3D and SURVEY results for Case 7.9.

- Core power distribution
- Core fast fluence distribution
- Graphite fast fluence distribution
- Average core temperatures

The end of Cycle 5 was selected as the time point for onset of the depressurized conduction cooldown event.

The radial and axial power factors for each of the fuel rings are tabulated in Tables 6-1 and 6-2. The initial core temperatures are listed in Table 6-3. The fast fluence values used for the core in the TAC2D model were generated by the SURVEY code, and are average values for Segments A and B. The reflector fast fluence values were obtained from DIF3D. The reflector fluence was based on end of life conditions. Each reflector and core node in the TAC2D model had a specific fluence value assigned.

Table 6-1. Radial Power Factors for DCC Event Analysis

Fuel Ring Number	Radial Power Factor
1 (Inner Ring)	0.795
2	1.091
3 (Outer Ring)	1.080

Table 6-2. Axial Power Factors for DCC Event Analysis

Fuel Block Number	Power Factor
1	1.092
2	1.226
3	1.151
4	1.093
5	1.025
6	0.968
7	0.934
8	0.921
9	0.832
10	0.750

Table 6-3. Initial Core Temperatures for DCC Event Analysis

Fuel Block Number	Temperature (°C)		
	Ring 1 (ID)	Ring 2	Ring 3 (OD)
1 (Top of core)	662	693	687
2	707	766	754
3	729	810	788
4	757	853	825
5	783	892	859
6	808	931	893
7	835	969	928
8	863	1010	963
9	886	1039	987
10 (Bottom of core)	909	1064	1010
Note: The core temperatures in the TAC2D model are weighted averages of the fuel and graphite temperatures at a given model location			

The results of the TAC2D thermal/hydraulics analysis are presented in Figures 6-1 through 6-3. These figures provide plots of the following parameters.

- The maximum core temperature (i.e., the maximum weighted average of the fuel and graphite temperature at any TAC2D calculation location)
- The mean core temperature
- The maximum inner reflector temperature
- The maximum outer reflector temperature
- The permanent side reflector temperature
- The core barrel temperature
- The maximum vessel temperature

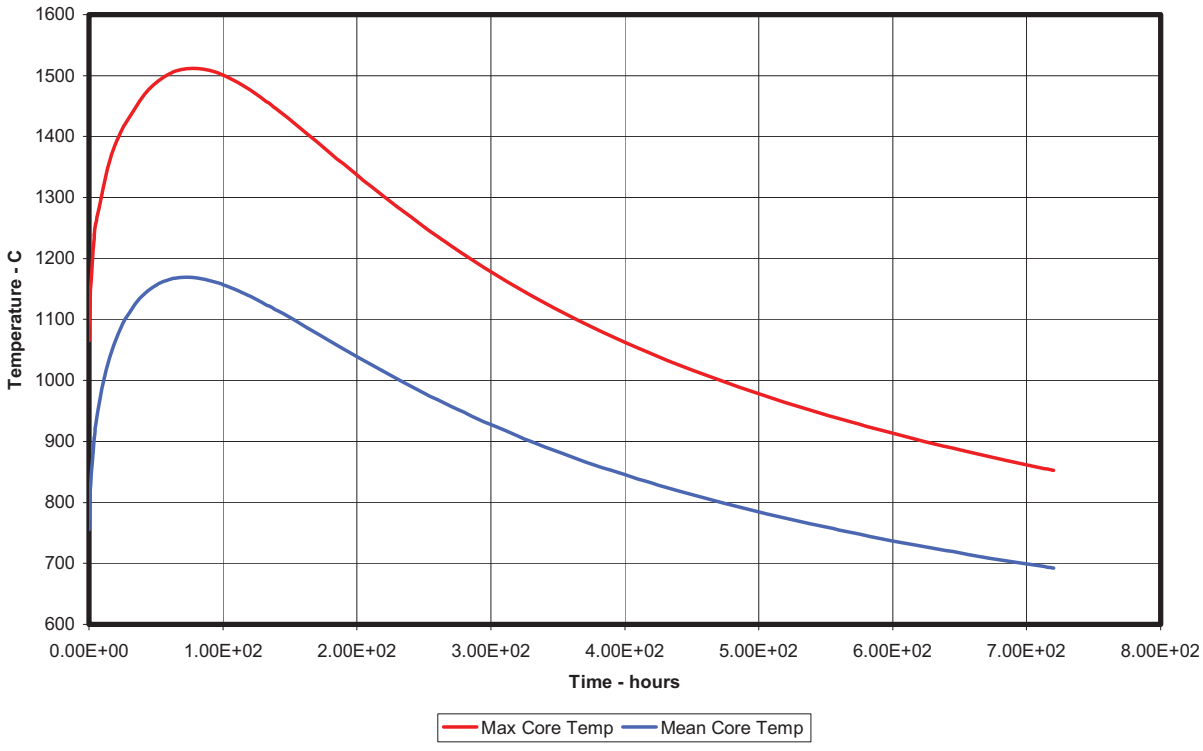

Figure 6-1. Maximum and Average Core Temperatures for DCC Event

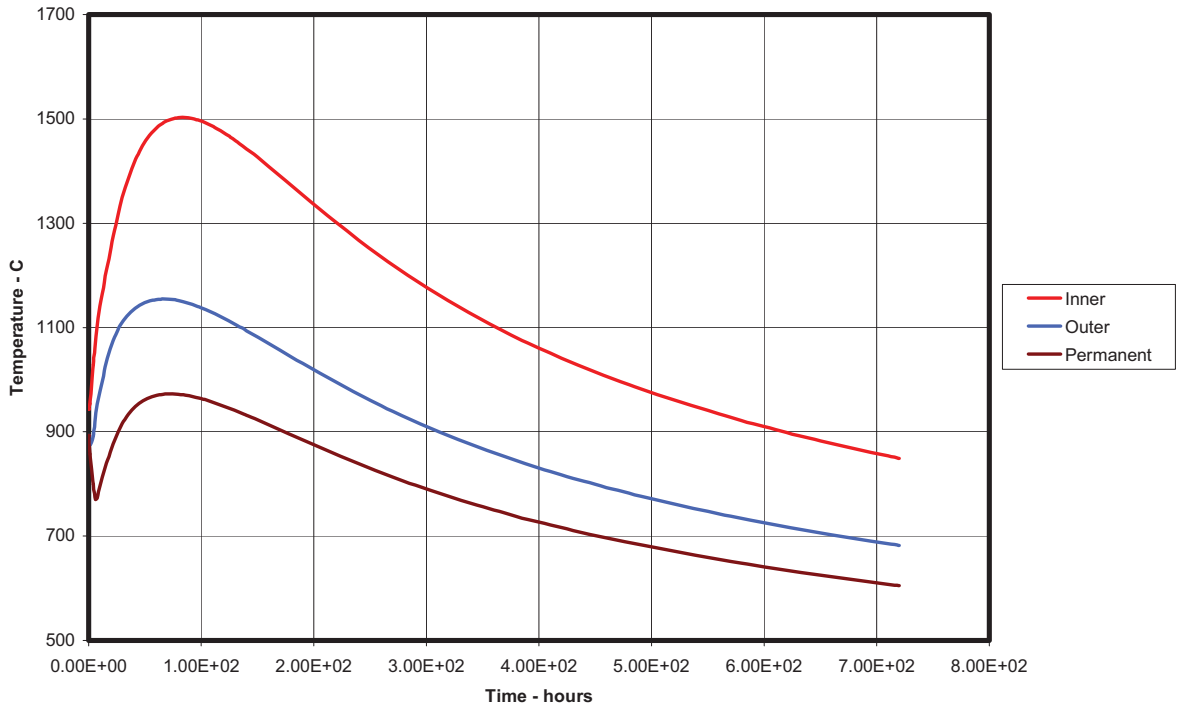

Figure 6-2. Maximum Graphite Reflector Block Temperatures for DCC Event

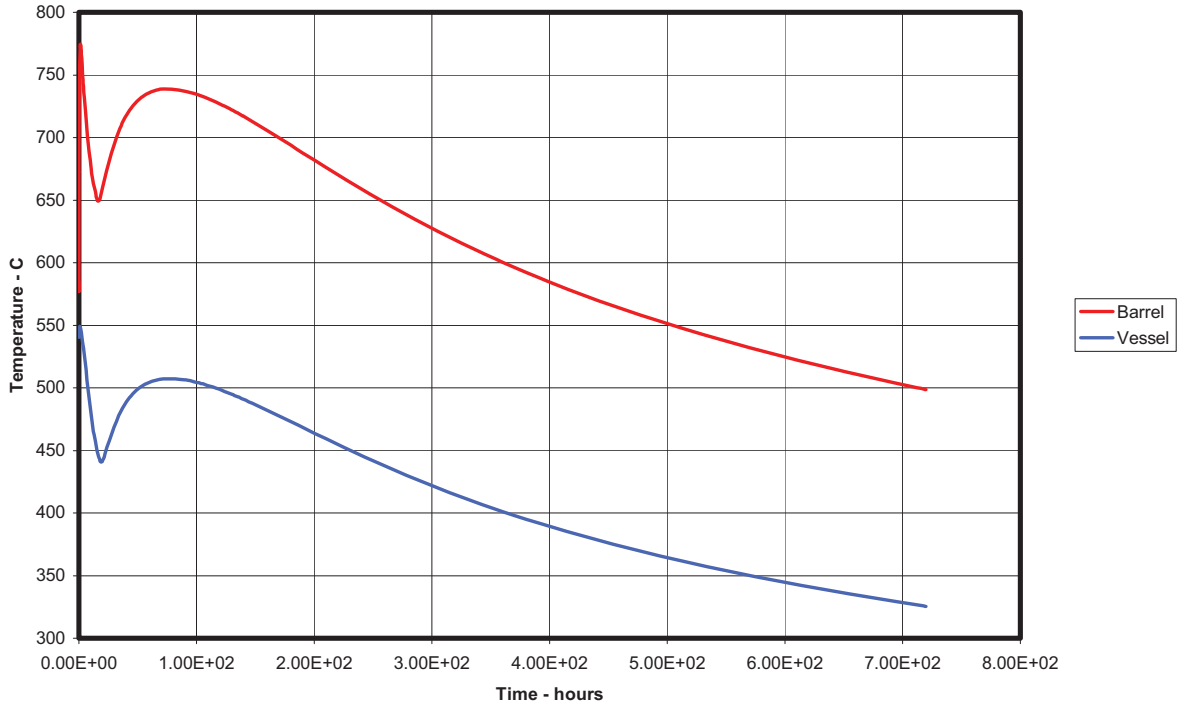

Figure 6-3. Maximum Core Barrel and Reactor Vessel Temperatures for DCC Event

As seen in Figure 6-1 the maximum core temperature is ~1510°C, which is well below the design guideline of 1600°C. The maximum vessel temperature is ~550°C at the onset of the transient, which is well above the ASME code limit for SA508/SA533. This is consistent with the conclusion from previous analyses that either a high-chrome steel vessel or direct cooling of a SA508/SA533 steel vessel will be needed for a reactor operating with a reactor outlet helium temperature of 900°C. The TAC2D model assumes a 9Cr-1Mo-V vessel.

Table 6-4 tabulates the maximum temperatures calculated for several other reactor components.

Table 6-4. Maximum Component Temperatures for DCC Event

Component	Maximum Temperature (°C)
Concrete Silo	56
Core Support	719
Upper Plenum Shroud	845
Startup Control Rod	1261*
Core Support Post	883
Vessel Support	540
RCCS Riser	319
RCCS Downcomer	239
Insulation	239
*Assuming that the control rod is inserted in the core during the DCC event, which is not the planned mode of operation for the startup control rods	

6.2 Fuel Performance Analysis

Fuel performance and fission product release during a depressurized conduction cooldown was analyzed for Case 7.9 using the SORS computer code [Cadwallader 1993]. The temperature transient for the fueled region of the core and its upper and lower reflectors were obtained from TAC2D as described in Section 6.1. The reflector temperatures are important for re-adsorption of metallic fission products released from the fuel and core graphite into the reflector graphite. Additional key inputs from SURVEY included fast neutron fluence, fissile and fertile fuel burnup, and the initial condition of the fuel particles such as exposed kernel fraction and the fraction of particles having a defective SiC layer but an intact OPyC layer. These inputs from SURVEY

were taken from the end of cycle 5, which is representative of the end of any of the subsequent equilibrium cycles. Table 6-5 lists the fuel particle initial conditions data used for the SORS analysis. Fuel element radionuclide inventories were obtained from the RADC computer code at the "maximum expected" level as reported in [Hanson 2008].

Table 6-5. Fuel Particle Initial Conditions

Parameter	Fertile Fraction	Fissile Fraction
Initially Exposed Kernels	1×10^{-5}	1×10^{-5}
Initially Failed SiC, Intact OPyC	8×10^{-5}	13×10^{-5}
Missing Buffer	0	0
Defective IPyC	4×10^{-6}	4×10^{-6}
Defective OPyC	1×10^{-4}	1×10^{-4}
Failed SiC	5×10^{-5}	5×10^{-5}
Heavy Metal Contamination	1×10^{-5}	

The results show that the dominant source of fission product release is heavy metal contamination for krypton, xenon, iodine, tellurium and other volatile and gaseous fission products. Cesium and strontium releases are due to initially exposed fuel kernels and initially failed SiC. Graphite retention significantly reduces these fuel particle releases such that the core fractional release is only 2×10^{-7}. For silver, intact fuel particles are the dominant source, but graphite retention provides significant holdup in both the core and reflector. Silver release after 720 hrs approaches 0.3% of total silver inventory. Figures 6-4 thru 6-8 present the core fission product release for design Case 7.9 for krypton, xenon, iodine, tellurium, cesium, strontium and silver.

The temperature transient causes an insignificant increase in exposed kernel fraction even in the hottest core location. Incremental failure of the SiC that leaves the OPyC intact is less than 1×10^{-5} in the hottest core location.

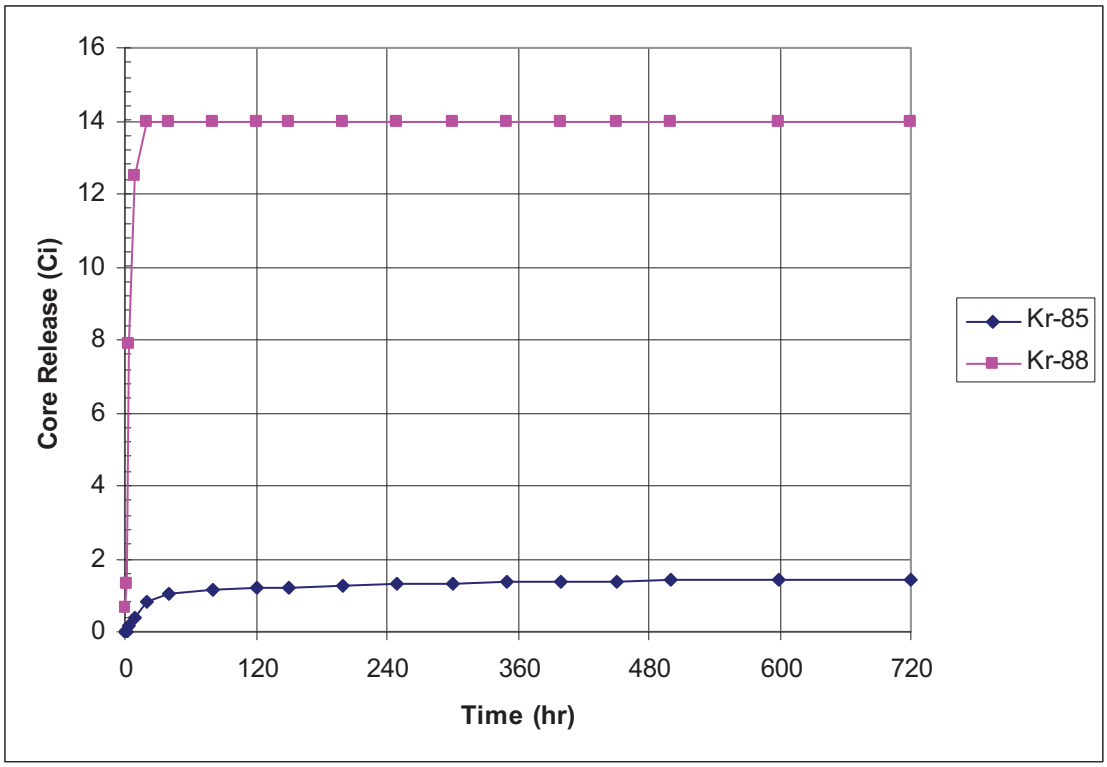

Figure 6-4. Krypton Release During Depressurized Conduction Cooldown

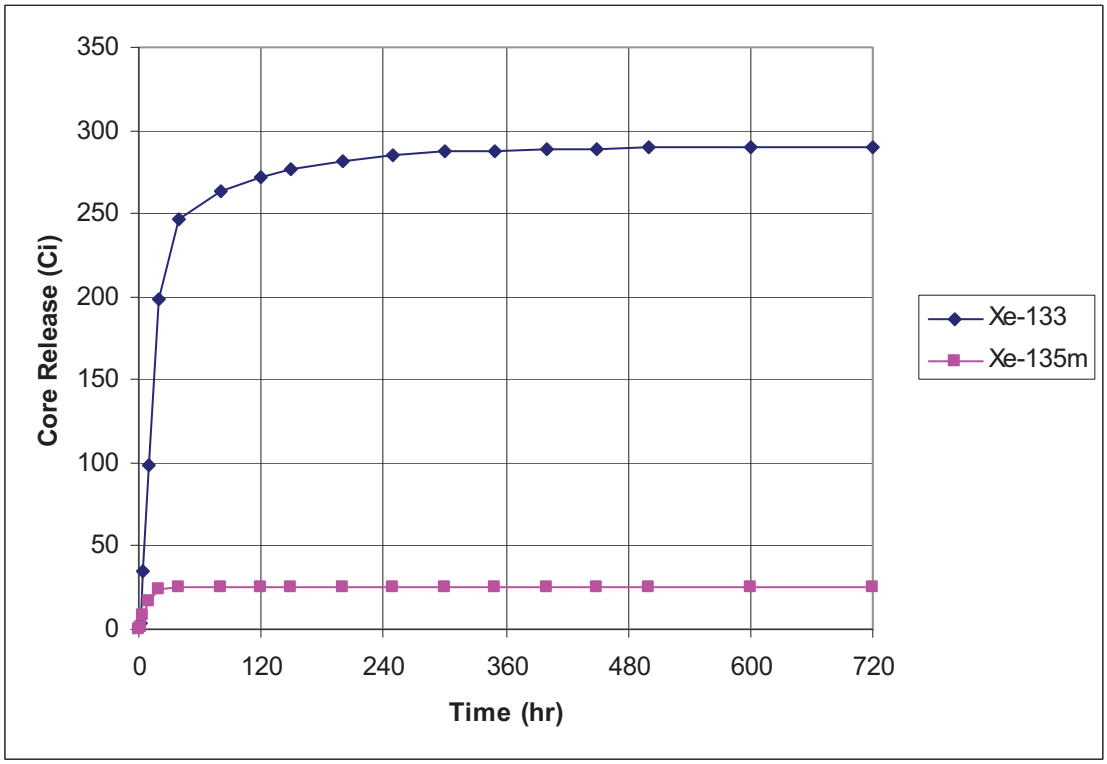

Figure 6-5. Xenon Release During Depressurized Conduction Cooldown

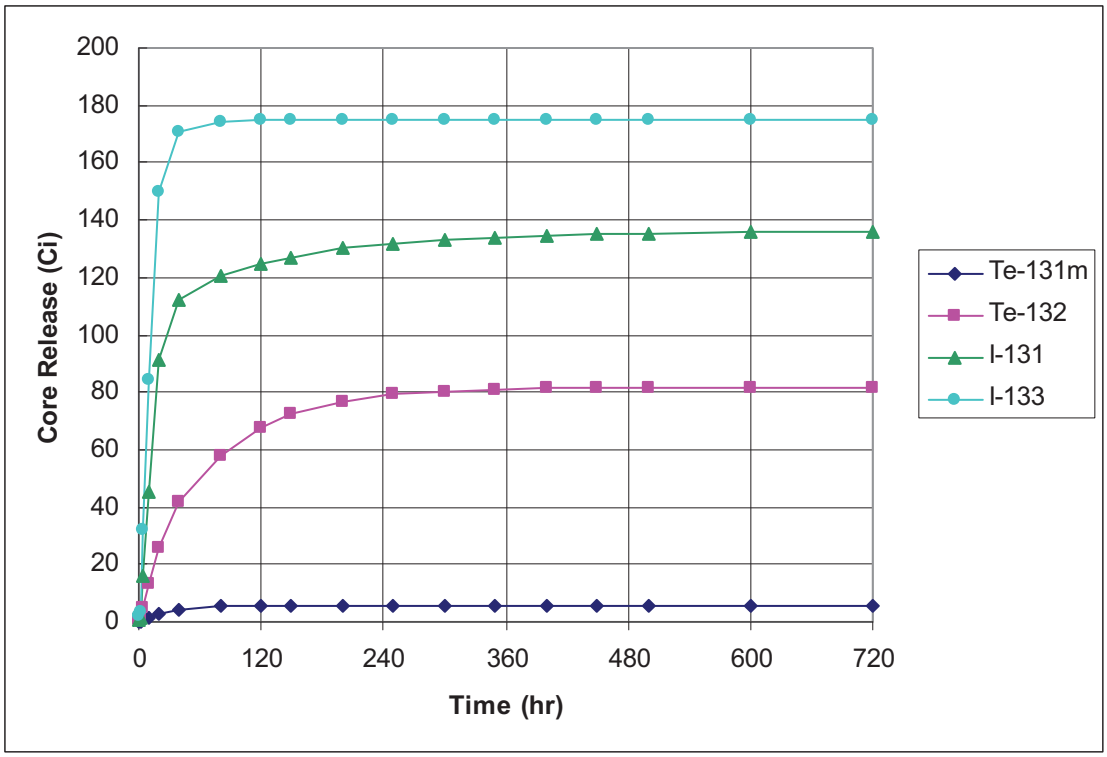

Figure 6-6. Tellurium and Iodine Release During Depressurized Conduction Cooldown

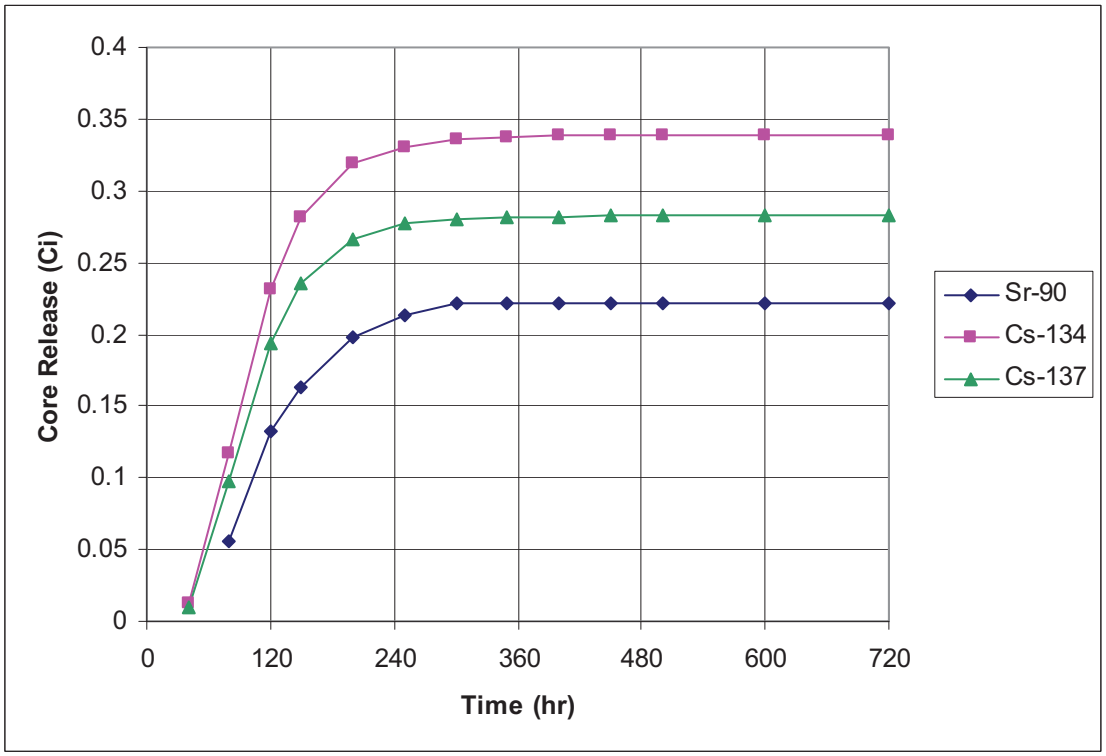

Figure 6-7. Strontium and Cesium Release During Depressurized Conduction Cooldown

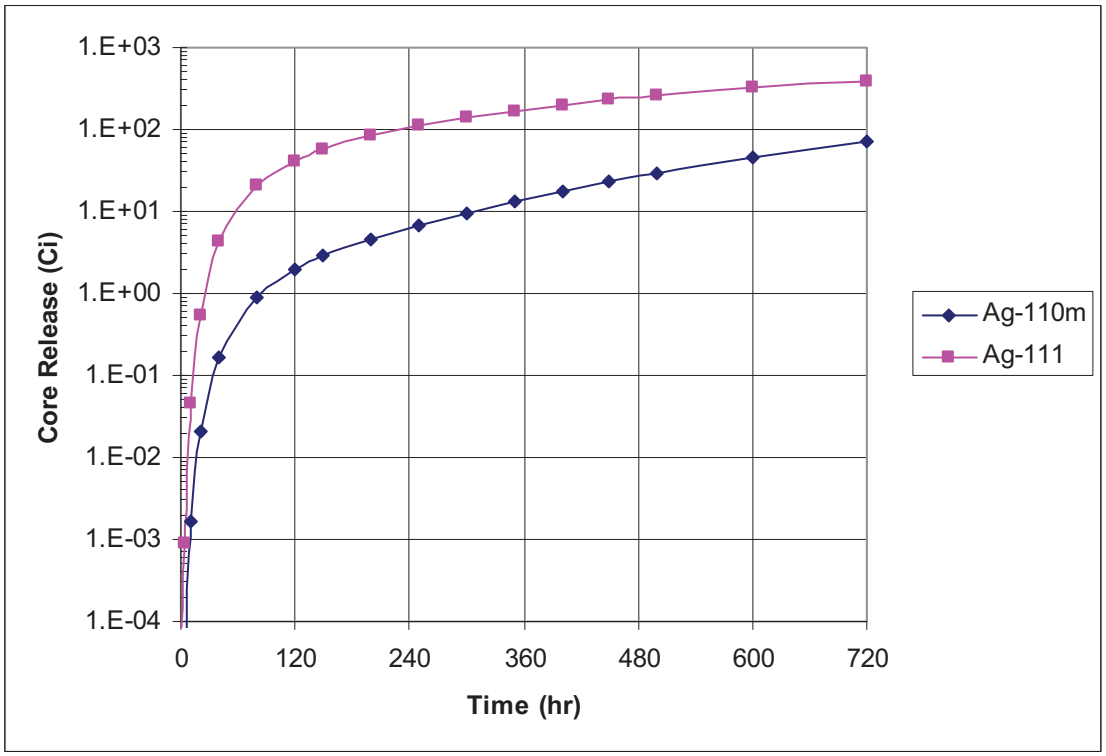

Figure 6-8. Silver Release During Depressurized Conduction Cooldown

7 CONCLUSIONS

After an extensive code development and verification effort, and evaluation of a large number of physics design iterations utilizing both a binary-fuel-particle system and a single fuel particle, GA was successful in producing binary-fuel-particle and single-fuel-particle core designs that: (1) meet the imposed cycle-length and PF requirements, the 1250°C design guideline for the time-averaged maximum fuel temperature, and the provisional "maximum expected" limit on in-service fuel failure; (2) have strong negative core temperature coefficients of reactivity; (3) have acceptable temperatures and fuel performance during a depressurized conduction cooldown event; and (4) have reasonable and similar axial and radial core power distributions and good uranium utilization. However, as shown in Table 7-1, neither the best binary-fuel-particle core design (Case 7.9) nor the best single-fuel-particle core design (Case 8.9.3) achieved in the CPA meet the provisional fission product release limits (from Section 2.3.3) for any of the fission products considered. Nevertheless, the results are encouraging for this initial core design effort given the relatively high fuel and graphite temperatures inherent in a prismatic MHR operating with an outlet helium temperature of 900°C and the potential that exists for further optimization of the core designs achieve in the CPA.

Table 7-1. Comparison of Core Performance Results with Provisional NGNP Requirements

Parameter	"Maximum Expected" Limit	Case 7.9	Case 8.9.3
Fuel failure during normal operation (exposed kernel fraction)	$\leq 5.0 \times 10^{-5}$	1.3×10^{-5} (fissile) 4.4×10^{-6} (fertile)	1.4×10^{-5}
In-service SiC failure	N/A	5.4×10^{-5}	1.0×10^{-4}
Kr-88 R/B	$\leq 8.3 \times 10^{-7}$	9.2×10^{-7}	1.1×10^{-6}
I-131 R/B	$\leq 2.0 \times 10^{-6}$	2.2×10^{-6}	2.5×10^{-6}
Cs-137 fractional release	$\leq 1.0 \times 10^{-5}$	4.2×10^{-5}	7.6×10^{-5}
Ag-110m fractional release	$\leq 5.0 \times 10^{-4}$	1.3×10^{-3}	5.7×10^{-3}

The results of the CPA work are considered to be supportive of an overall conclusion that use of a single fuel particle having either a single U-235 enrichment or two U-235 enrichments appears feasible for a prismatic MHR operating with a reactor outlet helium temperature of 900°C. This conclusion is based on the success of the CPA effort in producing a single-fuel-particle/single-enrichment core design (Case 8.9.3) that is comparable to the best binary-fuel-particle core design (Case 7.9) with respect to predicted fuel performance and gaseous fission product

release, and that has predicted metallic fission product release that is only about a factor of two to three higher than for Case 7.9. The increased Ag-110m and Cs-137 release in Case 8.9.3 relative to Case 7.9 is primarily due to the higher fuel temperatures in the single-fuel-particle core design as summarized in Table 7-2. This is as expected because a binary-fuel-particle system provides an inherent advantage relative to a single-fuel particle having a single U-235 enrichment because it allows U-235 enrichment zoning as well as uranium zoning and fixed burnable poison zoning. However, the differences in the results for the two designs are not particularly significant in view of the large uncertainties inherent in the calculation of fuel failure and fission product release.

Table 7-2. Maximum Fuel Temperatures in Hottest 5% Core Volume

	Case 7.9		Case 8.9.3	
Segment & Fuel Load	**Maximum (°C)**	**Approx. Range (°C)**	**Maximum (°C)**	**Approx. Range (°C)**
Segment 1				
Fuel Load 1	1254	1160 – 1254	1350	1200 – 1350
Fuel Load 2	1488	1350 – 1488	1534	1390 – 1534
Fuel Load 3	1456	1330 – 1456	1451	1310 – 1451
Segment 2				
Fuel Load 1	1341	1200 – 1341	1534	1340 – 1534
Fuel Load 2	1456	1290 – 1456	1483	1290 – 1483
Fuel Load 3	1419	1280 – 1419	1456	1280 - 1456

The primary challenge associated with achieving a single-fuel-particle/single-enrichment core design that meets all requirements will be to reduce the metallic fission product release, which is greatest during the approach-to-equilibrium reactor operating cycles. Specifically, the maximum Ag-110 and Cs-137 cumulative release fractions for Case 8.9.3 are greater than the “maximum expected” limits by factors of 11 and 7, respectively. Design improvements that reduce the very-high localized temperatures observed not only in Case 8.9.3 but in all of the various design iterations, particularly during the approach-to-equilibrium cycles, will be necessary to reduce the Ag-110m and Cs-137 release fractions. The substantially lower metallic fission product release predicted for Case 8.9.3 Cycle 5, is noteworthy in that it suggests that the metallic fission product release fractions can be significantly reduced if a better physics design for the initial and approach-to-equilibrium cycles can be developed.

The CPA effort also produced two single-fuel-particle/two-enrichment core designs (Cases 8.1 and 8.5) for which the predicted fuel performance and fission product release are approximately equivalent to the corresponding predictions for Case 7.9. Thus, the predicted Ag-110m and Cs-

137 release fractions for these designs would have to be reduced by only about a factor of four to meet the provisional requirements. Use of a single-fuel-particle design with two U-235 enrichments is a potential fall back if an acceptable core design cannot ultimately be achieved with a single fuel particle and single U-235 enrichment. This is because a single-fuel-particle design with two U-235 enrichments should still require qualification of only one fuel particle because the irradiation and accident condition performance of the fuel particle having the higher U-235 enrichment should be bounding for the fuel particle having the lower U-235 enrichment. However, the maximum PF in both Case 8.1 and Case 8.5 moderately exceed the limit imposed on the CPA, so some relaxation of the PF constraints would be needed to accommodate these designs.

With respect to the PF limits imposed on the CPA, the PF constraints combined with the fuel cycle length goal of 540 EFPD (which requires relatively heavy fuel loadings) significantly limited the flexibility to use fuel zoning as a means of minimizing radial and axial power peaking in the core in either a binary-fuel-particle or single-fuel-particle core design. Consideration should be given to allowing PFs to increase up to about 45% given that the capability to make fuel compacts up to this PF without breaking fuel particles has already been demonstrated by the NGNP/AGR Fuel Program.

Although the physics design methodology changes investigated in Cases 7.9.1 and 7.9.4 to mitigate the localized fission rate spikes and resultant very-high, but short-term localized fuel temperatures caused by large incremental control rod movements did not have the anticipated effect, it is still clear from the SURVEY results that the very-high temperatures in the bottom of the core are the result of control rod withdrawal. Another potential means of reducing the impact of control rod withdrawal would be to modify the control rod operating scheme. There are 36 control rods located in the outer reflector elements, and the current approach used in the CPA is to operate these control rods in banks of three (one control rod per 120° sector of the core) and to completely withdraw each rod bank before initiating withdrawal of the next rod bank. A modified control rod operating scheme in which the control rods are withdrawn in banks of six rather than banks of three was evaluated in binary-fuel-particle core design Case 7.4, but this approach unexpectedly resulted in much-higher axial power factors and was not pursued further. Other control rod operating schemes could be investigated; for example, one in which all operating control rod groups are initially inserted about half-way into the core as opposed to having six of the twelve banks fully inserted and the other six withdrawn, as in the present scheme. This would minimize control rod withdrawal for a required reactivity change and help to maintain an axial power shape tilted towards the top of the core.

In essentially all of the binary-fuel-particle and single-fuel-particle core design iterations, the highest calculated fuel temperatures are in the second and third cycles (i.e., the approach-to-

equilibrium cycles). Based on these results, it is concluded that the design iterations performed in this study did not achieve sufficient optimization of the initial core and initial reload segments, and that further design iterations could result in significant improvement with respect to the high fuel temperatures observed in these cycles. However, given the extent to which the predicted Ag-110m and Cs-137 release fractions exceed the "maximum expected" limits in Cases 7.9 and 8.9,3, it is doubtful that these limits can be met by fuel and FBP zoning alone. Rather, it is likely that improvements to DIF3D (such as a control search capability) and/or relaxation of the constraints on PF and/or cycle length will be necessary to reduce the Ag-110m and Cs-137 release fractions to these levels. For example, allowing shorter cycle lengths during the approach-to-equilibrium might significantly improve fuel performance during cycles 2 and 3 without relaxing the constraint on PF.

Another potential means of improving the temperature, fuel failure, and fission product release results obtained for Cases 7.9 and 8.9.3 would be to modify the physics calculations to take advantage of the inverse relationship between reactivity and temperature. This option is available because all the reactor physics calculations in the CPA were based on neutron cross sections generated for a single core-averaged temperature. This simplification minimized the complexity of the calculations to allow for reasonably-quick evaluation of many options, but it was also a conservatism that resulted in overestimation of peak power factors and temperatures to some degree.[16] If temperature-dependent sets of cross sections were used throughout the core, the effect of the core negative temperature coefficient would be to reduce the neutron flux, and hence the power in the high temperature regions and to increase power in the low temperature regions. This would have the beneficial effect of lowering the highest fuel temperatures. It is possible to use multiple cross section sets in the DIF3D calculations, so the degree of conservatism associated with the use of a single cross section set could (and should) be evaluated. If the use of multiple cross sections sets is found to significantly reduce peak fuel temperatures, this methodology should be adopted for future core physics design work.

As indicated above, the relatively high fission product release fractions obtained for both the binary-fuel-particle and single-fuel-particle core designs in the CPA are at least partially due to the relatively high fuel and graphite temperatures that are inherent in a prismatic MHR operating with an outlet helium temperature of 900°C. It is expected that for a given reactor design, a reduction in the reactor outlet helium temperature would have a beneficial impact on fuel and graphite temperatures and therefore on fuel performance and fission product release. Evaluation of the effect of reducing the reactor outlet helium temperature on fuel performance and fission product release was not within the scope of the CPA, but it was included in a

[16] Based on 2D (GAUGE) analyses of this effect in prior MHR design programs, GA considered the use of a single-temperature cross section set to be a reasonable, albeit conservative, approach for the CPA calculations.

companion task that was performed to develop fuel performance requirements and to ascertain the capability of various core designs to meet the requirements [Hanson 2009]. In the companion study, SURVEY and TRAFIC-FD calculations were performed for Case 7.9 from the CPA with a reactor outlet helium temperature of 750°C and a core inlet helium temperature of 390°C (thereby maintaining the same core temperature rise as for Case 7.9 in the CPA). The results for Case 7.9 with the different reactor outlet helium temperatures are compared in Table 7-3 and confirm the expected benefit from reducing the reactor outlet helium temperature.

Table 7-3. Case 7.9 Results for Different Reactor Outlet Helium Temperatures

Parameter	"Maximum Expected" Limit	Case 7.9 (900°C)	Case 7.9 (750°C)
Fuel failure during normal operation (exposed fissile kernel fraction)	$\leq 5.0 \times 10^{-5}$	1.3×10^{-5}	1.0×10^{-5}
In-service SiC failure	N/A	5.4×10^{-5}	1.4×10^{-6}
Kr-88 R/B	$\leq 8.3 \times 10^{-7}$	9.2×10^{-7}	5.3×10^{-7}
I-131 R/B	$\leq 2.0 \times 10^{-6}$	2.2×10^{-6}	1.6×10^{-6}
Cs-137 fractional release	$\leq 1.0 \times 10^{-5}$	4.2×10^{-5}	5.1×10^{-6}
Ag-110m fractional release	$\leq 5.0 \times 10^{-4}$	1.3×10^{-3}	4.4×10^{-5}

8 REFERENCES

[Acharya 1994] Acharya, R. T., “Transport of Silver in Particle Coatings and Graphite,” Memorandum 818:RTA:293:94, GA unpublished data, November 30, 1994

[Archibald 1983] R. J. Archibald, P. K. Koch, “A User’s and Programmer’s Guide to the GAUGE Two-Dimensional Neutron Diffusion Program”, General Atomics report GA-A16657, July 1983

[Boonstra 1976] Boonstra, R.H., “TAC2D – A General Purpose Two-Dimensional Heat Transfer Computer Code,” GA Report GA-A14032, July 15, 1976

[Cadwallader 1993] Cadwallader, G.J., and S.B. Inamati, “SORS/NP1 Code Description and Users Manual,” CEGA report CEGA-002092, September 1993

[Charman 2009] Charman, C., “Software Requirements Specification for Code Modifications to Accommodate Fuel Shuffling,” 911181, Rev. 0, General Atomics, to be issued

[DelBene 2000] Del Bene, J.V., “TAC2D Version 1.1 Verification Report and Independent Review’” General Atomics document 910351, November 2000

[Derstine 1984] K. L. Derstine, “DIF3D: A Code to Solve One-, Two-, and Three-Dimensional Finite-Difference Diffusion Theory Problems”, Argonne National Laboratory, ANL-82-64, April 1984

[Ellis 2009a] Ellis, C. P., “Core Physics Design Calculations for Next Generation Nuclear Plant (NGNP) Core Performance Analysis, Phase 1,” Report 911161, Rev. 0, General Atomics, February 2009

[Ellis 2009b] Ellis, C. P., “Core Physics Design Calculations for Next Generation Nuclear Plant (NGNP) Core Performance Analysis, Phase 2,” Report 911179, Rev. 0, General Atomics, to be issued

[Ellis 2009c] Ellis, C.P., “Core Physics Design Calculations for NGNP Core Performance Analysis of Single Fuel Particle, Phase 2,” Report 911185, Rev. 0, General Atomics, to be issued

[FDDM/F 1987] Myers, B. F., "Fuel Design Data Manual," General Atomics Report 901866, Issue F, August 1987 *(GA Proprietary Information)*

[GA 2009a] Ellis, C., A. Baxter, and D. Hanson, ”Final Report – NGNP Core Performance Analysis, Phase 1,” Report 911160, Rev. 0, General Atomics, March 2009

[GA 2009b] “Interim Report – NGNP Core Performance Analysis, Phase 2,” Report 911176, Rev. 0, General Atomics, September 2009

[GDDM/A 1984] Price, R. J., “Graphite Design Data Manual,” 906374, Rev. A, GA Technologies, September 1984.

[Hanson 2008] Hanson, D. L., “NGNP Contamination Control Study,” 911117, Rev. 0, General Atomics, April 2008

[Hanson 2009] Hanson, D. L., “Technical Basis for NGNP Fuel Performance and Quality Requirements,” Report 911168, Rev. 0, General Atomics, September 2009

[Jovanovic 1989] Jovanovic, V., “Radionuclide Control for MHTGR,” Report DOE-HTGR-88245, Rev. 1, General Atomics, August 1989

[Kapernick 1993] Kapernick. R., “POKE User's Manual,” CEGA-002928, Rev. N/C, CEGA Corporation, November 1993

[Martin 1993] Martin, R. C., “Compilation of Fuel Performance and Fission Product Transport Models and Database for MHTGR Design,” ORNL/NPR-91/6, Oak Ridge National Laboratory, October 1993

[Medwid 1993] Medwid, W., and A. Gillespie, “COMEDIE BD-1 Test Evaluation Report,” DOE-HTGR-88552, Rev. 0, General Atomics, October 1993

[Moormann 1987] Moormann, R., and K. Verfondern, “Methodik umfassneder probabilistischer Sicherheitsanalysen fuer zunkuenftige HTR-Anlagenkonzepte. Ein Statusbericht (Sand 1986); Band 3: Spaltproduktfreisetzung,” Juel-Spez-388/Bd. 3, Kernforschungsanlage Juelich, Mai 1987

[Munoz 1994] Munoz, S. P., “Fuel Product Specification [for the GT MHR],” DOE-GT-MHR-100209, Rev. 0, General Atomics, May 1994.

[PC-MHR 1994] “MHTGR Plutonium Consumption Study, Phase II Extension FY-94 Final Report,” GA/DOE-156-94, General Atomics, September 30, 1994

[PCDSR 2007] “NGNP and Hydrogen Production Preconceptual Design Studies Report,” Report 911107, Rev. 0, General Atomics, July 2007

[Pfremmer 2002] Pfremmer, R. D., “Software Description and User's Manual for GT-MHR Fuel Performance Code, SURVEY,” 911009, Rev. 0, General Atomics, April 2002

[Plan 2007] “Technical Program Plan for the Next Generation Nuclear Plant/Advanced Gas Reactor Fuel Development and Qualification Program,” Report INL/EXT-05-00465, Rev. 0, Idaho National Laboratory, July 2008

[Richards 2008a] Richards, M., and Meyer, R., “Reactor Pressure Vessel and Intermediate Heat Exchanger Pressure Vessel Alternatives Study Report,” Report 911118, Rev. 0, General Atomics, April 2008

[Richards 2008b] Richards, M., “NGNP Parametric Fuel and Reactor Pressure Vessel Temperature Calculations,” Report 911127, Rev. 0, General Atomics, November 2008

[Shenoy 1974] Shenoy, A. S., and D. W. McEachern, “HTGR Core Thermal Design Methods and Analysis, “ Report GA-A12985 (GA-LTR-17), General Atomic, December 1974

[Sherman 1993] R. Sherman, “BURP: A Macroscopic Cross Section Generation and Nuclide Depletion Program For Use With DIF3D”, CEGA Memo CEGA-M-93-1139, August 1993

[TAC2D 1975] Morcos, S.M. and Williams, K.A., “The TAC2D Code, Version TFMABC-75-1, Part C: Code Verification and Benchmark Problems,” General Atomics report GA-A13415, June 1975

[TECDOC 1997] [TECDOC-978] “Fuel Performance and Fission Product Behavior in Gas Cooled Reactors,” International Atomic Energy Agency, November 1997

[Walti 1972] P. Walti and P. Koch, “MICROX – A Two-Region Flux Spectrum Code for the Efficient Calculation of Group Cross Sections”, Gulf General Report Gulf-GA-A10827, April 1972

Appendix A

Monte Carlo Method Studies of the NGNP Design

A.1 Introduction

Monte Carlo radiation transport and burn-up methods can be used to confirm the results of deterministic codes based on neutron diffusion and transport theory for nuclear reactor calculations. Monte Carlo radiation transport methods have a number of advantages. For example, they are fully and explicitly three-dimensional, and virtually any geometry can be modeled in detail including very small features such as individual TRISO particles. Thus, many parameters that have to be determined or approximated a priori, for use in deterministic calculations, are implicitly included in the Monte Carlo model. In addition, continuous energy cross-sections are generally employed in Monte Carlo codes, whereas deterministic methods use cross sections averaged into broad groups from simplified models of the particular reactor under consideration. The continuous energy cross sections should allow more accurate calculation of the effects of resonance structures and their changes with reactor temperature when compared to the averaging methods that must be used with broad group cross-section sets. Further, Monte Carlo has flexibility in determining quite a number of quantities (such as directional flux/current across a surface, flux at a point or in a cell, energy deposition, reaction rates, etc.) that may be important in understanding a system and refining a design.

However, Monte Carlo has a significant disadvantage as compared with deterministic methods in that it is very time consuming. A typical simulation will generally take several times longer to run using Monte Carlo codes than an equivalent deterministic calculation. Also, if the geometry is fairly complex it may take longer to set up the model to include the necessary details. Therefore, many iterations of a design may be performed using deterministic methods in the time it takes to perform a single Monte Carlo transport and burn-up calculation. The bottom line is that Monte Carlo is a valuable tool in verifying a particular design and determining quantities that may refine the design.

A.2 Monte Carlo Model

A Monte Carlo calculation was performed for the initial cycle of the NGNP core design. At a later date, a multiple cycle Monte Carlo burn-up could be undertaken.

The code used was MCNPX version 2.7b [MCNPX 1] and [MCNPX 2], which was developed at LANL and provides an explicit 3-dimensional transport and burn-up capability for this type of simulation. Utilizing combinatorial geometry and repeated structure features, essentially any level of detail can be obtained for the model. The burn-up module of the code is based on

CINDER'90 which was also developed at LANL and has been tested and used extensively on a wide variety of nuclide depletion calculation applications. Each MCNPX release package contains a set of test problems and results, and these were used to verify correct code operation on the operating platform.

In the model all particle types (LEU, NU, and FBP) were modeled in complete detail, i.e. kernel, buffer, and coatings. The particles were arranged in a 100-particle lattice simulation that reflected the proper PF and mixing ratio of the particles, and were quasi-random. This model was then replicated and filled throughout a larger volume element (e.g., a fuel compact). The 100-particle lattice was developed in order to accommodate the mixed fuel specification of the system. Though initially this was not used for the fixed burnable poison (FBP) particles which are of only one type, and a simpler 2-particle cubic model was used.

Due to the number of coatings on the TRISO particles, this approach resulted in a large number of surfaces and cells (over 500 for each fuel segment). Therefore an input processing code was developed that calculated the particle matrix, and updated the model input for any design iteration. JEF-2.2 cross-section sets, evaluated at a number of temperatures, were used in the burn-up calculations. The sets included temperatures of 300^{o}K, 500^{o}K, 800^{o}K, 1000^{o}K, 1200^{o}K, and 1500^{o}K, so that the range of temperatures in the core could be adequately represented.

All fuel blocks (Standard, Control, and RSS) were modeled in detail. Fuel rods (both under dowels and not under dowels), coolant holes and passages, and tooling and handling holes, were included in each fuel element. Control rod and RSS holes were also modeled in the appropriate blocks. In addition, lateral gaps between the blocks were included. All reflector blocks were explicitly modeled except for the outer buffer region containing boron, and the upper and lower reflectors. The outer buffer region was simply modeled as an annular ring with a smeared composition. The upper and lower reflectors were included as slabs with no penetrations. The entire core was included in the model. 3-day time steps were used initially, then expanded to 7-days, and followed by 10-day time steps out to 580 EFPD.

A.3 Results

The Monte Carlo calculation was performed first using the Phase 1 GAUGE 6.0 nuclear design iteration for a two fuel particle (LEU and NU) core. The results showed reasonable agreement, within statistical errors, over the first 150-days in the initial cycle. At t = 0 both started out at a k-eff of approximately 1.11, decreased quickly to between 1.08 and 1.09, and began to rise. However, as shown in Figure A-1 below, at 150-days, the K_{eff} behavior began to diverge, with the GAUGE-calculated k-eff rolling over and decreasing, and the MCNPX-calculated k-eff showing a steady increase out to about 400-days before rolling over and decreasing.

Subsequent investigation of the MCNPX results showed that the FBP was burning off much faster than calculated by the GAUGE code. This result is non-physical, and was found to be due to an unexpected, higher flux in the FBP rods than in the fuel in the Monte Carlo models.

Further work on this problem was delayed until the completion of the final binary-fuel-particle design (Case 7.9). In the new study, the 100-particle lattice simulation was adopted for the FBP rods as well, since the particle locations take on a quasi-random structure which minimizes neutron streaming, which was believed to be the source of the earlier problems with the FBP burnup model for the Case 6.0 calculation. The PF of the FBP particles was also carefully reviewed and defined, since additional analysis showed that the MCNPX k-eff calculation seemed to be very sensitive to small changes in their values.

The results of the MCNPX analysis of the unrodded initial core reactivity behavior for Case 7.9 are shown in Figure A-2 below and compared to the similar DIF3D results. The standard deviation on the MCNPX k-eff values was 0.004 and is indicated in the figure. There is now much closer agreement between the two methods. An examination of the plot of k-eff versus time for both the MCNPX and DIF3D runs shows that MCNPX reactivity is lower than the DIF3D values for about the first 170 days, with some scatter in the MCNPX results. Past 170 days, MCNPX follows the DIF3D results fairly closely but has somewhat higher values until about 570 days where the MCNPX reactivity falls just below 1.0. As far as total burn-up is concerned, MCNPX and DIF3D agree reasonably well; at 580 days the values are 53,760 MWD/MTU for MCNPX and 53,831 MWD/MTU for DIF3D.

It now appears that the Monte Carlo and deterministic methods are in reasonable agreement, and the Monte Carlo model supports the deterministic model used in the NGNP design study. However, additional analysis is needed to ensure that the FBP modeling in the MCNPX code is completely accurate.

A.4 References

[MCNPX 1] “MCNPX User’s Manual, version 2.1.5,” Laurie S. Waters, Editor, LANL Report TPO-E83-G-UG-X-00001, Rev 0, November 1999

[MCNPX 2] “MCNPX 27b Extensions”, Dennis Pelowitz et al., LANL report LA-UR-09-04150, July 2009

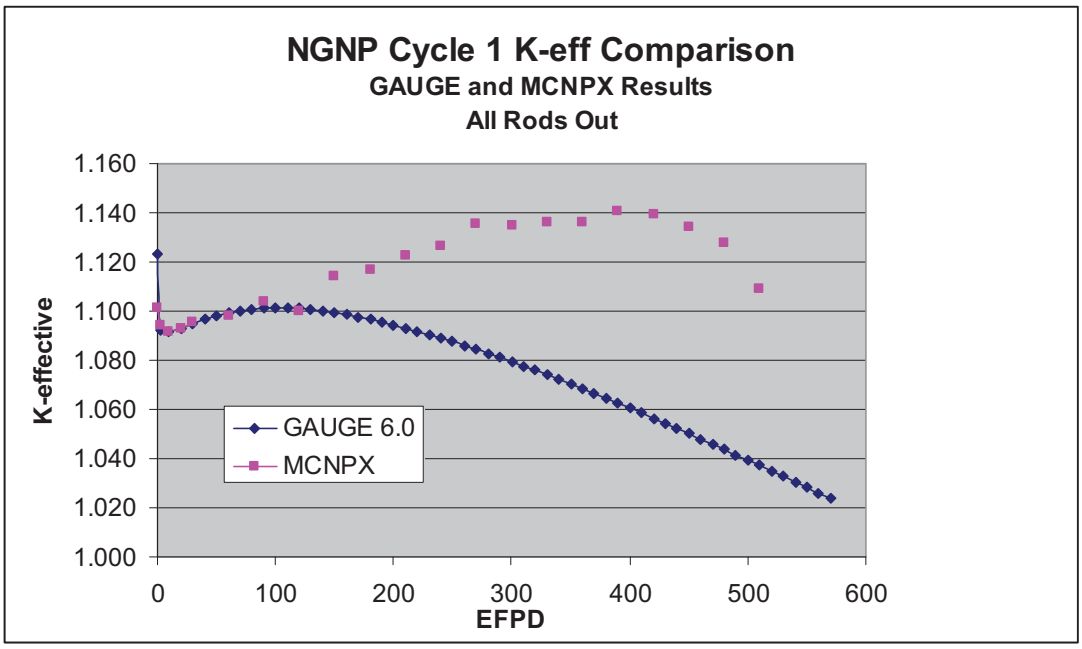

Figure A-1. Comparison of Monte Carlo and GAUGE Calculated K-eff for the Initial Core

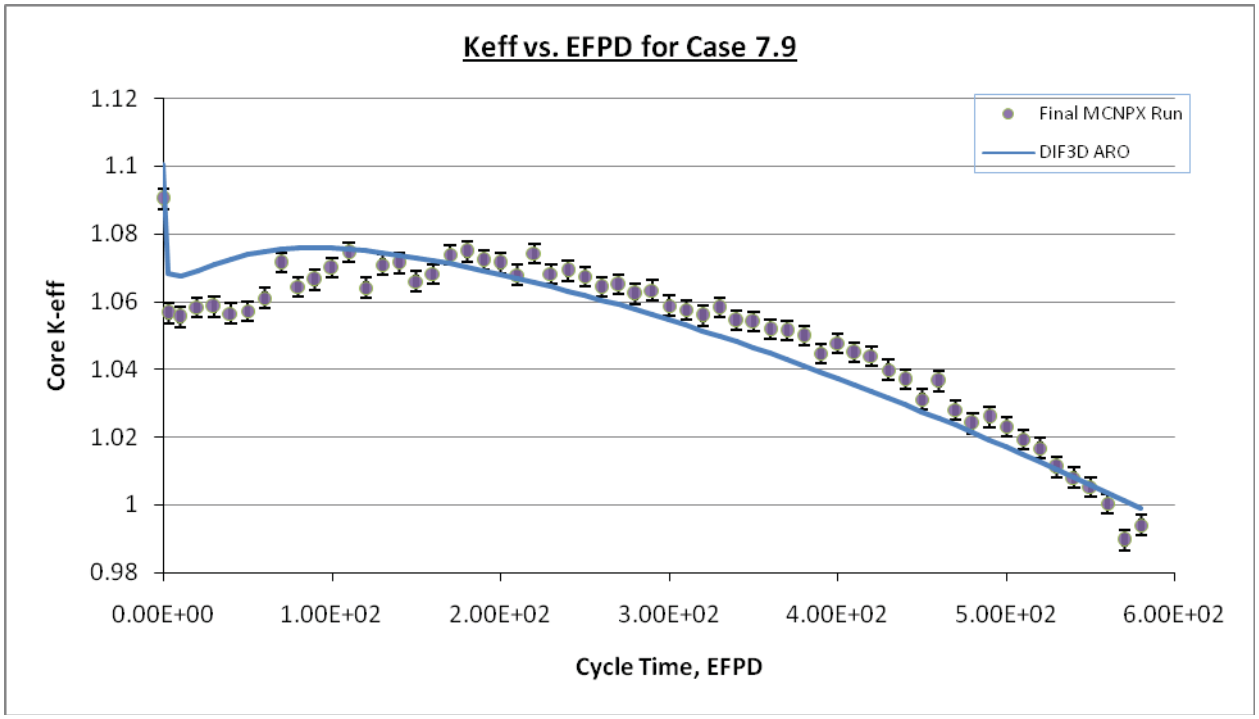

Figure A-2. MCNPX and DIF3D Unrodded K-eff Comparison for Case 7.9

P.O. BOX 85608 SAN DIEGO, CA 92186-5608 (858) 455-3000